BioMed Research International

Molecular Image-Guided Theranostic and Personalized Medicine 2014

Guest Editors:Hong Zhang, Mei Tian, Ignasi Carrio, Ali Cahid Civelek, and Yasuhisa Fujibayashi

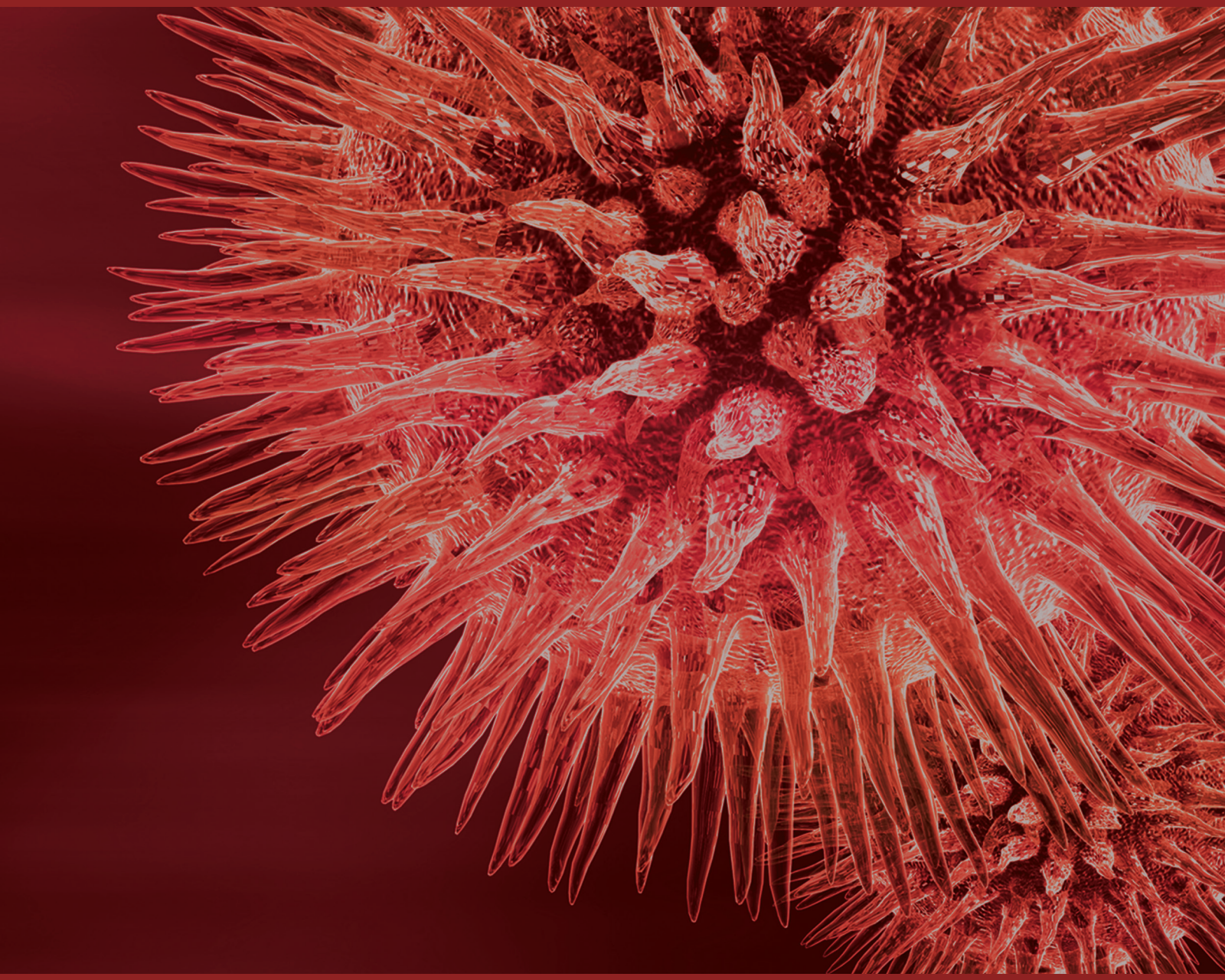

Molecular Image-Guided Theranostic and Personalized Medicine 2014

BioMed Research International

Molecular Image-Guided Theranostic and Personalized Medicine 2014

Guest Editors: Hong Zhang, Mei Tian, Ignasi Carrio, Ali Cahid Civelek, and Yasuhisa Fujibayashi

Contents

Molecular Image-Guided Theranostic and Personalized Medicine 2014, Hong Zhang, Mei Tian, Ignasi Carrio, Ali Cahid Civelek, and Yasuhisa Fujibayashi
Volume 2015, Article ID 258612, 2 pages

Adenocarcinoma with BAC Features Presented as the Nonsolid Nodule Is Prone to Be False-Negative on ^{18}F-FDG PET/CT, Hu-bing Wu, Lijuan Wang, Quan-shi Wang, Yan-jian Han, Hong-sheng Li, Wen-lan Zhou, and Ying Tian
Volume 2015, Article ID 243681, 7 pages

Prognostic Value of ^{99m}Tc-Pertechnetate Thyroid Scintigraphy in Radioiodine Therapy in a Cohort of Chinese Graves' Disease Patients: A Pilot Clinical Study, Haifeng Hou, Shu Hu, Rong Fan, Wen Sun, Xiaofei Zhang, and Mei Tian
Volume 2015, Article ID 974689, 4 pages

The Diagnostic Value of ^{18}F-FDG PET/CT in Association with Serum Tumor Marker Assays in Breast Cancer Recurrence and Metastasis, Ying Dong, Haifeng Hou, Chunyan Wang, Jing Li, Qiong Yao, Said Amer, and Mei Tian
Volume 2015, Article ID 489021, 5 pages

Molecular and Functional Imaging of Internet Addiction, Yunqi Zhu, Hong Zhang, and Mei Tian
Volume 2015, Article ID 378675, 9 pages

Ghrelin Improves Functional Survival of Engrafted Adipose-Derived Mesenchymal Stem Cells in Ischemic Heart through PI3K/Akt Signaling Pathway, Dong Han, Wei Huang, Sai Ma, Jiangwei Chen, Lina Gao, Tong Liu, Rongqing Zhang, Xiujuan Li, Congye Li, Miaomiao Fan, Yundai Chen, and Feng Cao
Volume 2015, Article ID 858349, 12 pages

Somatostatin Receptor Based Imaging and Radionuclide Therapy, Caiyun Xu and Hong Zhang
Volume 2015, Article ID 917968, 14 pages

Hindawi Publishing Corporation
BioMed Research International
Volume 2015, Article ID 258612, 2 pages
http://dx.doi.org/10.1155/2015/258612

Editorial

Molecular Image-Guided Theranostic and Personalized Medicine 2014

Hong Zhang,[1] Mei Tian,[2] Ignasi Carrio,[3] Ali Cahid Civelek,[4] and Yasuhisa Fujibayashi[5]

[1]*The Second Affiliated Hospital of Zhejiang University, Hangzhou, Zhejiang, China*
[2]*Hangzhou Binjiang Hospital of Zhejiang University, Hangzhou, Zhejiang, China*
[3]*San Paul Hospital, Autonomous University of Barcelona, Barcelona, Spain*
[4]*NIH Clinical Center, Bethesda, MD, USA*
[5]*National Institute of Radiological Sciences, Chiba, Japan*

Correspondence should be addressed to Hong Zhang; hzhang21@gmail.com

Received 2 March 2015; Accepted 2 March 2015

Molecular image-guided therapy has been demonstrated to be effective in improving diagnosis, prognosis, planning, and monitoring of personalized medication. Molecular imaging modalities include positron emission tomography (PET), single-photon emission-computed tomography (SPECT), magnetic resonance imaging (MRI), computed tomography (CT), ultrasound (US), and optical imaging (Ramen, quantum dots, and bioluminescence). Among clinical molecular imaging modalities, radionuclide imaging technique is the most sensitive one which could provide target-specific information as well as function, pathway activities, and cell migration in the intact organism. For instance, the radiotracer could noninvasively assess diseases treatment endpoints which are used to rely almost exclusively on biopsies and histopathological assays. New leads on the development of personalized theranostic (image and treat) agents would allow for more accuracy in the selection of patients who may respond to treatment.

Topics covered in this special issue include advances in molecular imaging modalities in oncological disease management, image-guided approach of brain function, stem cell technology, and receptor based imaging approach. For example, Q. Wang's group at Nanfang Hospital of Southern Medical University reported a retrospective study on 51 consecutive patients to investigate what causes the false negative of adenocarcinoma with BAC features on ^{18}F-FDG PET/CT. Their study demonstrated that different types of adenocarcinoma with BAC features exhibited different ^{18}F-FDG uptake patterns. False negative on ^{18}F-FDG PET/CT mainly occurs in those lesions presented as the nonsolid nodule on CT, but not the solid nodule. Y. Dong and her coauthors from Zhejiang University evaluated the efficacy of PET/CT in association with serum tumor maker assays in the follow-up of patients with breast cancer (BC). This study indicated that PET/CT was a highly efficient tool to follow-up patients with BC compared with CITs in terms of sensitivity and specificity, allowing for the detection of metastatic and/or recurrent cases. The high serum levels of CA 15-3 in confirmed positive PET/CT patients compared to negative ones indicated the clinical value of CA 15-3 in BC follow-up. H. Hou and his coauthors from the same institute reported a pilot study on the prognostic value of ^{99m}Tc-pertechnetate thyroid scintigraphy for predicting the outcomes of fixed dose (5 mCi) of radioiodine. A fixed dose of 5mCi radioiodine seems to be practical and effective for treating GD patients with thyroid mass ≤40.1 g and ^{99m}Tc-pertechnetate uptake ≤15.2%. This study demonstrates that ^{99m}Tc-pertechnetate thyroid scintigraphy is an important prognostic factor for predicting the outcomes of RIT.

Mesenchymal stem cells (MSCs) have been proposed as a promising cell population for cell therapy and regenerative medicine applications. However, the low retention and poor survival of engrafted cells hampered the therapeutic efficacy of engrafted MSCs. In this issue, F. Cao and her coauthors from Fourth Military Medical University and Chinese PLA General Hospital presented their work on the protective effects of ghrelin on engrafted adipose derived mesenchymal stem cells (ADMSCs) and its beneficial effects with cellular

therapy in mice myocardial infarction (MI). Their study revealed that ghrelin may serve as a promising candidate for hormone-driven approaches to improve the efficacy of mesenchymal stem cell-based therapy for cardiac ischemic disease via PI3K/AKT pathway.

Recently, a number of tracers have been introduced due to the encouraging results from the applications of radiolabeled ligand-receptor system. The current status of somatostatin receptor based imaging and radionuclide therapy is summarized and discussed in the review paper by C. Xu and her coauthor. The *hSSTr2* gene can act as not only a reporter gene for in vivo imaging, but also as a therapeutic gene for local radionuclide therapy. Even a second therapeutic gene can be transfected into the same tumor cells together with *hSSTr2* reporter gene to obtain a synergistic effect.

Neuroscience is a hot topic in recent years. Maladaptive use of the Internet results in Internet addiction (IA), which is associated with various negative consequences. Molecular and functional imaging approaches have been increasingly used for the analysis of neurobiological and neurochemical changes of the brain. Y. Zhu and his coauthors summarize the molecular and functional imaging findings on neurobiological mechanisms of IA, focusing on magnetic resonance imaging (MRI) and nuclear imaging modalities including positron emission tomography (PET) and single-photon emission-computed tomography (SPECT). MRI studies demonstrate that structural changes in frontal cortex are associated with functional abnormalities in Internet addicted subjects. Nuclear imaging findings indicate that IA is associated with dysfunction of the brain dopaminergic systems. Abnormal dopamine regulation of the prefrontal cortex (PFC) could underlie the enhanced motivational value and uncontrolled behavior over Internet overuse in addicted subjects.

In summary, molecular imaging could be applied to target characterization, underlying disease progression and evaluation of therapeutic response and stem cell and brain function. This special issue provides a platform of the efficacy of personalized medication from molecular imaging technology which may have high impact on patient care.

Hong Zhang
Mei Tian
Ignasi Carrio
Ali Cahid Civelek
Yasuhisa Fujibayashi

Hindawi Publishing Corporation
BioMed Research International
Volume 2015, Article ID 243681, 7 pages
http://dx.doi.org/10.1155/2015/243681

Research Article

Adenocarcinoma with BAC Features Presented as the Nonsolid Nodule Is Prone to Be False-Negative on ^{18}F-FDG PET/CT

Hu-bing Wu, Lijuan Wang, Quan-shi Wang, Yan-jian Han, Hong-sheng Li, Wen-lan Zhou, and Ying Tian

NanFang PET/CT Center, Nanfang Hospital, Southern Medical University, 1838 Guangzhou Avenue North, Guangzhou, Guangdong 510515, China

Correspondence should be addressed to Quan-shi Wang; wqslph@163.net

Received 8 September 2014; Revised 9 January 2015; Accepted 12 January 2015

Academic Editor: Ignasi Carrio

Purpose. The present study investigated which type of adenocarcinoma with BAC features was prone to be false-negative on 18F-FDG PET/CT. *Materials and Methods*. A retrospective study was performed on 51 consecutive patients with localized adenocarcinoma with BAC features. CT and PET were assessed for lesion size, GGO percentage, and SUVmax. Lesions with FDG uptake the same as or more than mediastinal blood-pool activity were considered as PET-positive. *Results*. Of the 51 cases, 19.6% presented as pure GGO nodules, 31.4% as mixed nodules, and 49.0% as solid nodules. None of the pure GGO nodules was 18F-FDG avid, compared with 37.5% of mixed nodules and 96.0% of solid nodules ($\chi^2 = 31.55$, $P = 0.000$). In the mixed nodule group, SUVmax was negatively correlated with GGO percentage ($r = -0.588$; $P = 0.021$). The positive detection rate of 18F-FDG PET/CT was 50.0%, 55.6%, and 100% in tumors 1.1–2.0 cm, 2.1–3.0 cm, and >3.0 cm in diameter, respectively ($\chi^2 = 5.815$, $P = 0.055$). General linear model factor analysis showed that the GGO was an important factor contributing to false-negative PET/CT results ($F = 23.992$, $P = 0.000$), but lesion size was not ($F = 0.602$, $P = 0.866$). *Conclusions*. The present study indicated that the adenocarcinoma with BAC features presented as nonsolid nodule is prone to be false negative on 18F-FDG PET/CT.

1. Introduction

Bronchioloalveolar carcinoma (BAC) is a subtype of adenocarcinoma that manifests as the lepidic growth of tumor cells along the alveoli without stromal invasion. Whereas, the adenocarcinoma with BAC features is a subtype of adenocarcinoma which comprises a heterogeneous group of tumors with BAC histology mixed with a varying population of invasive cells. Since the latest revision of the WHO/International Association for the Study of Lung Cancer Classification in 2004, the adenocarcinoma with aerogenous spread is referred to as adenocarcinoma with BAC features instead of pure BAC [1, 2]. Lung adenocarcinoma with BAC features is a form of adenocarcinoma with unique clinical, radiological, and epidemiological features. Most of them are noninvasive or minimally invasive carcinoma and associated with a markedly better prognosis compared with invasive adenocarcinoma and may be cured with surgical resection [3, 4].

Adenocarcinoma with BAC features has 3 subtypes: nonmucinous (most frequent), mucinous (25%), and mixed (exceedingly rare). Lee et al. [5] reported that all nonmucinous adenocarcinomas with BAC features appeared as pure ground-glass opacity (GGO) nodules, whereas mucinous ones could appear as solid or part-solid nodules (mixed nodule).

Positron emission tomography (PET)/CT with ^{18}F-fluorodeoxyglucose (FDG) is a noninvasive diagnostic technique that provides information about glucose metabolism in lesions and is used routinely for the preoperative staging of NSCLC because of its higher sensitivity and specificity than other diagnostic modalities [6, 7]. However, it has been reported that adenocarcinoma with BAC features has a lower ^{18}F-FDG uptake than other types of NSCLC, and is prone to be falsely negative on PET/CT [7, 8]. Nonetheless, it is clear that false-negative does not occur in all the lesions [9, 10]. Therefore, it is needed to determine which type of adenocarcinoma with BAC features is prone to be false-negative

and which patient will benefit from postoperative ^{18}F-FDG PET/CT surveillance. In the present study, we performed a retrospective study on 51 consecutive patients to investigate what causes the false negativity of adenocarcinoma with BAC features on ^{18}F-FDG PET/CT.

2. Materials and Methods

2.1. Patients. This study was approved by the Institutional Review Board of our hospital. Because of the retrospective nature of the study, the requirement of subject informed consent was waived.

We retrospectively reviewed the records of 51 consecutive patients with adenocarcinoma with BAC features who underwent preoperative PET/CT from December 2005 to January 2011. There were 31 males and 20 females with a mean age of 59 years (range, 35–87 years). Each patient had a focal nodule larger than 1.0 cm. Patients with multiple nodules were excluded. After PET/CT examination, all patients underwent surgical resection within 1 month and a final diagnosis of adenocarcinoma with BAC features was made by histological examination of the surgical specimen. All patients were stage pT1N0 or pT2N0. None of the patients had received prior anticancer treatment before the PET/CT scan, and no patients had insulin dependent diabetes.

2.2. ^{18}F-FDG PET/CT Examination. PET/CT examinations were performed using a GE Discovery LS PET/CT scanner (GE Healthcare, Waukesha, WI). Patients were instructed to fast for at least 6 hours before the scan, and blood glucose level was monitored by finger stick immediately prior to the study to ensure that their glucose level was within normal levels (<7 mmol/L). Approximately 60 minutes after an intravenous injection of 277 to 444 MBq (7.50–12.00 mCi, 0.15 mCi/kg) of ^{18}F-FDG, whole-body PET/CT was performed according to the guidelines for tumor imaging with ^{18}F-FDG PET/CT 1.0 [11]. A spiral CT scan was performed using an 0.8 s rotation time, 80 mA, 140 kVp, and a 5 mm slice thickness in high-speed mode with the patient's arms raised over their head. Whole-body ^{18}F-FDG PET/CT scan was acquired in the 2-dimensional acquisition mode with 3 min/bed position. After data acquisition, attenuation correction of the PET emission data was performed by CT-based attenuation correction (CTAC). Image reconstruction was performed with an ordered-subset expectation maximization (OSEM) iterative algorithm (2 iterations, 28 subsets).

The acquired PET and CT images were sent to an Xeleris (GE Medical Systems) workstation for registration and fusion. The PET image, CT image, and fused PET/CT image were reviewed by 2 experienced physicians each with more than 10 years of experience in nuclear medicine. For qualitative analysis, the degree of FDG activity in the nodules was defined as either negative (i.e., less than mediastinal blood-pool activity) or positive (i.e., same as or greater than mediastinal blood-pool activity). For semiquantitative analysis, the region of interest (ROI) was drawn along the margin of the lesion for the measurement of the maximum standardized uptake value (SUVmax). In patients with negative PET/CT images, ROIs were drawn on the chest CT and copied to same region on the PET/CT image. SUVmax was measured to represent the ^{18}F-FDG uptake of the lesion.

2.3. Thin-Section CT Examination. Thin-section CT of the nodules was performed using the GE Discovery LS PET/CT scanner with 140 kVp, 160 mA, and a pitch of 0.875. Thin-section CT images were reconstructed into 1.0 mm-thick sections using high-frequency algorithms.

The thin-section CT images were displayed with lung (level, −600 HU; width, 1700 HU) and mediastinal (level, 30 HU; width, 400 HU) window settings in a multiplanar format and were reviewed separately by two experienced chest radiologists. On CT images, nodules were classified into GGO, solid and mixed nodules. GGO was defined as focal nodular areas of hazy increased lung attenuation with preservation of bronchial and vascular margins. Solid nodule was defined as an opacity with the density similar to that of soft tissue. The mixed nodule was considered when GGO and solid component were mixed in an opacity. The percentage of GGO was calculated as $[(D_{GGO} - D)/D_{GGO}] \times 100$, where D_{GGO} is the greatest diameter of the lesion, including the GGO area and D is the greatest diameter of the lesion without GGO [12].

2.4. Statistical Analysis. The descriptive data were expressed as mean ± standard deviation. One-way ANOVA was used to analyze continuous variables, and the Pearson Chi-Square test was used to compare categorical variables between groups. The SUVmax was correlated with GGO percentage with linear regression analysis. General linear model factor analysis was used to analyze the influence of GGO and lesion size on false-negative PET/CT results. A P value of 0.05 or less was considered significant. SPSS 13.0 software (SPSS, Inc., Chicago, IL) was used for all analyses.

3. Results

The ^{18}F-FDG PET/CT results were positive in 58.8% (30/51) of patients with adenocarcinoma with BAC features, and, in 21 patients, the ^{18}F-FDG PET/CT results were negative. The SUVmax of the PET/CT positive BAC group was significantly higher than that of the PET/CT negative BAC group (7.79 ± 4.08 versus 1.29 ± 0.63, resp.; $t = 7.20$, $P = 0.000$).

Of the 51 cases, 19.6% of patients presented with GGO nodules, 31.4% with mixed nodules, and 49.0% with solid nodules. The different types of lesions exhibited different ^{18}F-FDG uptake on PET/CT images. ^{18}F-FDG PET/CT demonstrated positive detection in 0.0% of the pure GGO nodules, 37.5% of the mixed nodules, and 96.0% of solid nodules (Table 1). Examples of the different types of lesions with different ^{18}F-FDG uptake patterns were shown in Figures 1–3. In the mixed nodule group, the SUVmax of the nodules was negatively correlated with GGO percentage (mean, 68%; range, 54–93%) ($r = -0.588$, $P = 0.021$). Similar to the visual analysis, ^{18}F-FDG uptake in the lesions of the 3 groups

Table 1: GGO component, lesion size, SUVmax, and PET/CT positivity in adenocarcinoma lesions with BAC features.

Tumor	Number	PET/CT positivity, no. (%) of nodules	SUVmax
GGO component		$\chi^2 = 31.55$, $P = 0.000$	$F = 20.827$, $P = 0.000$
GGO nodule	10	0 (0.0)	1.04 ± 0.43
Mixed nodule	16	6 (37.5)	2.93 ± 2.99
Solid nodule	25	24 (96.0)	8.14 ± 4.11
Lesion size (cm)		$\chi^2 = 5.815$, $P = 0.055$	$F = 21.463$, $P = 0.000$
1.1–2.0	26	13 (50.0)	2.20 ± 2.51
2.1–3.0	18	10 (55.6)	7.46 ± 3.59
>3.0	7	7 (100)	9.88 ± 5.10

BAC, bronchoalveolar cell carcinoma; GGO, ground-glass opacity; SUVmax, maximum standardized uptake value.

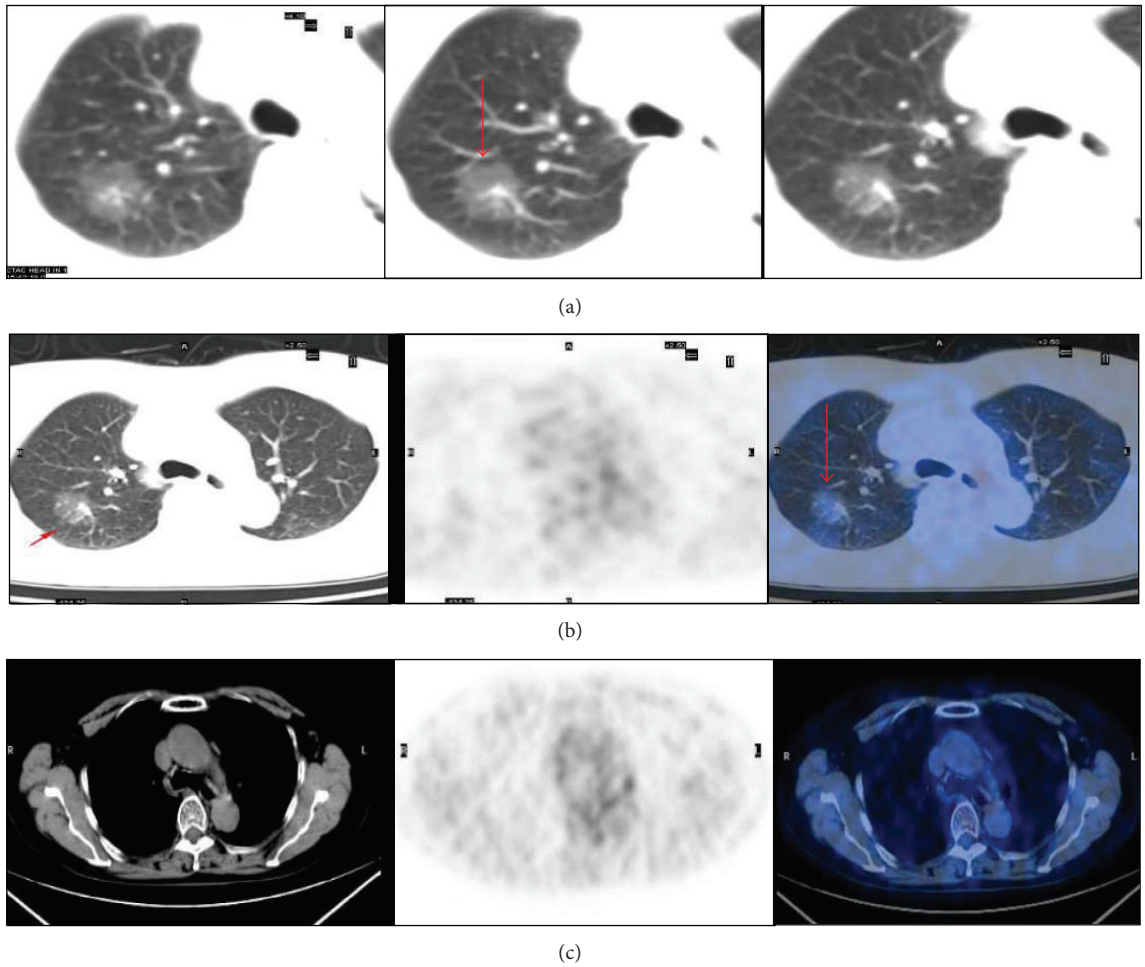

Figure 1: A 75-year-old female with an adenocarcinoma lesion with BAC features (red arrow). (a) Axial thin section CT images revealed a 2.8 cm pure ground-glass opacity in the right upper lobe. (b, c) ^{18}F-FDG PET/CT was negative for the lesion, and the maximum standardized uptake value = 0.8.

were significantly different ($F = 20.827$, $P = 0.000$, Table 1). The SUVmax of GGO nodule and mixed nodule groups was significantly lower than that of the solid nodules group ($P = 0.000$). No significant difference between the SUVmax of the GGO nodules group and mixed nodules group was observed ($P = 0.170$).

Twenty patients had tumors from 1.1 to 2.0 cm in diameter, 18 from 2.1 to 3.0 cm in diameter, and 7 > 3.0 cm in diameter. Analysis showed that SUVmax was significantly positively correlated with tumor size ($r = 0.60$, $P < 0.01$). Lower ^{18}F-FDG uptake in lesions 1.2–2.0 cm in diameter was noted as compared with lesions 2.1–3.0 cm and lesions >

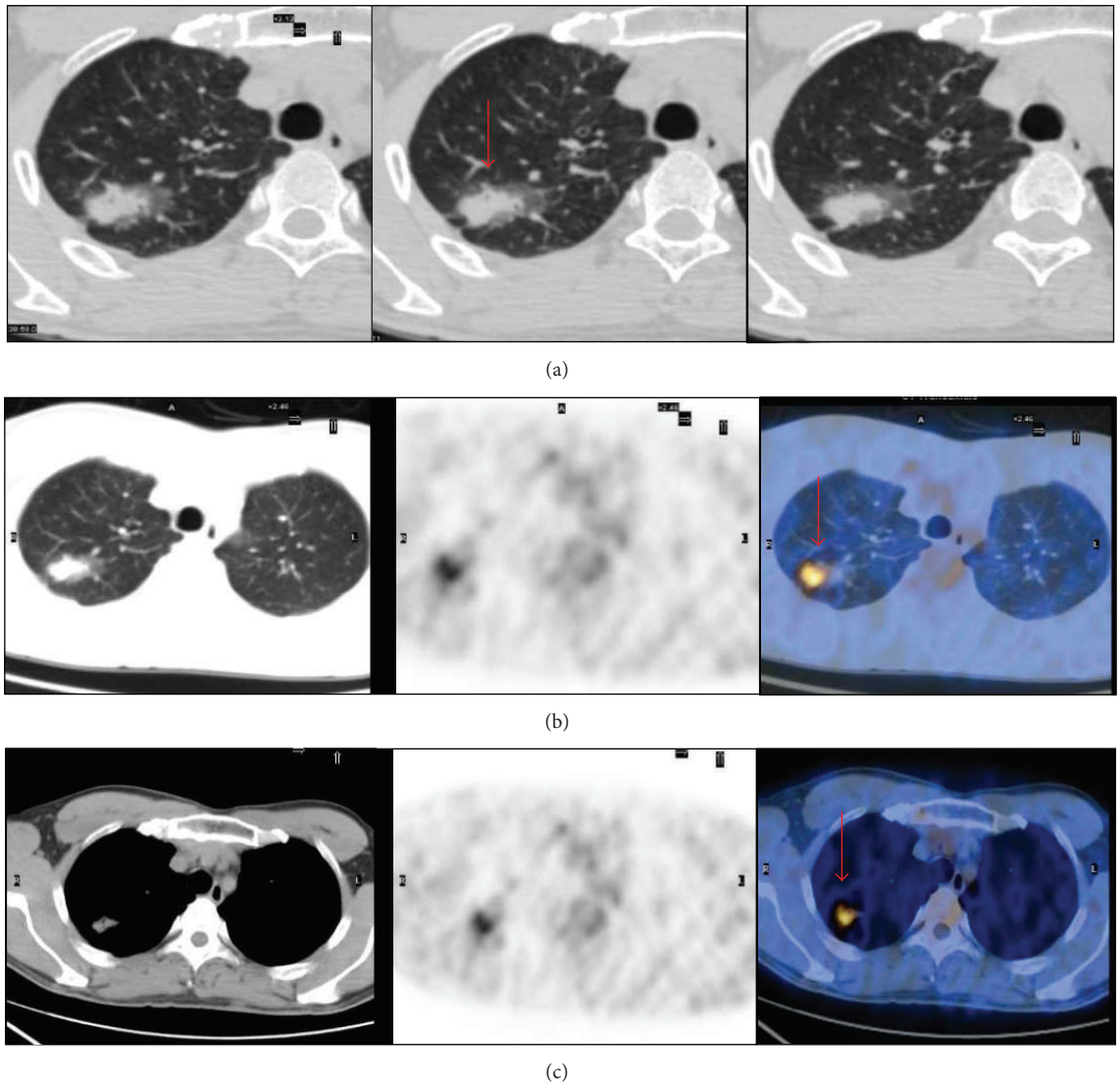

Figure 2: A 47-year-old male with an adenocarcinoma lesion with BAC features (red arrow). (a) Axial thin section CT image revealed a 2.3 cm mixed ground-glass opacity nodule in right upper lobe. (b, c) ^{18}F-FDG PET/CT was positive for the lesion, and the maximum standardized uptake value = 3.59. Focal hypermetabolism was localized in the soft part of the lesion but not in the ground-glass part.

3.0 cm in diameter (both, $P = 0.000$). However, ^{18}F-FDG PET/CT exhibited no significant difference in the positive detection rate among the 3 tumor size groups ($\chi^2 = 5.815$, $P = 0.055$, Table 1). Approximately the same positive detection rate was found in the 1.1–2.0 cm and 2.1–3.0 cm diameter groups (50.0% versus 55.6%, resp.; $P > 0.05$), but all lesions > 3.0 cm in diameter were ^{18}F-FDG avid (Table 1).

Factorial design ANOVA was used to analyze the influence of GGO and lesion size on false negativity of PET/CT results. Analysis demonstrated that GGO had a statistically significant effect on false-negative PET/CT results of BAC lesions ($F = 23.992$, $P = 0.000$); however, lesion size had no effect ($F = 0.602$, $P = 0.866$). The results also showed that there was no interaction between GGO and lesion size with respect to false-negative PET/CT results ($F = 1.069$, $P = 0.446$).

4. Discussion

Although ^{18}F-FDG PET/CT is a valuable imaging modality for the diagnosis and staging of lung cancer, it has several pitfalls. Focal adenocarcinoma with BAC features has been reported as often being negative on ^{18}F-FDG PET/CT scans [7, 8, 13, 14]. Sun et al. [15] reported that the SUVmax of adenocarcinoma with BAC (mean, 7.2) was significantly lower than that of other subtypes of NSCLC (mean, 13.33) ($P < 0.0001$). A low sensitivity (72%) of ^{18}F-FDG PET/CT for detecting adenocarcinoma with BAC features was reported by Khandani et al. [16] Heyneman and Patz Jr. [17] also reported that PET/CT failed to identify 40% of adenocarcinoma lesions with BAC features. In the present study, ^{18}F-FDG PET/CT showed a similar low sensitivity (58.8%) for diagnosing adenocarcinoma with BAC features.

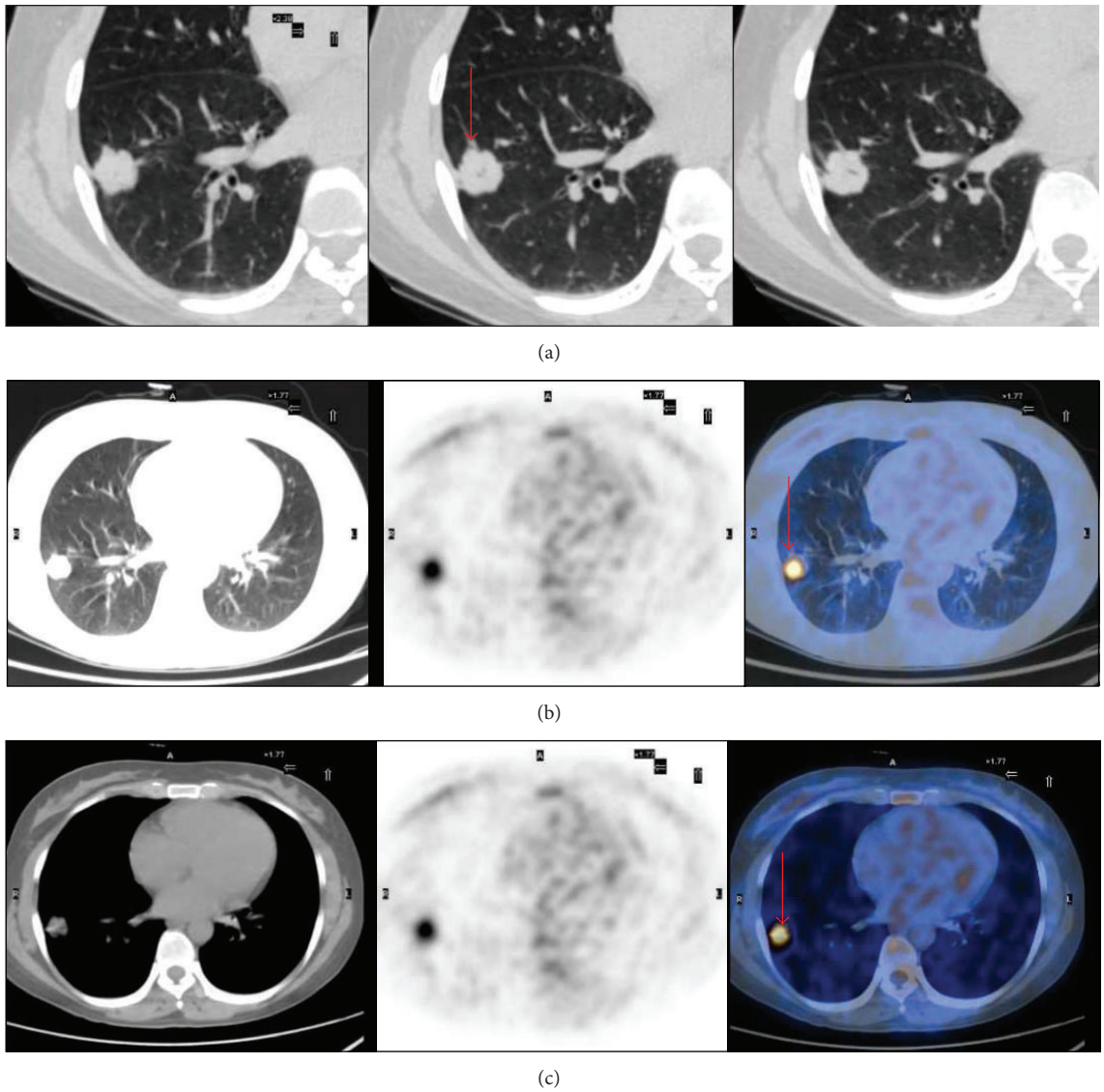

(a)

(b)

(c)

Figure 3: A 47-year-old woman with an adenocarcinoma lesion with BAC features (red arrow). (a) Axial thin section CT image revealed a 2.2 cm solid nodule (arrow) in right lower lobe. (b, c) ^{18}F-FDG PET/CT was positive for the lesion, and the maximum standardized uptake value = 5.66.

Because of the low positive detection rate, ^{18}F-FDG PET/CT seems to be unsuitable for imaging adenocarcinoma with BAC features. However, the results of the present study indicated that about 50% of adenocarcinoma with BAC features were PET/CT positive, and patients with adenocarcinoma with BAC features that are PET/CT positive may also potentially benefit from PET/CT staging or postoperative surveillance. However, the problem lies in predicting which type of adenocarcinoma with BAC features may potentially benefit from PET/CT.

In the present study, none of the BAC lesions with pure GGO was positive on PET/CT. A similar result was reported by Nomori et al. [18] that false-negative PET/CT results were found in 90% of GGO lesions. Very low ^{18}F-FDG uptake in pure GGO lesions was also reported by Goudarzi et al. [19]. In their study, a total of 26 pure GGO lesions had a median SUVmax of 1.48 (range, 0.63–4.54), and a SUVmax < 2.5 was found in 81% of the lesions. GGO is commonly seen in adenocarcinoma lesions with BAC features and is thought to be derived from the combined effects of reduction of alveolar air spaces and increased cellular components with alveolar cuboidal cell hyperplasia, thickening of alveolar septa, and partial filling of the alveolar air spaces by tumor cells [7, 20]. Lower ^{18}F-FDG uptake in GGO lesions may be the result of the low metabolic demand of slow-growing lesions or a very small number of active malignant cells in these lesions.

Being contrast to the pure GGO lesions, the present study demonstrated that nearly all of the solid nodules were positive of ^{18}F-FDG PET. It is similar to the results reported by Lee et al. [21]. Their results showed that the mean SUVmax 2.3 ± 1.9 for mucinous BACs, which appear as solid or part-solid nodules on CT, was significantly higher than that of

0.5 ± 0.8 for nonmucinous BACs, which present as pure GGO nodules ($P = 0.007$). The solid nodules may be predominantly composed of actively growing malignant cells and thus a high glucose demand. Because pure GGO nodule and solid nodule showed a nearly completely different ^{18}F-FDG uptake pattern, we suggested that ^{18}F-FDG PET/CT might be suitable for imaging of adenocarcinoma lesions with BAC features which present as solid nodule on CT and should not be used for imaging of those as GGO nodule.

The present study also suggests that it is the proportion of the solid component in the adenocarcinoma lesions with BAC features which actually determines whether the tumor is positive or not on PET/CT. Liu et al. found that the percentage of GGO was negatively correlated with the ^{18}F-FDG uptake in the lesion [22]. The present study demonstrated a similar tendency in the mixed nodule group ($r = -0.588$; $P = 0.021$). As shown in Figure 2, focal hypermetabolism was localized in the soft part of the lesion but not in the ground-glass part. Mixed nodules may represent an intermediate stage of tumor growth, that is, from the indolent stage of a pure GGO lesion to active tumor. Because of the low positive detection rate, we suggested that ^{18}F-FDG PET/CT might not be suitable for imaging of adenocarcinoma lesions with BAC features which present as mixed nodules on CT.

Small NSCLC lesions are often found to have low ^{18}F-FDG uptake and are prone to be false-negative on PET/CT [10, 23]. Although the present study also demonstrated the SUVmax of BAC lesions and tumor size had a significant positive correlation ($r = 0.657$, $P = 0.000$), the factorial design ANOVA study indicated the tumor size was not associated with false-negative PET/CT results. Approximately the same positive detection rate of ^{18}F-FDG PET/CT was found for lesions 1.1–2.0 cm and lesions 2.1–3.0 cm in diameter (50% versus 55.6%, resp.; $P > 0.05$). Factorial design ANOVA demonstrated that GGO had a statistically significant effect on false-negative PET/CT results of adenocarcinoma lesions with BAC features but not lesion size. This result was different from what was found in the adenocarcinoma lesions without BAC features. In the adenocarcinoma lesions without BAC features, the lesion size was often significantly associated with ^{18}F-FDG uptake [24]. This difference may result from the different presentations between them. Most adenocarcinoma lesions without BAC features are solid lesions; however, ground-glass changes are commonly seen in adenocarcinoma lesions with BAC features.

A limitation of the present study is the small sample size of the mixed nodule group, and all of the lesions were ≥ 1.0 cm. Further studies with a larger patient group, including patients with adenocarcinoma lesions with BAC features < 1.0 cm are needed. In addition, the retrospective nature of the study may limit the interpretation of the results.

5. Conclusion

Adenocarcinoma with BAC features is considered as the main cause of falsely negative finding on ^{18}F-FDG PET/CT. However, the present study demonstrated that different types of adenocarcinoma with BAC features exhibited different ^{18}F-FDG uptake patterns. False-negative on ^{18}F-FDG PET/CT mainly occurs in those lesions which presented as the nonsolid nodule on CT but not the solid nodule. A patient diagnosed with adenocarcinoma lesions with BAC features may still benefit from postoperative ^{18}F-FDG PET/CT surveillance when the lesion presented as a solid nodule on the preoperative CT images. Further research is needed to confirm the present results.

Disclosure

Hu-bing Wu is first author.

Conflict of Interests

The authors declare that there is no conflict of interests regarding the publication of this paper.

Acknowledgments

The authors would like to thank their colleagues in the Department of Pathology, Nanfang Hospital, who provided and reviewed the histopathologic data. The National Natural Science Foundation Project of China supported this study financially (81071175).

References

[1] W. D. Travis, K. Garg, W. A. Franklin et al., "Evolving concepts in the pathology and computed tomography imaging of lung adenocarcinoma and bronchioloalveolar carcinoma," *Journal of Clinical Oncology*, vol. 23, no. 14, pp. 3279–3287, 2005.

[2] W. L. Read, N. C. Page, R. M. Tierney, J. F. Piccirillo, and R. Govindan, "The epidemiology of bronchioloalveolar carcinoma over the past two decades: analysis of the SEER database," *Lung Cancer*, vol. 45, no. 2, pp. 137–142, 2004.

[3] D. Arenberg, "Bronchioloalveolar carcinoma," *Seminars in Respiratory and Critical Care Medicine*, vol. 32, no. 1, pp. 52–61, 2011.

[4] M. Gaeta, A. Blandino, S. Pergolizzi et al., "Patterns of recurrence of bronchioloalveolar cell carcinoma after surgical resection: a radiological, histological, and immunohistochemical study," *Lung Cancer*, vol. 42, no. 3, pp. 319–326, 2003.

[5] H. Y. Lee, K. S. Lee, J. Han et al., "Mucinous versus nonmucinous solitary pulmonary nodular bronchioloalveolar carcinoma: CT and FDG PET findings and pathologic comparisons," *Lung Cancer*, vol. 65, no. 2, pp. 170–175, 2009.

[6] H. AL-Jahdali, A. N. Khan, S. Loutfi, and A. S. Al-Harbi, "Guidelines for the role of FDG-PET/CT in lung cancer management," *Journal of Infection and Public Health*, vol. 5, supplement 1, pp. S35–S40, 2012.

[7] V. Ambrosini, S. Nicolini, P. Caroli et al., "PET/CT imaging in different types of lung cancer: an overview," *European Journal of Radiology*, vol. 81, no. 5, pp. 988–1001, 2012.

[8] H. Y. Lee and K. S. Lee, "Ground-glass opacity nodules: histopathology, imaging evaluation, and clinical implications," *Journal of Thoracic Imaging*, vol. 26, no. 2, pp. 106–118, 2011.

[9] T.-W. Huang, L.-F. Lin, C.-M. Hsieh et al., "Positron emission tomography in bronchioloalveolar carcinoma of the lung,"

European Journal of Surgical Oncology, vol. 38, no. 12, pp. 1156–1160, 2012.

[10] N. Suzawa, M. Ito, S. Qiao et al., "Assessment of factors influencing FDG uptake in non-small cell lung cancer on PET/CT by investigating histological differences in expression of glucose transporters 1 and 3 and tumour size," *Lung Cancer*, vol. 72, no. 2, pp. 191–198, 2011.

[11] D. Delbeke, R. E. Coleman, M. J. Guiberteau et al., "Procedure guideline for tumor imaging with ^{18}F-FDG PET/CT 1.0," *Journal of Nuclear Medicine*, vol. 47, no. 5, pp. 885–895, 2006.

[12] T. J. Kim, C. M. Park, J. M. Goo, and K. W. Lee, "Is there a role for FDG PET in the management of lung cancer manifesting predominantly as ground-glass opacity?" *The American Journal of Roentgenology*, vol. 198, no. 1, pp. 83–88, 2012.

[13] J. J. Erasmus and H. A. MacApinlac, "Low-sensitivity FDG-PET studies: less common lung neoplasms," *Seminars in Nuclear Medicine*, vol. 42, no. 4, pp. 255–260, 2012.

[14] S. L. Aquino, E. F. Halpern, L. B. Kuester, and A. J. Fischman, "FDG-PET and CT features of non-small cell lung cancer based on tumor type," *International Journal of Molecular Medicine*, vol. 19, no. 3, pp. 495–499, 2007.

[15] J. S. Sun, K. J. Park, S. S. Sheen et al., "Clinical usefulness of the fluorodeoxyglucose (FDG)-PET maximal standardized uptake value (SUV) in combination with CT features for the differentiation of adenocarcinoma with a bronchioloalveolar carcinoma from other subtypes of non-small cell lung cancers," *Lung Cancer*, vol. 66, no. 2, pp. 205–210, 2009.

[16] A. H. Khandani, K. D. Whitney, S. M. Keller, C. R. Isasi, and M. Donald Blaufox, "Sensitivity of FDG PET, GLUT1 expression and proliferative index in bronchioloalveolar lung cancer," *Nuclear Medicine Communications*, vol. 28, no. 3, pp. 173–177, 2007.

[17] L. E. Heyneman and E. F. Patz Jr., "PET imaging in patients with bronchioloalveolar cell carcinoma," *Lung Cancer*, vol. 38, no. 3, pp. 261–266, 2002.

[18] H. Nomori, K. Watanabe, T. Ohtsuka, T. Naruke, K. Suemasu, and K. Uno, "Evaluation of F-18 fluorodeoxyglucose (FDG) PET scanning for pulmonary nodules less than 3 cm in diameter, with special reference to the CT images," *Lung Cancer*, vol. 45, no. 1, pp. 19–27, 2004.

[19] B. Goudarzi, H. A. Jacene, and R. L. Wahl, "Diagnosis and differentiation of bronchioloalveolar carcinoma from adenocarcinoma with bronchioloalveolar components with metabolic and anatomic characteristics using PET/CT," *Journal of Nuclear Medicine*, vol. 49, no. 10, pp. 1585–1592, 2008.

[20] T. Kushihashi, H. Munechika, K. Ri et al., "Bronchioloalveolar adenoma of the lung: CT-pathologic correlation," *Radiology*, vol. 193, no. 3, pp. 789–793, 1994.

[21] H. Y. Lee, J. Han, K. S. Lee et al., "Lung adenocarcinoma as a solitary pulmonary nodule: prognostic determinants of CT, PET, and histopathologic findings," *Lung Cancer*, vol. 66, no. 3, pp. 379–385, 2009.

[22] S. Liu, H. Cheng, S. Yao et al., "The clinical application value of PET/CT in adenocarcinoma with bronchioloalveolar carcinoma features," *Annals of Nuclear Medicine*, vol. 24, no. 7, pp. 541–547, 2010.

[23] Y. Tsunezuka, Y. Shimizu, N. Tanaka, T. Takayanagi, and M. Kawano, "Positron emission tomography in relation to Noguchi's classification for diagnosis of peripheral non-small-cell lung cancer 2 cm or less in size," *World Journal of Surgery*, vol. 31, no. 2, pp. 314–317, 2007.

[24] S. Iwano, S. Ito, K. Tsuchiya, K. Kato, and S. Naganawa, "What causes false-negative PET findings for solid-type lung cancer?" *Lung Cancer*, vol. 79, no. 2, pp. 132–136, 2013.

Hindawi Publishing Corporation
BioMed Research International
Volume 2015, Article ID 974689, 4 pages
http://dx.doi.org/10.1155/2015/974689

Clinical Study

Prognostic Value of ^{99m}Tc-Pertechnetate Thyroid Scintigraphy in Radioiodine Therapy in a Cohort of Chinese Graves' Disease Patients: A Pilot Clinical Study

Haifeng Hou,[1,2,3,4] Shu Hu,[5] Rong Fan,[5] Wen Sun,[5] Xiaofei Zhang,[6] and Mei Tian[1,2,3,4]

[1] *Department of Nuclear Medicine and PET Center, The Second Affiliated Hospital of Zhejiang University School of Medicine, 88 Jiefang Road, Hangzhou, Zhejiang 310009, China*
[2] *Zhejiang University Medical PET Center, Hangzhou, Zhejiang 310009, China*
[3] *Institutes of Nuclear Medicine and Molecular Imaging, Zhejiang University, Hangzhou, Zhejiang 310009, China*
[4] *Key Laboratory of Medical Molecular Imaging of Zhejiang Province, Hangzhou, Zhejiang 310009, China*
[5] *Department of Nuclear Medicine, Peking University Shenzhen Hospital, Shenzhen, Guangdong 518036, China*
[6] *Department of Clinical Epidemiology and Biostatistics, The Second Affiliated Hospital of Zhejiang University School of Medicine, Hangzhou, Zhejiang 310009, China*

Correspondence should be addressed to Mei Tian; meitian@gmail.com

Received 16 July 2014; Accepted 31 August 2014

Academic Editor: Hong Zhang

Objectives. This study is to assess the prognostic value of ^{99m}Tc-pertechnetate thyroid scintigraphy for predicting the outcomes of fixed low dose of radioiodine therapy (RIT) in a cohort of Chinese Graves' disease (GD) patients. *Materials and Methods*. This is a retrospective study of GD patients who received RIT with a single dose of radioiodine (5 mCi). All the patients received ^{99m}Tc-pertechnetate thyroid scintigraphy prior to RIT. Thyroid mass, ^{99m}Tc-pertechnetate uptake, gender, age at diagnosis, duration of the disease, ophthalmopathy, and serum levels of FT4, FT3, TT4, and TT3 prior to RIT were analyzed as potential interference factors for outcomes of RIT. *Results*. One hundred and eighteen GD patients who completed RIT were followed up for 12 months. The outcomes (euthyroidism, hypothyroidism, and hyperthyroidism) were found to be significantly associated with thyroid mass and ^{99m}Tc-pertechnetate uptake. Patients with thyroid mass ≤ 40.1 g or ^{99m}Tc-pertechnetate uptake ≤ 15.2% had higher treatment success. *Conclusions*. A fixed low dose of 5 mCi radioiodine seems to be practical and effective for the treatment of Chinese GD patients with thyroid mass ≤ 40.1 g and ^{99m}Tc-pertechnetate uptake ≤ 15.2%. This study demonstrates ^{99m}Tc-pertechnetate thyroid scintigraphy is an important prognostic factor for predicting the outcomes of RIT.

1. Introduction

Radioiodine therapy (RIT) is considered to be the effective treatment for Graves' disease (GD); however, the optimal radioiodine dose (administered activity) in the treatment of GD remains unsettled [1]. Although it is generally accepted that cure rates of GD may increase with the radioiodine dose, higher dose of radioiodine might cause unnecessary radiation exposure. Elevated risk of cancers (especially cancer of the stomach, kidney, and breast) was found in association with the cumulative increase of radioiodine dose [2].

In addition to controversial results on the optimal dose of radioiodine administered, consensus on the predictive factors for RIT is still missing among the radionuclide therapy communities. Previously, age, gender, clinical symptoms, thyroid mass, serum TSH receptor antibodies (TRAb) levels, thyroid uptake, and history of thyrostatic drugs use have been reported to be correlated with the success rates of RIT [1]. However, until now, the response to RIT in patients with GD remains unpredictable, and factors postulated to predict the outcomes have not been proved clinically useful or widely adopted in clinical practice.

In the present study, we used a fixed comparatively low dose radioiodine (5 mCi) and reported the value of ^{99m}Tc-pertechnetate thyroid scintigraphy for predicting the outcomes of RIT in a cohort of Chinese GD patients.

2. Patients and Methods

2.1. Patients. One hundred and twenty-eight GD patients treated with a fixed dose of radioiodine (5 mCi) in the Nuclear Medicine Clinic were retrospectively evaluated from January, 2011, to June, 2012. All patients came from iodine-sufficient areas in the East China. Among all the patients, 80 were initially treated with methimazole (MMI) or propylthiouracil (PTU) for at least 12 months but still had hyperthyroidism after withdrawal or reducing the medication dosage. Before being referred to RIT, the antithyroid drugs (ATDs) treated GD patients remained medication free for at least 1 month. The other 48 patients had not taken ATDs because of self-selection or significant side effect (agranulocytosis, posttherapy liver failure or allergy). All the patients received RIT with a fixed dose of 5 mCi radioiodine at the Nuclear Medicine Clinic and signed the written informed consents. This study has been approved by the local ethics committee.

Patients were followed up for at least 12 months after RIT. RIT was considered successful if euthyroidism or hypothyroidism was achieved, which was diagnosed on the basis of thyroid function tests. RIT was considered as a failure, when the patients remained hyperthyroid, had to use ATDs, or received a second dose of RIT before the end of the followup. Ten patients were excluded from the data analysis due to the failure of follow-up.

The gender, age at diagnosis, duration of the disease, thyroid mass, ^{99m}Tc-pertechnetate uptake, ophthalmopathy, and serum levels of FT4, FT3, TT4, and TT3 prior to RIT were studied as potential interference factors for RIT.

2.2. Thyroid Scintigraphy. All GD patients were instructed to follow a low iodine diet and avoid iodine-rich products for 15 days prior to thyroid scintigraphy. Thyroid scan and uptake were performed at 20 min after intravenous injection of 185 MBq (5 mCi) of ^{99m}Tc-pertechnetate (Atom High Tech Co., Ltd., Shanghai, China). A SPECT scintillation camera equipped with a low-energy, high-resolution, and parallel-hole collimator (E.CAM, Siemens Medical Solutions) was used for thyroid scintigraphic scan. The method for the calculation of thyroid mass and ^{99m}Tc-pertechnetate uptake was previously described by Ramos et al. [3].

2.3. Statistical Analysis. All statistical analyses were carried out using SPSS version 16.0 for Windows (SPSS Inc., Chicago, IL, USA). Data were expressed as mean ± standard deviation (SD). The chi-squared test and Mann-Whitney U test were performed to compare variables in the two groups (hypothyroid and euthyroid versus hyperthyroid patients). Logistic regression analysis was used to identify the associated factors with RIT success (euthyroidism and hypothyroidism). Stepwise method was used for variables selection. The receiver operator characteristic (ROC) curve was used to identify the optimal threshold for thyroid mass and ^{99m}Tc-pertechnetate uptake to discriminate RIT success or failure (persistence of hyperthyroidism) of RIT. The significance level was set at 5%.

Table 1: Pre-RIT laboratory and clinical characteristics of patients.

Variables	Values
Gender	
Male	41 (34.75%)
Female	77 (65.25%)
Age (years)	40.35 ± 12.69 (17–77)
Disease duration (years)	4.20 ± 4.80 (0.08–30)
Ophthalmopathy	
Yes	73 (61.86%)
No	45 (38.14%)
Hormone levels of pre-RIT	
FT4 (pmol/L)	55.63 ± 27.19 (22.71–140.08)
FT3 (pmol/L)	19.99 ± 7.36 (7.46–44.39)
TT4 (nmol/L)	260.62 ± 80.07 (16.7–387.31)
TT3 (nmol/L)	7.08 ± 2.99 (1.01–12.32)
Thyroid mass of pre-RIT (g)	41.13 ± 8.85 (22.68–61.60)
Thyroid ^{99m}Tc-pertechnetate uptake of pre-RIT (%)	15.23 ± 7.59 (2.80–36.80)
Outcome of post-RIT	
Hypothyroidism	35 (29.66%)
Euthyroidism	49 (41.53%)
Hyperthyroidism	34 (28.81%)

All values are expressed as mean ± SD for continuous variables and as the number of patients (percentage) for categorical variables.

3. Results

3.1. Patients and Outcomes after RIT. Baseline, pre-RIT patient laboratory and clinical characteristics are listed in Table 1. A total of 118 patients treated by RIT were included in this study, of which 49 patients (41.53%) were euthyroid, 35 patients (29.66%) were hypothyroid, and 34 patients (28.81%) remained hyperthyroid. Patients were followed up after RIT for at least 12 months.

3.2. Comparative Analysis between the Variables and the Outcomes after RIT. Thyroid mass ($P < 0.001$), ^{99m}Tc-pertechnetate uptake ($P < 0.001$), and TT3 ($P = 0.048$) prior to RIT were found significantly associated with the outcomes of RIT by using the Mann-Whitney U test (Table 2). No statistical associations were found between post-RIT thyroid function and the following parameters: age at diagnosis, disease duration, FT4, FT3, and TT4. And no statistically significant association was found between post-RIT thyroid function (euthyroidism and hypothyroidism versus hyperthyroidism) and gender ($P = 0.937$) or ophthalmopathy ($P = 0.395$) by using the chi-squared test.

Table 2: Comparative analysis on pre-RIT variables in different groups.

Variables	Patients group with different outcome of RIT		P
	Hypothyroidism and euthyroidism ($n = 84$)	Hyperthyroidism ($n = 34$)	
Age (years)	39.83 ± 12.88	41.62 ± 12.32	0.377
Disease duration (years)	4.37 ± 5.27	3.77 ± 3.40	0.631
Hormone levels			
FT4 (pmol/L)	54.20 ± 26.26	59.17 ± 29.47	0.463
FT3 (pmol/L)	19.44 ± 7.43	21.35 ± 7.09	0.152
TT4 (nmol/L)	255.46 ± 77.06	273.37 ± 86.95	0.470
TT3 (nmol/L)	6.80 ± 2.92	7.75 ± 3.09	0.048
Thyroid mass (g)	38.28 ± 7.34	48.18 ± 8.41	<0.001
^{99m}Tc-pertechnetate uptake (%)	12.83 ± 6.05	21.19 ± 7.80	<0.001

3.3. Thyroid Mass. We analyzed the estimated thyroid mass by using the ROC analysis to differentiate the patients who achieved treatment success (euthyroidism or hypothyroidism) from those who remained hyperthyroid (treatment failure) and found that patients of treatment success had a thyroid mass threshold of 40.1 g, with sensitivity of 85.3% and specificity of 65.5% (Figure 1(a)).

3.4. Thyroid ^{99m}Tc-Pertechnetate Uptake. ROC analysis was used to analyze the ^{99m}Tc-pertechnetate uptake obtained prior to radioiodine therapy to differentiate the group of patients who achieved success with treatment (euthyroidism and hypothyroidism) from those who remained hyperthyroid (treatment failure). We found treatment success patients had an uptake threshold of 15.2%, with sensitivity of 82.4% and specificity of 69.0% (Figure 1(b)).

3.5. Logistic Regression Analysis. Univariate logistic regression analysis showed statistical differences when comparing RIT success (euthyroidism and hypothyroidism) with failure (hyperthyroidism) to thyroid mass ($P < 0.001$) and ^{99m}Tc-pertechnetate uptake ($P < 0.001$). There was no influence of gender ($P = 0.939$), ophthalmopathy ($P = 0.395$), age at diagnosis ($P = 0.487$), disease duration ($P = 0.535$), FT4 ($P = 0.366$), FT3 ($P = 0.199$), TT4 ($P = 0.269$), and TT3 ($P = 0.118$).

The multivariate logistic regression analysis demonstrated that the patients with thyroid mass ≤ 40.1 g showed a 6.35-fold higher probability of RIT success (odds ratio (OR) = 6.35, $P = 0.002$, 95% CI = 1.99–20.99) and patients with ^{99m}Tc-pertechnetate uptake ≤ 15.2% presented a 4.77-fold higher probability of success (OR = 4.77, $P = 0.007$, 95% CI = 1.53–14.91). Kendall's correlation coefficient between thyroid mass and ^{99m}Tc-pertechnetate uptake was 0.426 ($P < 0.001$).

4. Discussion

In the present study, GD patients received RIT with a single fixed dose of radioiodine (5 mCi). After RIT, 71.19% of the GD patients succeed (euthyroidism or hypothyroidism), but 25.51% of the patients still remained hyperthyroid. Moreover, patients with thyroid mass ≤ 40.1 g (odds ratio (OR) = 6.35) or ^{99m}Tc-pertechnetate uptake ≤ 15.2% (OR = 4.77) had higher treatment success. However, we did not find a satisfied correlation coefficient between thyroid mass and ^{99m}Tc-pertechnetate uptake ($r = 0.426$), which indicated a relative independence between the two predictive variables for thyroid function after RIT.

Although RIT for the treatment of GD has been used since the 1940s, there remains controversy about the optimal dosage of radioiodine. Theoretically, the RIT success rate increases with radioiodine dose, but incidence of hypothyroidism might also elevate, which might need a life-long hormone-replacement medication causing inconvenience to daily life. Often fixed activities of 370 or 555 MBq (10 or 15 mCi) are used, which will result in hypothyroidism in 69% to 90% of patients [4–7]. Fear of hypothyroidism also is the main reason for rejecting RIT as the first-line treatment for many GD patients in China [8]. In the present study, a fixed comparatively low dose radioiodine (5 mCi) was used with only 29.66% of GD patients becoming hypothyroid after RIT, but the overall RIT success (euthyroidism or hypothyroidism) is similar to the other previous studies [6, 7, 9, 10].

Thyroid scintigraphy is a conventional nuclear medicine procedure which provides valuable information regarding both thyroid anatomy and physiology and plays an integral role in the diagnosis and management of GD [11]. Thyroid scintigraphy using ^{99m}Tc-pertechnetate has been proven to be more advantageous than with radioiodine, since the images have better quality, the procedure is faster, and the patient is submitted to a lower radiation dose [3]. As in just one visit, the patient receives an intravenous injection of ^{99m}Tc-pertechnetate, the thyroid mass and ^{99m}Tc-pertechnetate uptake can be measured after 20 min, and the radioiodide can be administered immediately afterwards. In the present study, we found that thyroid mass and ^{99m}Tc-pertechnetate can be used to predict the outcomes of RIT. The results of this study will be very helpful in optimizing the therapeutical dose of radioiodine for GD patient, receiving a satisfactory rate of remission but providing the lowest possible radiation to the rest of the body.

In conclusion, in the present study, we found a fixed dose of 5 mCi radioiodine seems to be practical and effective,

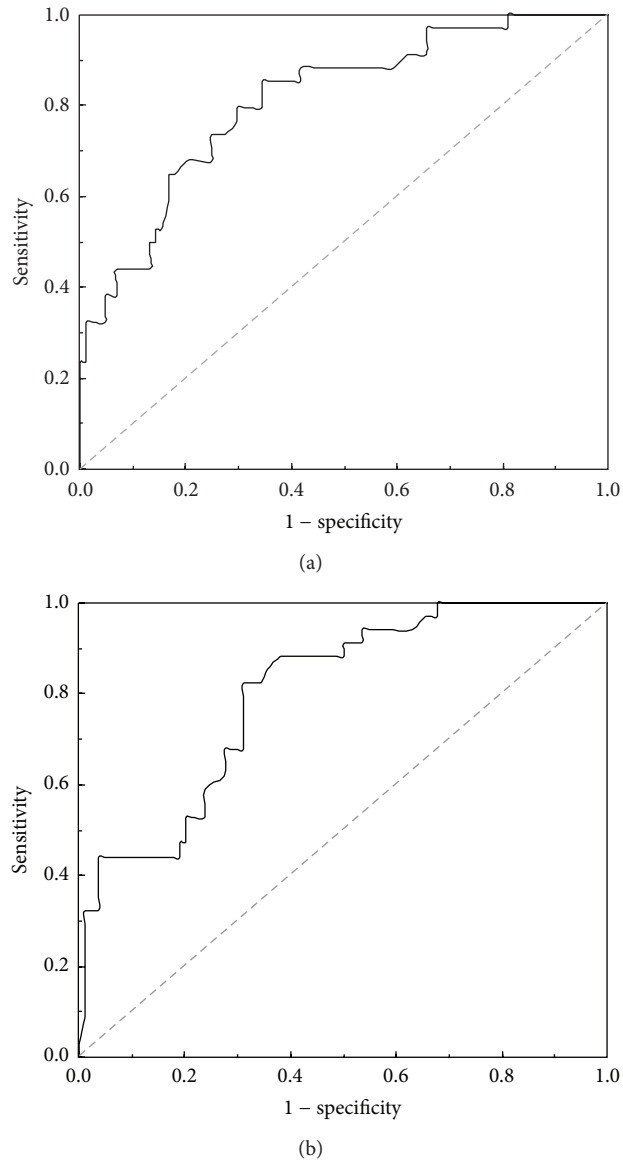

Figure 1: ROC curve used to identify cut-off values related to RIT success in patients with GD. (a) Thyroid mass. The area under the curve (AUC) was 0.811. The cut-off point of thyroid mass for prediction was estimated at 40.1 g, with 85.3% sensitivity and 65.5% specificity. (b) ^{99m}Tc-pertechnetate uptake. AUC was 0.801. The cut-off point was estimated at 15.2%, with 82.4% sensitivity and 69.0% specificity.

especially for the GD patients with thyroid mass ≤ 40.1 g and ^{99m}Tc-pertechnetate uptake ≤ 15.2%. For GD patients larger goiter (> 40.1 g) and markedly increased ^{99m}Tc-pertechnetate uptake (> 15.2%) prior to RIT can be considered as important predictive factors of RIT failure. These patients should be better candidates for receiving higher radioiodine doses or to be referred for thyroidectomy. Thus, ^{99m}Tc-pertechnetate thyroid scintigraphy is an important prognostic factor for predicting the outcomes of RIT and it might also be helpful in optimizing the radioiodine dose of RIT.

Conflict of Interests

The authors declare that there is no conflict of interests regarding the publication of this paper.

References

[1] D. S. Ross, "Radioiodine therapy for hyperthyroidism," *The New England Journal of Medicine*, vol. 364, no. 6, pp. 542–550, 2011.

[2] S. Metso, A. Auvinen, H. Huhtala, J. Salmi, H. Oksala, and P. Jaatinen, "Increased cancer incidence after radioiodine treatment for hyperthyroidism," *Cancer*, vol. 109, no. 10, pp. 1972–1979, 2007.

[3] C. D. Ramos, D. E. Zantut Wittmann, E. C. Etchebehere, M. A. Tambascia, C. A. Moreira Silva, and E. E. Camargo, "Thyroid uptake and scintigraphy using ^{99m}Tc pertechnetate: standardization in normal individuals," *Sao Paulo Medical Journal*, vol. 120, no. 2, pp. 45–48, 2002.

[4] A. Collier, S. Ghosh, M. Hair, I. Malik, and J. McGarvie, "Comparison of two fixed activities of radioiodine therapy (370 vs. 555 MBq) in patients with Graves' disease," *Hormones*, vol. 8, no. 4, pp. 273–278, 2009.

[5] H. Peters, C. Fischer, U. Bogner, C. Reiners, and H. Schleusener, "Radioiodine therapy of Graves' hyperthyroidism: standard vs. calculated 131iodine activity. Results from a prospective, randomized, multicentre study," *European Journal of Clinical Investigation*, vol. 25, no. 3, pp. 186–193, 1995.

[6] A. Moura-Neto, C. Mosci, A. O. Santos et al., "Predictive factors of failure in a fixed 15 mCi 131I-iodide therapy for Graves' disease," *Clinical Nuclear Medicine*, vol. 37, no. 6, pp. 550–554, 2012.

[7] D. E. Zantut-Wittmann, C. D. Ramos, A. O. Santos et al., "High pre-therapy [99mTc]pertechnetate thyroid uptake, thyroid size and thyrostatic drugs: Predictive factors of failure in [131I]iodide therapy in Graves' disease," *Nuclear Medicine Communications*, vol. 26, no. 11, pp. 957–963, 2005.

[8] Chinese-Society-of-Nuclear-Medicine, "Guideline of 131I-iodide treatment for graves' disease," *Chinese Journal of Nuclear Medicine and Molecular Imaging*, vol. 33, no. 2, pp. 83–95, 2013.

[9] E. K. Alexander and P. R. Larsen, "High dose 131I therapy for the treatment of hyperthyroidism caused by Graves' disease," *Journal of Clinical Endocrinology and Metabolism*, vol. 87, no. 3, pp. 1073–1077, 2002.

[10] J. A. F. de Jong, H. M. Verkooijen, G. D. Valk, P. M. J. Zelissen, and B. de Keizer, "High failure rates after 131I therapy in graves hyperthyroidism patients with large thyroid volumes, high iodine uptake, and high iodine turnover," *Clinical Nuclear Medicine*, vol. 38, no. 6, pp. 401–406, 2013.

[11] O. E. Okosieme, D. Chan, S. A. Price, J. H. Lazarus, and L. D. K. E. Premawardhana, "The utility of radioiodine uptake and thyroid scintigraphy in the diagnosis and management of hyperthyroidism," *Clinical Endocrinology*, vol. 72, no. 1, pp. 122–127, 2010.

Hindawi Publishing Corporation
BioMed Research International
Volume 2015, Article ID 489021, 5 pages
http://dx.doi.org/10.1155/2015/489021

Research Article

The Diagnostic Value of ^{18}F-FDG PET/CT in Association with Serum Tumor Marker Assays in Breast Cancer Recurrence and Metastasis

Ying Dong,[1] Haifeng Hou,[2,3,4,5] Chunyan Wang,[6] Jing Li,[2,3,4,5] Qiong Yao,[2,3,4,5] Said Amer,[7] and Mei Tian[2,3,4,5]

[1]*Department of Oncology, The Second Affiliated Hospital of Zhejiang University School of Medicine, Hangzhou 310009, China*
[2]*Department of Nuclear Medicine, The Second Affiliated Hospital of Zhejiang University School of Medicine, Hangzhou 310009, China*
[3]*Zhejiang University Medical PET Center, Hangzhou 310009, China*
[4]*Institute of Nuclear Medicine and Molecular Imaging, Zhejiang University, Hangzhou 310009, China*
[5]*Key Laboratory of Medical Molecular Imaging of Zhejiang Province, Hangzhou 310009, China*
[6]*Beijing 307 Hospital, Beijing 100071, China*
[7]*Department of Zoology, Faculty of Science, Kafr El Sheikh University, Kafr El Sheikh 33516, Egypt*

Correspondence should be addressed to Haifeng Hou; houhf@pku.edu.cn and Mei Tian; meitian@gmail.com

Received 20 August 2014; Accepted 22 September 2014

Academic Editor: Hong Zhang

Background. After initial treatment of breast cancer (BC), monitoring locoregional recurrence and distant metastases is a great clinical challenge. *Objective*. To evaluate the efficacy of PET/CT in association with serum tumor makers in BC follow-up. *Methods*. Twenty-six women with a history of modified radical mastectomy were evaluated by ^{18}F-FDG PET/CT. The results of PET/CT were compared with those of conventional imaging techniques (CITs) (including mammography, chest radiography, CT, MRI, ultrasound, and bone scintigraphy). Serum tumor markers of CEA, CA 125, and CA 15-3 in the BC patients were also analyzed in association with the results of PET/CT. *Results*. Compared with CITs, PET/CT was more sensitive to detect the malignant foci and had better patient-based sensitivity and specificity. The mean CA 15-3 serum level was significantly higher in the confirmed positive patients of PET/CT results than in the confirmed negative ones, while there were no significant differences in the serum levels of CEA and CA 125 of both groups. *Conclusion*. PET/CT is a highly efficient tool for BC follow-up compared with CITs. The high serum levels of CA 15-3 in confirmed positive PET/CT patients indicated the clinical value of CA 15-3 in BC follow-up.

1. Introduction

Breast cancer (BC) is recognized as the most leading cause of death in women worldwide, with progressively increased incidence over the last few decades [1]. Approximately 30% of patients diagnosed with BC are at the risk of developing locoregional recurrence or metastasis to distant organs [2].

After initial treatment of BC, follow-up based on clinical examination and conventional imaging techniques (CITs) is common practice. However, localization of metastases or recurrences remains a serious challenge, requiring an extensive diagnostic workup. Mammography is of high value in the follow-up of BC and is recommended to diagnose or exclude local recurrence [3, 4], but it encounters obvious challenge to detect the remote metastases. The use and efficacy of other modalities such as chest radiography, computed tomography (CT), magnetic resonance imaging (MRI), ultrasound, or bone scintigraphy (BS) remain controversial [5–8].

Previous studies have suggested that fluorine-18 fluorodeoxyglucose-positron emission tomography (FDG-PET) might improve the sensitivity of detection recurrence of BC compared to CITs [9, 10]. Moreover, FDG-positron emission tomography/computed tomography (PET/CT) generates invaluable data on the functional activity of the

recurrence sites and a general picture based on whole-body acquisition, with a high signal-to-noise ratio [11].

Blood levels of tumor markers (TMs) seem to be correlated with the tumor mass and considered as useful tool in both diagnosis and follow-up of certain cancers. In recent decades, TMs such as carcinoembryonic antigen (CEA) and cancer-associated antigen 15-3 (CA 15-3) have been used as reliable evidence of distant metastasis of BC [12, 13]. Cancer-associated antigen 125 (CA 125) is commonly used in ovarian cancer [14] and showed elevated levels in ~84% of metastatic breast patients [15, 16]. And the PET/CT has also been recognized as valuable modality for the follow-up of BC patients with elevated levels of TMs [11, 17].

The aim of this study was to evaluate the efficacy of using ^{18}F-FDG PET/CT along with serum TMs (CEA, CA 125, and CA 15-3) in monitoring the recurrence and metastasis of BC in order to optimize their utility in clinical practice.

2. Patients and Methods

2.1. Patients. The retrospective study was done on a total of 26 female patients (aged 33–84 years; mean ± SD, 54.9 ± 12.1 years) with a history of modified radical mastectomy (MRM), at the Second Affiliated Hospital of Zhejiang University School of Medicine, Hangzhou, China. The patients were diagnosed as suspicion of recurrence and referred to for whole-body ^{18}F-FDG PET/CT scanning at the PET Center from July 2013 to January 2014. The median time interval from initial MRM to ^{18}F-FDG PET/CT was 6.3 (1–34 years). The current study was performed under informed written consent of all patients who contributed in the study. Particular attention was paid to maintain good wellbeing of all patients.

2.2. ^{18}F-FDG PET/CT Scanning and Image Analysis. ^{18}F-FDG was produced by the cyclotron (Sumitomo CYPRIS HM-12S) and PET/CT was performed using the PET/CT system (Siemens Biograph mCT). All patients were instructed to fast for at least 6 hours before imaging. At the time of the tracer injection, patients should have had a blood glucose level of less than 140 mg/dL. Before and after injection, patients were kept lying comfortably in a quiet, dimly lit room. Image acquisition was started 1 hour ± 10 minutes after intravenous administration of FDG (7.4 MBq/kg body weight).

The PET/CT images were assessed by 2 experienced physicians in consensus. In the case of divergent evaluation, a third nuclear medicine specialist served as a referee. The PET images were inspected visually for regions of focally increased glucose uptake and quantitatively by detecting the maximum standardized uptake value. In equivocal findings, a standardized uptake value (SUV) of greater than 2 was considered as malignant, except the liver, where SUV higher than 2 in the difference of the focus and the surrounding normal tissue was considered as malignant [17]. Focally increased uptake located in the lung was considered as malignant in all cases. To be classified as confirmed positive, a recurrence confirmation was required, based on CITs, pathology, or clinical follow-up. To be classified as negative or false positive, a minimum of 6 months of follow-up was required, with negative CITs and/or repeated PET/CT imaging and clinical examination.

2.3. CITs Imaging. CT, chest radiography, and ultrasound were performed for all patients, mammography in 12 patients, MRI in 4 patients, and BS in 12 patients. All results of CITs in the time period of 3 months before and after PET/CT were collected for further analysis.

2.4. Tumor Markers. The protocols used to measure CEA, CA 125, and CA 15-3 concentrations were standardized for all patients. The serum CEA, CA 125, and CA 15-3 concentrations were determined by the electrochemiluminescence method. The serum CEA, CA 125, and CA 15-3 of 5.0 ng/mL, 35 U/mL and 30 U/mL, respectively, were adopted as the upper limits of normal. In combined use of the three TMs, we classified patients into "TM positive" if at least one of these markers exceeded its cut-off value.

2.5. Statistical Analysis. Generated data were analyzed statistically using SPSS software, version 16.0 (SPSS Inc., Chicago, IL). Results were expressed as the mean ± SD. McNemar test was used to analyze findings of PET/CT and CITs. The serum levels of CEA, CA 125, and CA 15-3 in the BC patients with confirmed positive PET/CT results were compared to the confirmed negative ones using the Mann-Whitney test. Values of $P < 0.05$ were considered significant.

3. Results

In the present study, CITs detected a total of 47 suspicious lesions in 18 out of 26 patients, with 28 lesions being proved to be malignant. The CITs revealed 2 local recurrences in 2 patients and detected brain metastases in one case. Four cases were identified to have 7 suspicious lung metastases, and 6 lesions were proved to be malignant in 3 patients by follow-up. In addition, 3 lymphatic metastases were detected in one case but only one lymph node metastasis located in the axilla was proved after biopsy. A total of 34 suspicious bone metastases were detected in 12 women and 18 of these lesions were proved to be malignant by clinical follow-up and rechecked by CITs. Of these, 6 were located in the ribs, 4 in the pelvis, 5 in the spine, 2 in the extremities, and 1 in the scapula.

PET/CT detected a total of 135 suspicious malignant foci in 21 out of 26 patients, with 122 lesions being proved to be malignant in follow-up or recheck by CITs. Of these, 4 were revealed to be local recurrences in 2 cases. A total of 17 foci were lymphatic metastases in 5 cases, with 3 being detected in the axilla, 13 in the mediastinum, and one in inguina. The PET/CT revealed 91 bone metastases in 9 patients, of which 24 were in the ribs, 27 in the pelvis, 26 in the spine, 2 in the scapula, and 12 in the extremities. Also, one metastasis was detected in the liver of one patient, one metastasis in brain of another patient, and 8 pulmonary metastases in 4 patients.

Collected results (Table 1) indicate that PET/CT detected significantly ($P < 0.01$) more malignant foci, at all anatomical niches but the brain, compared to CITs. The PET/CT was

Table 1: Suspected and confirmed malignant foci of CITs and PET/CT.

Locations	Malignant lesions detected by CITs		Malignant lesions detected by PET/CT		Total confirmed malignancy*
	Suspected	Confirmed	Suspected	Confirmed	
Local recurrence	2	2	5	4	4
Lung	7	6	9	8	8
Liver	0	0	1	1	1
Brain	1	1	1	1	1
Lymph nodes	3	1	22	17	18
Mediastinal	0	0	17	13	14
Axilla	3	1	4	3	3
Others	0	0	1	1	1
Bone	34	18	97	91	101
Ribs	8	5	27	24	28
Pelvis	5	5	27	27	30
Spine	18	5	29	26	29
Extremities	2	2	12	12	12
Scapula	1	1	2	2	2

*Confirmation of positive cases was done based on recurrence of cancer as indicated by CITs, pathology, and/or clinical follow-up. Confirmation of negative cases was done based on absence of abnormality as indicated by CITs, repeated PET/CT imaging as well as clinical follow-up for a period of 6 months.

superior in detecting recurrence (4 versus 2) as well as metastases in lymph node (17 versus 1), bone (91 versus 18), and lung (8 versus 6). A liver metastasis was only detectable by PET/CT.

The patient-based sensitivity and specificity of PET/CT were 95.0% and 71.43% compared to 78.95% and 57.14% for CITs. The negative and positive predictive values were 100.0% and 90.48% for PET/CT versus 50.0% and 83.33% for CITs, respectively.

CEA, CA 125, and CA 15-3 levels were determined in the sera of 20 out of 26 patients. A total of 6 BC patients were classified as TM positive. Serum levels of CEA in 2 patients, CA 125 in 1 patients, and CA 15-3 in 2 patients were above normal values. Only one patient had higher serum CEA, CA 125, and CA 15-3 concentrations than normal values simultaneously. According to the PET/CT results of these 20 patients, 13 were confirmed positive and 7 were confirmed negative. There was no significant difference in CEA serum levels of confirmed positive compared to confirmed negative PET/CT patients (7.90 ± 20.34 versus 2.57 ± 2.86 ng/mL; $P = 0.35$), as well as CA 125 (15.77 ± 26.69 versus 7.41 ± 2.26 U/mL; $P = 0.96$). But the mean CA 15-3 serum level was significantly higher in the positive compared to negative ones (18.42 ± 12.13 versus 11.8 ± 9.64 U/mL; $P = 0.04$).

4. Discussion

Early detection and adequate localization of recurrence are essential for guiding optimal therapy for BC patients [18]. Recent studies have shown the relevance of ^{18}F-FDG PET/CT in detecting distant metastasis in patients with clinical suspicion of recurrence [8–11] and in patients with confirmed locoregional recurrence [19]. Furthermore, PET/CT has been reported to have a major impact on managing BC patients with elevated TMs levels [11, 20], subsequently, leading to change of management protocols of 36%–54% of patients. The combined anatomical-molecular PET/CT imaging technique has been shown to improve significantly the specificity of FDG-PET and CT [21, 22].

Results of the present study confirmed that ^{18}F-FDG PET/CT was an accurate technique for the appropriate detection of BC metastasis and/or recurrence compared to CITs. Compared with CITs, PET/CT detected more malignant foci overall ($P < 0.01$) (Figure 1). In addition, PET/CT was superior on CITs in terms of patient-based sensitivity, specificity, positive predictive value, and absolute negative predictive value in detecting metastases and/or recurrence. There occurred only 11 false-positive findings, 1 in the lung and 4 in the lymph nodes because of inflammatory disorder. The other 3 false-positive foci were in ribs for old fractures.

For many malignancies, the potential uses of serum TMs include aiding early diagnosis, determining prognosis, prospectively predicting response, or resistance to specific therapies, surveillance after primary surgery, and monitoring therapy in patients with advanced disease. However, in BC, the role of serum TMs is less well established [12, 23]. Recently, in the study of Yerushalmi et al. [16], TM elevation of CA 15-3, CEA, and/or CA 125 was documented in the majority of patients with metastatic BC, with CA 15-3 occurring most commonly. Zissimopoulos et al. [8] reported CA 15-3 showed a sensitivity of 67%, specificity of 74%, positive predictive value of 63%, and negative predictive value of 77% in revealing bone metastasis. Further, in the asymptomatic BC patients with elevated TMs (CA 15-3 or CEA), ^{18}FDG-PET/CT imaging is an efficient technique to detect BC recurrence [11]. In our present study, 30.77% (4/13) patients of confirmed positive PET/CT results showed rising

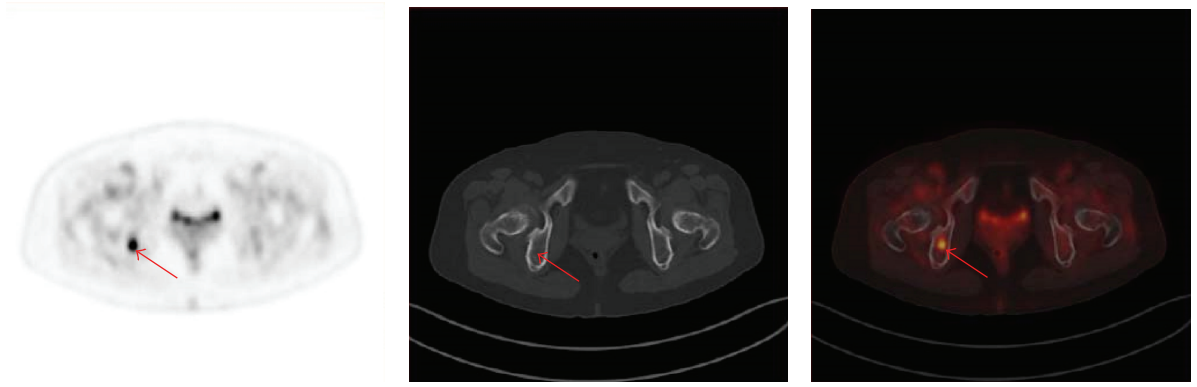

(a) (b) (c)

Figure 1: The PET image (c) demonstrates focal increased FDG uptake in right body of ischium (red arrow), which is considered as malignant. In the CT image (b), no abnormality is seen. The PET/CT (a) is considered as suspicious malignant because of the PET findings. Bone metastatic involvement of the right body of ischium was proved by follow-up.

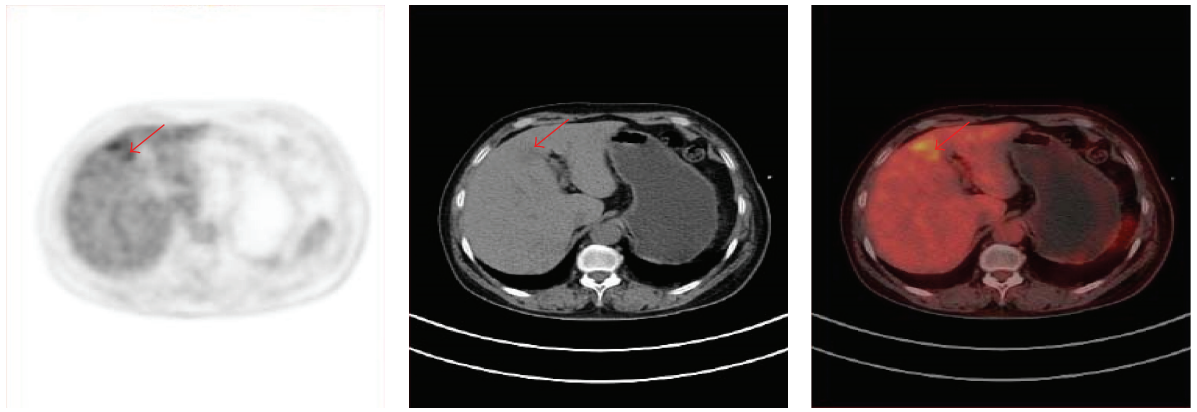

(a) (b) (c)

Figure 2: PET, CT and PET/CT of a 59 year old patient, referred for restaging because of elevated CA 15-3 level 12 years after surgically resected breast carcinoma of the left breast. The PET demonstrates a focal increased FDG uptake in the liver (red arrow), which is considered as malignant. The CT shows a slightly low dense area in the left lobe of liver. The PET/CT is considered as suspicious because of the PET findings. Metastatic involvement of the liver was proved by follow-up.

TMs (CEA, CA 125, or CA 15-3). There were also 2 patients with confirmed negative PET/CT results to show increased CEA or CA 15-3. Although no significant difference in the CEA and CA 125 serum level between confirmed positive and confirmed negative PET/CT groups was found, CA 15-3 serum level was significantly higher in the confirmed positive ones (Figure 2). This finding was in consistence with previous study [11], which reported highly increased CA 15-3 serum level was more frequently observed in cases of multiple lesions.

The number of patients involved in the present study is relatively small, which might limit the ability to generalize the generated results. Further study on a larger population is required before drawing a more definitive conclusion. For the calculation of sensitivity and specificity, a patient-based approach was used instead of lesion-based. In general, treatment decisions are generally made based on the presence of recurrent or metastatic disease, rather than on the number of lesions involved. Consequently, it is clinically more relevant to consider the patient-based data rather than the lesion-based analyses.

5. Conclusion

The findings of the present study indicate that PET/CT might be advantageous in the follow-up of patients with BC compared to CITs, providing a sensitive tool for detecting metastases and locally recurrent disease. The higher CA 15-3 serum level found in the confirmed positive PET/CT patients than the confirmed negative ones indicated the increased likelihood of BC recurrence and metastasis and the clinical value of CA 15-3 in BC follow-up.

Conflict of Interests

The authors have no conflict of interests to declare for this paper.

Authors' Contribution

Ying Dong, Haifeng Hou, and Chunyan Wang contributed equally to this paper.

Acknowledgments

This work is partly sponsored by Grants from the National Key Basic Research Program of China (2014CB744505), the Health Bureau of Zhejiang Province (2013RCA021), the National Science Foundation of China (81101835), the Startup Fund of Zhejiang Provincial Key Discipline Construction of Medical Imaging and Nuclear Medicine (188310+710211/058/001), the Scientific Research Foundation for Doctors of the Second Affiliated Hospital of Zhejiang University School of Medicine (Y560252013), and the Science Foundation of Zhejiang Province (Y2110299). Cordial thanks are for all patients who contributed in the present study.

References

[1] A. Jemal, R. Siegel, E. Ward, Y. Hao, J. Xu, and M. J. Thun, "Cancer statistics, 2009," *CA: Cancer Journal for Clinicians*, vol. 59, no. 4, pp. 225–249, 2009.

[2] J. A. van Dongen, A. C. Voogd, I. S. Fentiman et al., "Long-term results of a randomized trial comparing breast-conserving therapy with mastectomy: European organization for research and treatment of cancer 10801 trial," *Journal of the National Cancer Institute*, vol. 92, no. 14, pp. 1143–1150, 2000.

[3] C. S. Giess, D. M. Keating, M. P. Osborne, and R. Rosenblatt, "Local tumor recurrence following breast-conservation therapy: correlation of histopathologic findings with detection method and mammographic findings," *Radiology*, vol. 212, no. 3, pp. 829–835, 1999.

[4] T. J. Smith, N. E. Davidson, D. V. Schapira et al., "American Society of Clinical Oncology 1998 update of recommended breast cancer surveillance guidelines," *Journal of Clinical Oncology*, vol. 17, no. 3, pp. 1080–1082, 1999.

[5] E. Joseph, M. Hyacinthe, G. H. Lyman et al., "Evaluation of an intensive strategy for follow-up and surveillance of primary breast cancer," *Annals of Surgical Oncology*, vol. 5, no. 6, pp. 522–528, 1998.

[6] M. P. Rojas, E. Telaro, A. Russo et al., "Follow-up strategies for women treated for early breast cancer," *Cochrane Database of Systematic Reviews*, vol. 25, no. 1, 2005.

[7] D. Pavic, M. A. Koomen, C. M. Kuzmiak, Y. H. Lee, and E. D. Pisano, "The role of magnetic resonance imaging in diagnosis and management of breast cancer," *Technology in Cancer Research and Treatment*, vol. 3, no. 6, pp. 527–541, 2004.

[8] A. Zissimopoulos, D. Matthaios, E. Matthaiou, E. Mantadakis, and I. Karaitianos, "Association between bone scintigraphy and serum levels of tumor markers in the detection of bone disease in breast cancer patients," *Journal of BUON*, vol. 12, no. 4, pp. 505–511, 2007.

[9] L. Pan, Y. Han, X. Sun, J. Liu, and H. Gang, "FDG-PET and other imaging modalities for the evaluation of breast cancer recurrence and metastases: a meta-analysis," *Journal of Cancer Research and Clinical Oncology*, vol. 136, no. 7, pp. 1007–1022, 2010.

[10] C. R. Isasi, R. M. Moadel, and M. D. Blaufox, "A meta-analysis of FDG-PET for the evaluation of breast cancer recurrence and metastases," *Breast Cancer Research and Treatment*, vol. 90, no. 2, pp. 105–112, 2005.

[11] L. Champion, E. Brain, A.-L. Giraudet et al., "Breast cancer recurrence diagnosis suspected on tumor marker rising," *Cancer*, vol. 117, no. 8, pp. 1621–1629, 2011.

[12] M. Yildiz, B. Oral, M. Bozkurt, and A. Cobaner, "Relationship between bone scintigraphy and tumor markers in patients with breast cancer," *Annals of Nuclear Medicine*, vol. 18, no. 6, pp. 501–505, 2004.

[13] R. Kokko, K. Holli, and M. Hakama, "Ca 15-3 in the follow-up of localised breast cancer: a prospective study," *European Journal of Cancer*, vol. 38, no. 9, pp. 1189–1193, 2002.

[14] T. Meyer and G. J. S. Rustin, "Role of tumour markers in monitoring epithelial ovarian cancer," *British Journal of Cancer*, vol. 82, no. 9, pp. 1535–1538, 2000.

[15] A. Berruti, M. Tampellini, M. Torta, T. Buniva, G. Gorzegno, and L. Dogliotti, "Prognostic value in predicting overall survival of two mucinous markers: CA 15-3 and CA 125 in breast cancer patients at first relapse of disease," *European Journal of Cancer Part A: General Topics*, vol. 30, no. 14, pp. 2082–2084, 1994.

[16] R. Yerushalmi, S. Tyldesley, H. Kennecke et al., "Tumor markers in metastatic breast cancer subtypes: frequency of elevation and correlation with outcome," *Annals of Oncology*, vol. 23, no. 2, pp. 338–345, 2012.

[17] A. R. Haug, G. P. Schmidt, A. Klingenstein et al., "F-18-fluoro-2-deoxyglucose positron emission tomography/computed tomography in the follow-up of breast cancer with elevated levels of tumor markers," *Journal of Computer Assisted Tomography*, vol. 31, no. 4, pp. 629–634, 2007.

[18] A. Cochet, S. David, K. Moodie et al., "The utility of 18 F-FDG PET/CT for suspected recurrent breast cancer: impact and prognostic stratification," *Cancer Imaging*, vol. 14, no. 1, pp. 1–9, 2014.

[19] T. S. Aukema, E. J. T. Rutgers, W. V. Vogel et al., "The role of FDG PET/CT in patients with locoregional breast cancer recurrence: a comparison to conventional imaging techniques," *European Journal of Surgical Oncology*, vol. 36, no. 4, pp. 387–392, 2010.

[20] A. Buck, H. Schirrmeister, T. Kühn et al., "FDG uptake in breast cancer: correlation with biological and clinical prognostic parameters," *European Journal of Nuclear Medicine*, vol. 29, no. 10, pp. 1317–1323, 2002.

[21] L. Radan, S. Ben-Haim, R. Bar-Shalom, L. Guralnik, and O. Israel, "The role of FDG-PET/CT in suspected recurrence of breast cancer," *Cancer*, vol. 107, no. 11, pp. 2545–2551, 2006.

[22] M. Tatsumi, C. Cohade, K. A. Mourtzikos, E. K. Fishman, and R. L. Wahl, "Initial experience with FDG-PET/CT in the evaluation of breast cancer," *European Journal of Nuclear Medicine and Molecular Imaging*, vol. 33, no. 3, pp. 254–262, 2006.

[23] M. J. Duffy, "Serum tumor markers in breast cancer: are they of clinical value?" *Clinical Chemistry*, vol. 52, no. 3, pp. 345–351, 2006.

Hindawi Publishing Corporation
BioMed Research International
Volume 2015, Article ID 378675, 9 pages
http://dx.doi.org/10.1155/2015/378675

Review Article

Molecular and Functional Imaging of Internet Addiction

Yunqi Zhu,[1,2,3,4] Hong Zhang,[1,2,3,4] and Mei Tian[1,2,3,4]

[1] *Department of Nuclear Medicine, The Second Hospital of Zhejiang University School of Medicine, 88 Jiefang Road, Hangzhou, Zhejiang 310009, China*
[2] *Zhejiang University Medical PET Center, Hangzhou 310009, China*
[3] *Institute of Nuclear Medicine and Molecular Imaging, Zhejiang University, Hangzhou 310009, China*
[4] *Key Laboratory of Medical Molecular Imaging of Zhejiang Province, Hangzhou 310009, China*

Correspondence should be addressed to Mei Tian; meitian@zju.edu.cn

Received 18 July 2014; Accepted 8 October 2014

Academic Editor: Ali Cahid Civelek

Maladaptive use of the Internet results in Internet addiction (IA), which is associated with various negative consequences. Molecular and functional imaging techniques have been increasingly used for analysis of neurobiological changes and neurochemical correlates of IA. This review summarizes molecular and functional imaging findings on neurobiological mechanisms of IA, focusing on magnetic resonance imaging (MRI) and nuclear imaging modalities including positron emission tomography (PET) and single photon emission computed tomography (SPECT). MRI studies demonstrate that structural changes in frontal cortex are associated with functional abnormalities in Internet addicted subjects. Nuclear imaging findings indicate that IA is associated with dysfunction of the brain dopaminergic systems. Abnormal dopamine regulation of the prefrontal cortex (PFC) could underlie the enhanced motivational value and uncontrolled behavior over Internet overuse in addicted subjects. Further investigations are needed to determine specific changes in the Internet addictive brain, as well as their implications for behavior and cognition.

1. Introduction

Addiction to substances or activities can profoundly affect people's health and sometimes lead to serious social problems [1–3]. For example, maladaptive use of the Internet can result in the development of a behavioral addiction, leading to significantly clinical impairment or distress [4]. Recently, research about Internet addiction (IA), especially Internet gaming disorder (IGD), has increased both in quantity and in quality [5, 6]. IA is usually defined as an inability of individuals to control their Internet use, resulting in marked psychological, social, and/or work difficulties [7]. IA is associated with various negative consequences, such as sacrificing real-life activities, lack of attention, aggression and hostility, stress, dysfunctional coping, worse academic achievement, low well-being, and high loneliness [5].

While IA has drawn growing attention from scientific world, there are currently no standard diagnostic criteria. Several diagnostic criteria have been proposed to quantify IA. The most widely used diagnostic criterion is Young's Diagnostic Questionnaire [8–10]. Based on the Diagnostic and Statistical Manual of Mental Disorders (DSM-IV), Young initially developed a short eight-item questionnaire that assessed IA [8]. In employing these criteria, participants with five or more of the eight criteria presented during the past 6 months were classified as suffering from IA. Young also created a 20-item questionnaire, called the Internet Addiction Test [10]. In the 20-item questionnaire, each item is based on a 5-point Likert scale evaluating the degree of problems caused by Internet use. Scores over 50 indicate occasional or frequent internet related problems and scores over 80 indicate significant IA-related life problems [10]. The Internet Addiction Test was proved to be a valid and reliable instrument that can be used in classifying IA [11]. Other diagnostic criteria and screening instruments have also been created and used to assess IA [12–16].

As an important subtype of IA, IGD has gained more and more attention from the whole world. IGD has been included

in the appendix of the DSM-V, with a goal of encouraging additional studies [4]. The DSM-V describes IGD as a "persistent and recurrent use of the Internet to engage in games, often with other players, leading to clinically significant impairment or distress as indicated by five or more (criteria) in a 12-month period" [5].

In the past few years, molecular and functional imaging techniques have been increasingly used to study the neurobiological mechanism underlying IA. Molecular imaging is a rapidly developing field aimed to provide disease-specific molecular information through diagnostic imaging studies [17]. The term molecular imaging can be broadly defined as the in vivo characterization and measurement of biologic processes at the cellular and molecular level [18]. In order to prevent and treat IA, it is important to have a clear understanding of its underlying mechanisms. Technological advances have led to great use of both structural and functional brain imaging modalities, for example, magnetic resonance imaging (MRI), positron emission tomography (PET), and single photon emission computed tomography (SPECT), to assist with the diagnosis of different clinical diseases as well as the study of IA. Here we review recent molecular and functional imaging studies that have provided considerable insight into the neurobiological mechanisms of IA, focusing particularly on MRI and PET imaging approaches.

2. MRI Findings

MRI is a highly versatile imaging modality which uses magnet and radiofrequency energy to visualize the internal structure and soft tissue morphology of the body [19]. The primary advantage of MRI as a molecular imaging modality is its high spatial resolution (micrometers), which allows physiological and anatomical information to be extracted simultaneously. Functional MRI (fMRI) is a noninvasive technique which can be used to monitor metabolic activity changes in brain [20]. It has been verified that an increase in neuronal activity within a certain brain region leads to a net increase in the amount of oxygenated blood flow in that specific region [21]. Since deoxygenated hemoglobin is paramagnetic, and oxygenated hemoglobin is diamagnetic, the blood-oxygen-level-dependent (BOLD) contrast enables the examination of regional brain functioning across different contexts and cognitive demands.

2.1. Structural Changes. Using MRI, some studies have shown that brain structural changes are associated with IA. Using the Stroop color-word test [22], which has been widely used for assessing inhibitory control, a study reported that adolescents with IGD showed impaired cognitive control ability [23]. Imaging results demonstrated that brain regions associated with executive function, for example, the left lateral orbitofrontal cortex (OFC), insula cortex, and entorhinal cortex, showed decreased cortical thickness in IGD subjects compared with controls (Figure 1). Moreover, the authors also reported that the reduced cortical thickness of the left lateral OFC was correlated with the impaired cognitive control ability in IGD adolescents. Consistent with this, another study also reported reduced thickness in the OFC of Internet addicted adolescents [24]. Given the view that the OFC is implicated in the pathology of drug and behavioral addictions [25, 26], the authors suggest that IA shares similar neurobiological mechanism with other addictions. Apart from the decreased cortical thickness, increased cortical thickness was also observed in the left precentral cortex, precuneus, middle frontal cortex, and inferior temporal and middle temporal cortices [23] (Figure 1). The precuneus is associated with visual imagery, attention, and memory retrievals [27]. The inferior temporal cortex and the middle frontal cortex have been shown to engage in craving induced by drug cues [28, 29]. Therefore, these results suggest that the increased cortical thickness areas in IGD may be associated with craving of gaming cues.

Voxel-based morphometry is an unbiased technique for characterizing regional cerebral volume and tissue concentration differences in structural magnetic resonance images [30, 31]. Voxel-based morphometry has been useful in identifying subtle structural abnormalities in a variety of neurological diseases. Voxel-based morphometry studies demonstrated that IGD adolescents had lower grey matter density in the left anterior cingulate cortex (ACC), left posterior cingulate cortex (PCC), left insula, and left lingual gyrus [32]. Using the same technique, decreased gray matter volume was found in the bilateral dorsolateral PFC, supplementary motor area, OFC, cerebellum, and left rostral ACC in another group of Internet addicted adolescents [33]. Additionally, a third Voxel-based morphometry study reported gray matter atrophy in the right OFC, bilateral insula, and right supplementary motor area of IGD [34]. The results of gray matter atrophy among these studies were not consistent, which may be due to different data processing methods. The PFC has been implicated in planning complex cognitive behavior, personality expression, and decision making, which consists of the dorsolateral PFC, ACC, and OFC [35]. Numerous imaging studies have brought to light the role of the PFC in addiction [36]. Now it is commonly recognized that the OFC plays a key role in impulse control and decision making [26, 37]. Functional brain imaging studies have revealed that the dorsolateral PFC and rostral ACC were involved in cognitive control [38, 39]. Reduced gray matter volume in the PFC may be associated with uncontrolled behavior in Internet addicts, which may explain fundamental symptoms of IA. The insula has been proposed to play a crucial role in addiction [40]. A number of functional imaging studies provide evidence that the insula is necessary for the explicit motivation to take drugs, and this function is common among drug abusers [41, 42]. Therefore, these results are in agreement with previous findings and verified the necessary role of the PFC and insula for addiction.

Diffusion tensor imaging (DTI) is an approach available to track brain white matter fibers noninvasively. Water molecules' diffusion was found to be much faster along the white matter fibers than perpendicular to them. The difference between these two motions is the basis of DTI [43, 44]. DTI provides a framework for acquisition, analysis, and quantification of the diffusion properties of white matter. In

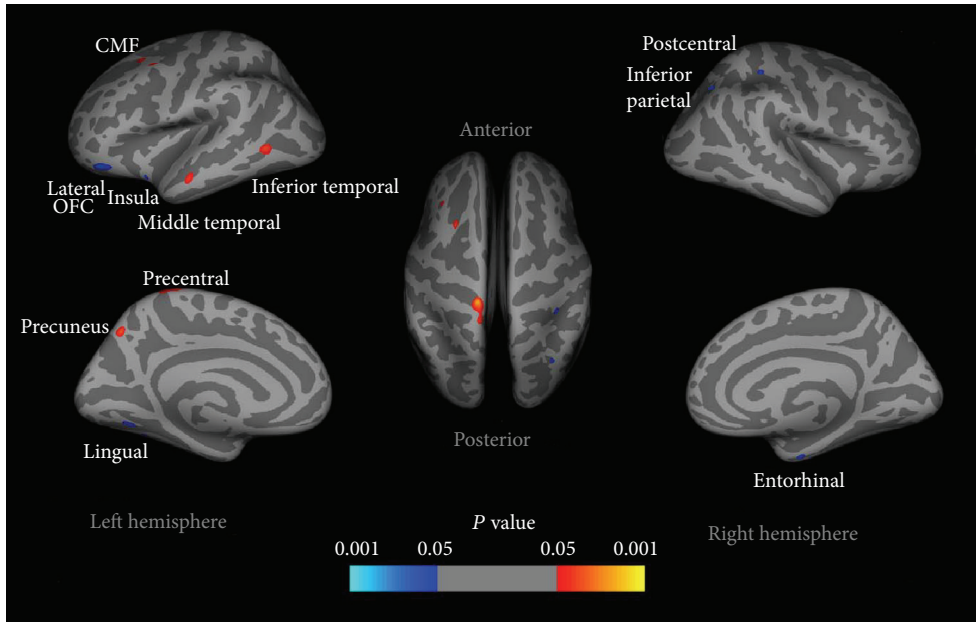

Figure 1: Cortical thickness differences in adolescents with IGD compared with healthy controls. Increased cortical thickness was observed in several regions in adolescents with IGD compared to healthy controls, that is, the left precentral cortex, precuneus, middle frontal cortex, and inferior temporal and middle temporal cortices. Reduced cortical thickness in the left lateral OFC, insula cortex, and lingual gyrus, along with the right postcentral gyrus, entorhinal cortex, and inferior parietal cortex were detected in adolescents with IGD [23].

addition to gray matter abnormalities, white matter abnormalities have also been suggested in IGD. Using DTI, a study assessed white matter integrity in individuals with IGD [45]. Higher fractional anisotropy was reported in the thalamus and left PCC in IGD relative to healthy controls. Moreover, higher fractional anisotropy in the thalamus was associated with greater severity of IGD. White matter abnormalities were also reported in other brain regions by other studies. For example, both enhanced and reduced fractional anisotropy were reported in a study, with enhanced fractional anisotropy in the left posterior limb of the internal capsule and reduced fractional anisotropy in the right parahippocampal gyrus [33]. In another study, significantly lower fractional anisotropy was reported throughout Internet addicts' brain, including the PFC and ACC [46]. However, no areas of higher fractional anisotropy were found. Similar results were also reported in another group of adolescents with IGD [34]. These findings suggest that IA disorder exhibit widespread white matter abnormalities, which may be linked to some behavioral impairment. It should be noted that the fractional anisotropy alterations in brain areas are not consistent in these studies, and the inconsistency in these studies needs further investigation.

2.2. Functional Abnormalities. Using arterial spin-labeling perfusion fMRI, Feng et al. investigated the effects of IGD on resting cerebral blood flow in adolescents [47]. Compared with control subjects, adolescents with IGD showed significantly higher global cerebral blood flow in the left inferior temporal lobe/fusiform gyrus, left parahippocampal gyrus/amygdala, right medial frontal lobe/ACC, left insula, right insula, right middle temporal gyrus, right precentral gyrus, left supplementary motor area, left cingulate gyrus, and right inferior parietal lobe. Most of these areas were included in a model proposed by Volkow et al. in which addiction emerges as an imbalance in information processing and integration among various brain circuits and functions [48]. Among these brain areas, the amygdala and hippocampus are part of a circuit involved in learning and memory that has been associated with craving in response to drug-associated cues [49]. Both the insula and the PFC are known to play a crucial role in addiction [36, 40]. Decreased cerebral blood flow was found in the left middle temporal gyrus, left middle occipital gyrus, and right cingulate gyrus in IGD adolescents. The results demonstrate that IGD alters cerebral blood flow distribution in adolescents' brain. However, it is unclear whether these cerebral blood flow alterations reflected primarily neurological lesions or secondary changes to compensate for such damage.

Functional connectivity impairments are also observed in individuals with IA. A recent study showed that subjects with IGD exhibited increased functional connectivity in the bilateral cerebellum posterior lobe and middle temporal gyrus compared with the control group [50]. The bilateral inferior parietal lobe and right inferior temporal gyrus exhibited decreased connectivity. Another study reported that adolescents with IA showed reduced functional connectivity mainly involving cortico-subcortical circuits, and bilateral

putamen was the most extensively involved subcortical brain region [51]. These results suggest that IA is associated with a widespread and significant decrease of functional connectivity spanning a distributed network.

It has been reported that impulsivity is associated with IA [52]. The ability to suppress a planned motor response is usually investigated using stop-signal or go/no-go paradigms [53]. A recent study evaluated response inhibition and error processing in subjects with IGD [54]. All subjects performed event-related go/no-go task under fMRI and completed questionnaires related to IA and impulsivity. The IGD group got a higher score for impulsivity and exhibited higher brain activation when processing response inhibition over the left OFC and bilateral caudate nucleus than controls. The OFC has been associated with response inhibition [37, 55]. Therefore, these results support the fact that the fronto-striatal network involved response inhibition. A similar study examined the neural correlations of response inhibition in males with IA using an event-related fMRI Stroop color-word task [56]. The IA group demonstrated significantly greater "Stroop effect"-related activity in the ACC and PCC compared with healthy controls. The ACC has been shown to be involved in conflict monitoring and cognitive control [57, 58]. The greater ACC recruitment during Stroop color-word task may reflect diminished "cognitive efficiency" in the IA group. The PCC is a central part of the default mode network and has implicated in attentional processes [59]. The greater activation in the PCC could indicate incomplete disengagement of the default mode network resulting in failure to optimize task related attentional resources in the IA group. These results suggest that individuals with IA exhibit diminished efficiency of response-inhibition processes.

Regional homogeneity is a widely used method in fMRI studies that measures the functional coherence of a given voxel with its nearest neighbors, and it can be used to evaluate resting-state brain activities based on the hypothesis that spatially neighboring voxels should have similar temporal patterns [60]. IGD subjects showed a significant increase in regional homogeneity in the inferior parietal lobe, left posterior cerebellum, and left middle frontal gyrus and decreased regional homogeneity in temporal, occipital, and parietal brain regions compared with healthy controls [61]. The results suggest that long-time online game playing enhanced brain synchronization in sensory-motor coordination related brain regions and decreased excitability in visual and auditory related brain regions.

Several studies investigated brain areas associated with cue-induced gaming urges [62–65]. The participants were presented with gaming pictures while undergoing fMRI. These studies showed increased signal activity in distributed brain areas (e.g., dorsolateral PFC, inferior parietal lobe, ACC, parahippocampal gyrus, OFC, and PCC) in addicted group compared with control group. The activated brain regions were positively correlated with self-reported gaming urges. Abnormalities in these brain regions have been implicated in addiction by numerous studies and may be associated with dysfunctions in cognitive control, craving, goal-directed behavior, and working memory in IGD subjects [66].

An interesting study compared IGD subjects with subjects in remission from IGD and controls in cue-induced craving to play online games [67]. Bilateral dorsolateral PFC, precuneus, left parahippocampal gyrus, PCC, and right ACC were activated in response to gaming cues in the IGD group compared with the control group. These activated brain regions represent brain circuit corresponding to the mechanism of substance addiction [38, 39, 59]. Furthermore, the remission group showed reduced activation over right dorsolateral PFC and left parahippocampal gyrus than did the IGD group. Thus, the authors suggest that the two areas would be candidate markers for current addiction to online gaming.

MRI has also been used to assess therapeutic effects of specific pharmacological treatment on IA. Bupropion is a norepinephrine/dopamine reuptake inhibitor, which has been used in the treatment of patients with substance abuse. A study explored the possible effectiveness of bupropion, assessed brain activity in response to game cues using fMRI [68]. IGD showed higher activation in the left occipital lobe, left dorsolateral PFC, and left parahippocampal gyrus than controls. After 6 weeks of bupropion treatment, the craving and the total time spent gaming were lower. The cue-induced brain activity in dorsolateral PFC was also decreased, which indicated that bupropion was effective. As previously mentioned, IGD individuals in remission showed reduced activation over right dorsolateral PFC and left parahippocampal gyrus [67]. Therefore, molecular imaging has the potential to help clinicians determine the most appropriate treatment for individual patients and monitor their progress toward recovery.

3. Nuclear Imaging Findings

Nuclear imaging approaches, which include SPECT and PET, have the advantages of high intrinsic sensitivity, unlimited depth penetration, and a broad range of clinically available molecular imaging agents [70]. SPECT and PET provide insight into energy metabolism in vivo by quantifying glucose consumption, cerebral perfusion, and oxygen consumption. In neuroscience research, this allows the study of neural activity, as well as disease processes, based on the brain's metabolism and function [71]. PET has the additional advantages of providing higher spatial resolution than SPECT. In addition to measurements of cerebral metabolism, PET and SPECT also enable more specific analyses of neurotransmitter binding site density through the use of specific neuroreceptor radiotracers [72].

3.1. PET Imaging of Brain Metabolic Changes. Using ^{18}F-fluoro-deoxyglucose (^{18}F-FDG) PET imaging, a study investigated the differences of cerebral glucose metabolism at resting state between young individuals with IGD and those with normal use [73]. Imaging results indicated that IGD had increased glucose metabolism in the right middle OFC, left caudate nucleus, and right insula and decreased metabolism in the bilateral postcentral gyrus, left precentral gyrus, and bilateral occipital regions compared with normal users. The results suggest that IGD may be associated with neurobiological abnormality in the OFC, striatum, and

sensory regions, which are implicated in impulse control, reward processing, and somatic representation of previous experiences.

3.2. Nuclear Imaging of Neuroreceptor Abnormalities. Emerging evidence has shown that the dopaminergic system is involved in drug addiction [74, 75]. A pilot study conducted by Koepp et al. used ^{11}C-labelled raclopride and PET scans to investigate endogenous dopamine release in the human striatum during a video game [76]. Binding of the radioligand ^{11}C-raclopride to dopamine D2 receptors is sensitive to levels of endogenous dopamine, which can be detected as changes in binding potential of the radioligand. The authors reported that binding of ^{11}C-raclopride to dopamine receptors in the striatum was significantly reduced during the video game compared with baseline levels of binding, which suggested increased release and binding of dopamine to its receptors. Moreover, they showed that there is a significant correlation between performance level during the task and reduced ^{11}C-raclopride binding potential in the striatum. Similar results have been reported in people with IA [77]. Individuals with IA had reduced dopamine D2 receptor availability in the striatum compared with controls. Furthermore, there was a negative correlation of dopamine receptor availability with IA severity. These findings are supportive of Han et al. who investigated the genetic polymorphisms of the dopaminergic system in a group of excessive Internet game players [78]. They reported that individuals with increased genetic polymorphisms in genes coding for the dopamine D2 receptor and dopamine degradation enzyme were more susceptible to excessive Internet gaming compared with age-matched controls.

Dopamine transporter is a plasma membrane protein that actively translocates released dopamine from the extracellular space into the presynaptic neurons [79]. Altered dopamine transporter concentration in the striatum following chronic substance administration has been reported previously [80, 81]. Using SPECT with the radiotracer ^{99}mTc-TRODAT-1, our group investigated striatal dopamine transporter density in IA subjects to identify potential presynaptic abnormalities [82]. We showed that dopamine transporter expression level was significantly decreased and the volume, weight, and ^{99}mTc-TRODAT-1 uptake ratio of corpus striatum were greatly reduced in individuals with IA compared with controls. Taken together, these results suggest that IA is associated with dysfunction of the brain dopaminergic systems.

In a more in-depth study, our group investigated both dopamine D2 receptor and glucose metabolism in the same individuals using PET with ^{11}C-N-methylspiperone (^{11}C-NMSP) and ^{18}F-FDG, in both states of resting and internet gaming task [69]. A significant decrease in glucose metabolism was observed in the prefrontal, temporal, and limbic systems in IGD subjects. In the resting state, low level of ^{11}C-NMSP binding was found in the right inferior temporal gyrus in the IGD subjects compared to normal controls (Figure 2(a)). After Internet gaming task, ^{11}C-NMSP binding potential in the striatum was significantly lower in IGD subjects compared with controls, indicating reduced level of dopamine D2 receptor (Figure 2(b)). Dysregulation of dopamine D2 receptor was correlated to years of Internet overuse (Figure 2(d)). Importantly, in IGD subjects, low level of dopamine D2 receptor in the striatum was correlated with decreased glucose metabolism in the OFC. These results suggest that dopamine D2 receptor mediated dysregulation of the OFC could underlie a mechanism for loss of control and compulsive behavior in IGD subjects.

From these results, it appears that IA shares similar neurobiological mechanisms with drug addiction. However, there is evidence indicates that there are substantial differences in the neurobiological mechanisms of different drug addiction [83]. In a perspective article, Badiani et al. provided evidence that opiate addiction and psychostimulant addiction are behaviorally and neurobiologically distinct, and these differences might also apply to other addictions [83]. Thus, understanding the neurobiological mechanisms underlying IA is essential for the development of specific and effective treatment approaches.

4. Conclusions and Future Perspectives

Emerging evidence has shown that changes in brain structure and activity related to IA are relevant to brain regions involved in reward, motivation, and memory, as well as cognitive control. Molecular and functional imaging techniques have been increasingly applied to IA research, contributing significantly to our understanding of the neurobiological mechanism. Most of the previous literatures have studied IA individuals only under resting state, verified structural and functional abnormalities in the OFC, dorsolateral PFC, ACC, and PCC. Those regions may play crucial roles in salience attribution, inhibitory control, and decision making. So far, only one PET study with ^{11}C-NMSP and ^{18}F-FDG was conducted under both resting and Internet gaming task states in the same individuals (either with IGD or not) and found that dopamine D2 receptor mediated dysregulation of the OFC could underlie a mechanism for loss of control and compulsive behavior in IGD subjects.

As IA has become a serious problem worldwide, a need for effective treatment is becoming increasingly urgent. Both psychological and pharmacological treatment approaches have been applied to treat IA. Several drugs have shown to be promising in treating IA, such as antidepressants, antipsychotics, and opioid receptor antagonists [84]. Cognitive-behavioral therapy has been applied to treat substance abuse [85]. Since IA appears to share similar mechanism with substance abuse, cognitive-behavioral therapy has also been verified to be effective in treating IA [86]. Further research using various specific radiotracers to target other neurotransmitter systems affected by IA will provide a more complete picture of the neurobiological mechanism that underlie IA. Moreover, specific radiotracers could be used to assess therapeutic effects of specific pharmacological treatment, for example, using ^{11}C-carfentanil to study the mu-opioid receptor availability and predict treatment outcomes of opioid receptor antagonists and help clinicians determine the most appropriate treatment for individual patients.

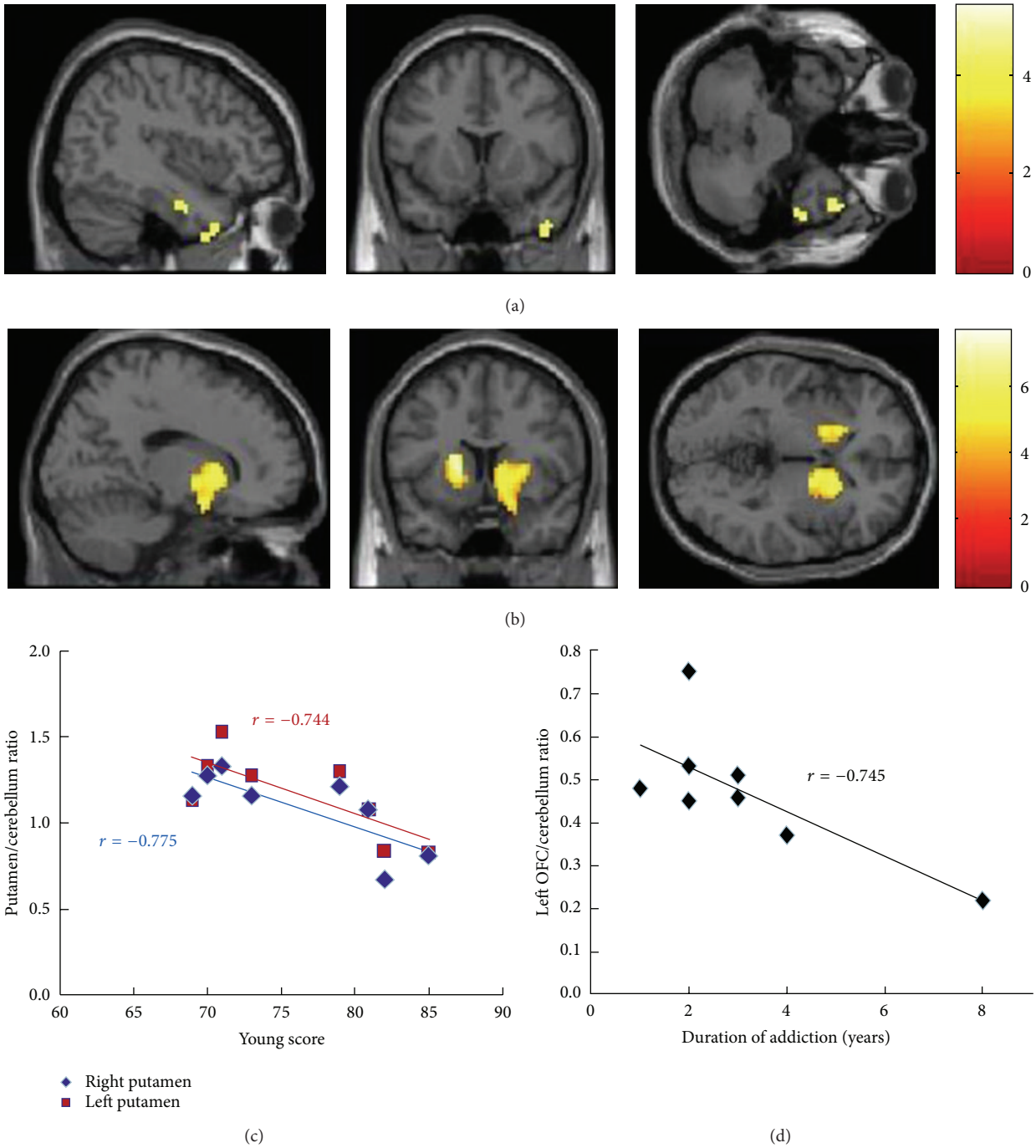

Figure 2: ^{11}C-NMSP PET imaging of dopamine D2 receptor availability in IGD subjects. (a) In the resting state, low level of ^{11}C-NMSP binding was found in the right inferior temporal gyrus in the IGD subjects compared to controls (yellow color) ($P < 0.001$ uncorrected, $k = 100$). (b) In the game task state, ^{11}C-NMSP binding in the putamen was significantly lower in the IGD group than the control group, especially in the right side (yellow color) ($P < 0.001$ uncorrected, $k = 100$). (c) Both right ($P = 0.024$, $r = -0.775$) and left putamen ^{11}C-NMSP binding potential ($P = 0.034$, $r = -0.744$) correlated negatively with the Young score in the IGD subjects. (d) The left OFC to the cerebellum ratio of ^{11}C-NMSP binding correlated negatively with the duration of internet overuse ($P = 0.034$, $r = -0.745$) [69].

Conflict of Interests

The authors declare that there is no conflict of interests regarding the publication of this paper.

Acknowledgments

This work is partly sponsored by Grants from the National Key Basic Research Program of China (2013CB329506),

National Science Foundation of China (NSFC) (81271601), and Ministry of Science and Technology of China (2011CB-504400).

References

[1] A. I. Leshner, "Addiction is a brain disease, and it matters," *Science*, vol. 278, no. 5335, pp. 45–47, 1997.

[2] T. E. Robinson and K. C. Berridge, "Addiction," *Annual Review of Psychology*, vol. 54, pp. 25–53, 2003.

[3] D. Sulzer, "How addictive drugs disrupt presynaptic dopamine neurotransmission," *Neuron*, vol. 69, no. 4, pp. 628–649, 2011.

[4] N. M. Petry, F. Rehbein, D. A. Gentile et al., "An international consensus for assessing internet gaming disorder using the new DSM-5 approach," *Addiction*, vol. 109, no. 9, pp. 1399–1406, 2014.

[5] D. J. Kuss, "Internet gaming addiction: current perspectives," *Psychology Research and Behavior Management*, vol. 6, pp. 125–137, 2013.

[6] D. E. Greydanus and M. M. Greydanus, "Internet use, misuse, and addiction in adolescents: current issues and challenges," *International Journal of Adolescent Medicine and Health*, vol. 24, no. 4, pp. 283–289, 2012.

[7] K. Yuan, W. Qin, Y. Liu, and J. Tian, "Internet addiction: neuroimaging findings," *Communicative and Integrative Biology*, vol. 4, no. 6, pp. 637–639, 2011.

[8] K. S. Young, "Internet addiction: the emergence of a new clinical disorder," *Cyberpsychology and Behavior*, vol. 1, no. 3, pp. 237–244, 1998.

[9] K. W. Beard and E. M. Wolf, "Modification in the proposed diagnostic criteria for Internet addiction," *Cyberpsychology and Behavior*, vol. 4, no. 3, pp. 377–383, 2001.

[10] K. S. Yong, *Caught in the Net: How to Recognize the Signs of Internet Addiction and a Winning Strategy for Recovery*, John Wiley & Sons, New York, NY, USA, 1998.

[11] L. Widyanto and M. McMurran, "The psychometric properties of the internet addiction test," *Cyberpsychology and Behavior*, vol. 7, no. 4, pp. 443–450, 2004.

[12] R. Tao, X. Huang, J. Wang, H. Zhang, Y. Zhang, and M. Li, "Proposed diagnostic criteria for internet addiction," *Addiction*, vol. 105, no. 3, pp. 556–564, 2010.

[13] C.-H. Ko, J.-Y. Yen, S.-H. Chen, M.-J. Yang, H.-C. Lin, and C.-F. Yen, "Proposed diagnostic criteria and the screening and diagnosing tool of Internet addiction in college students," *Comprehensive Psychiatry*, vol. 50, no. 4, pp. 378–384, 2009.

[14] N. A. Shapira, M. C. Lessig, T. D. Goldsmith et al., "Problematic internet use: proposed classification and diagnostic criteria," *Depression and Anxiety*, vol. 17, no. 4, pp. 207–216, 2003.

[15] C. H. Ko, J. Y. Yen, C. C. Chen, S. H. Chen, and C. F. Yen, "Proposed diagnostic criteria of internet addiction for adolescents," *Journal of Nervous and Mental Disease*, vol. 193, no. 11, pp. 728–733, 2005.

[16] G.-J. Meerkerk, R. J. J. M. van Den Eijnden, A. A. Vermulst, and H. F. L. Garretsen, "The Compulsive Internet Use Scale (CIUS): some psychometric properties," *Cyberpsychology and Behavior*, vol. 12, no. 1, pp. 1–6, 2009.

[17] M. L. James and S. S. Gambhir, "A molecular imaging primer: modalities, imaging agents, and applications," *Physiological Reviews*, vol. 92, no. 2, pp. 897–965, 2012.

[18] R. Weissleder and U. Mahmood, "Molecular imaging," *Radiology*, vol. 219, no. 2, pp. 316–333, 2001.

[19] A. M. Blamire, "The technology of MRI—the next 10 years?" *British Journal of Radiology*, vol. 81, no. 968, pp. 601–617, 2008.

[20] N. K. Logothetis, "The neural basis of the blood-oxygen-level-dependent functional magnetic resonance imaging signal," *Philosophical Transactions of the Royal Society B: Biological Sciences*, vol. 357, no. 1424, pp. 1003–1037, 2002.

[21] N. K. Logothetis and B. A. Wandell, "Interpreting the BOLD signal," *Annual Review of Physiology*, vol. 66, pp. 735–769, 2004.

[22] C. M. MacLeod and P. A. MacDonald, "Interdimensional interference in the Stroop effect: uncovering the cognitive and neural anatomy of attention," *Trends in Cognitive Sciences*, vol. 4, no. 10, pp. 383–391, 2000.

[23] K. Yuan, P. Cheng, T. Dong et al., "Cortical thickness abnormalities in late adolescence with online gaming addiction," *PLoS ONE*, vol. 8, no. 1, Article ID e53055, 2013.

[24] S.-B. Hong, J.-W. Kim, E.-J. Choi et al., "Reduced orbitofrontal cortical thickness in male adolescents with internet addiction," *Behavioral and Brain Functions*, vol. 9, no. 1, article 11, 2013.

[25] B. J. Everitt, D. M. Hutcheson, K. D. Ersche, Y. Pelloux, J. W. Dalley, and T. W. Robbins, "The orbital prefrontal cortex and drug addiction in laboratory animals and humans," *Annals of the New York Academy of Sciences*, vol. 1121, pp. 576–597, 2007.

[26] F. Lucantonio, T. A. Stalnaker, Y. Shaham, Y. Niv, and G. Schoenbaum, "The impact of orbitofrontal dysfunction on cocaine addiction," *Nature Neuroscience*, vol. 15, no. 3, pp. 358–366, 2012.

[27] A. E. Cavanna and M. R. Trimble, "The precuneus: a review of its functional anatomy and behavioural correlates," *Brain*, vol. 129, no. 3, pp. 564–583, 2006.

[28] S. Grant, E. D. London, D. B. Newlin et al., "Activation of memory circuits during cue-elicited cocaine craving," *Proceedings of the National Academy of Sciences of the United States of America*, vol. 93, no. 21, pp. 12040–12045, 1996.

[29] C. D. Kilts, J. B. Schweitzer, C. K. Quinn et al., "Neural activity related to drug craving in cocaine addiction," *Archives of General Psychiatry*, vol. 58, no. 4, pp. 334–341, 2001.

[30] J. Ashburner and K. J. Friston, "Voxel-based morphometry—the methods," *NeuroImage*, vol. 11, no. 6 I, pp. 805–821, 2000.

[31] J. L. Whitwell, "Voxel-based morphometry: an automated technique for assessing structural changes in the brain," *Journal of Neuroscience*, vol. 29, no. 31, pp. 9661–9664, 2009.

[32] Y. Zhou, F.-C. Lin, Y.-S. Du et al., "Gray matter abnormalities in internet addiction: a voxel-based morphometry study," *European Journal of Radiology*, vol. 79, no. 1, pp. 92–95, 2011.

[33] K. Yuan, W. Qin, G. Wang et al., "Microstructure abnormalities in adolescents with internet addiction disorder," *PLoS ONE*, vol. 6, no. 6, Article ID e20708, 2011.

[34] C.-B. Weng, R.-B. Qian, X.-M. Fu et al., "Gray matter and white matter abnormalities in online game addiction," *European Journal of Radiology*, vol. 82, no. 8, pp. 1308–1312, 2013.

[35] E. K. Miller and J. D. Cohen, "An integrative theory of prefrontal cortex function," *Annual Review of Neuroscience*, vol. 24, pp. 167–202, 2001.

[36] R. Z. Goldstein and N. D. Volkow, "Dysfunction of the prefrontal cortex in addiction: neuroimaging findings and clinical implications," *Nature Reviews Neuroscience*, vol. 12, no. 11, pp. 652–669, 2011.

[37] G. Schoenbaum, M. R. Roesch, and T. A. Stalnaker, "Orbitofrontal cortex, decision-making and drug addiction," *Trends in Neurosciences*, vol. 29, no. 2, pp. 116–124, 2006.

[38] A. W. MacDonald III, J. D. Cohen, V. A. Stenger, and C. S. Carter, "Dissociating the role of the dorsolateral prefrontal and anterior cingulate cortex in cognitive control," *Science*, vol. 288, no. 5472, pp. 1835–1838, 2000.

[39] D. C. Krawczyk, "Contributions of the prefrontal cortex to the neural basis of human decision making," *Neuroscience and Biobehavioral Reviews*, vol. 26, no. 6, pp. 631–664, 2002.

[40] N. H. Naqvi and A. Bechara, "The hidden island of addiction: the insula," *Trends in Neurosciences*, vol. 32, no. 1, pp. 56–67, 2009.

[41] N. H. Naqvi, D. Rudrauf, H. Damasio, and A. Bechara, "Damage to the insula disrupts addiction to cigarette smoking," *Science*, vol. 315, no. 5811, pp. 531–534, 2007.

[42] M. Contreras, F. Ceric, and F. Torrealba, "Inactivation of the interoceptive insula disrupts drug craving and malaise induced by lithium," *Science*, vol. 318, no. 5850, pp. 655–658, 2007.

[43] D. Le Bihan, J.-F. Mangin, C. Poupon et al., "Diffusion tensor imaging: concepts and applications," *Journal of Magnetic Resonance Imaging*, vol. 13, no. 4, pp. 534–546, 2001.

[44] D. S. Tuch, T. G. Reese, M. R. Wiegell, and V. J. Wedeen, "Diffusion MRI of complex neural architecture," *Neuron*, vol. 40, no. 5, pp. 885–895, 2003.

[45] G. Dong, E. DeVito, J. Huang, and X. Du, "Diffusion tensor imaging reveals thalamus and posterior cingulate cortex abnormalities in internet gaming addicts," *Journal of Psychiatric Research*, vol. 46, no. 9, pp. 1212–1216, 2012.

[46] F. Lin, Y. Zhou, Y. Du et al., "Abnormal white matter integrity in adolescents with internet addiction disorder: a tract-based spatial statistics study," *PLoS ONE*, vol. 7, no. 1, Article ID e30253, 2012.

[47] Q. Feng, X. Chen, J. Sun et al., "Voxel-level comparison of arterial spin-labeled perfusion magnetic resonance imaging in adolescents with internet gaming addiction," *Behavioral and Brain Functions*, vol. 9, no. 1, article 33, 2013.

[48] N. D. Volkow, G.-J. Wang, J. S. Fowler, D. Tomasi, F. Telang, and R. Baler, "Addiction: decreased reward sensitivity and increased expectation sensitivity conspire to overwhelm the brain's control circuit," *BioEssays*, vol. 32, no. 9, pp. 748–755, 2010.

[49] C. P. O'Brien, A. R. Childress, R. Ehrman, and S. J. Robbins, "Conditioning factors in drug abuse: can they explain compulsion?" *Journal of Psychopharmacology*, vol. 12, no. 1, pp. 15–22, 1998.

[50] W.-N. Ding, J.-H. Sun, Y.-W. Sun et al., "Altered default network resting-state functional connectivity in adolescents with internet gaming addiction," *PLoS ONE*, vol. 8, no. 3, Article ID e59902, 2013.

[51] S.-B. Hong, A. Zalesky, L. Cocchi et al., "Decreased functional brain connectivity in adolescents with internet addiction," *PLoS ONE*, vol. 8, no. 2, Article ID e57831, 2013.

[52] H. W. Lee, J.-S. Choi, Y.-C. Shin, J.-Y. Lee, H. Y. Jung, and J. S. Kwon, "Impulsivity in internet addiction: a comparison with pathological gambling," *Cyberpsychology, Behavior, and Social Networking*, vol. 15, no. 7, pp. 373–377, 2012.

[53] A. R. Aron, D. Shohamy, J. Clark, C. Myers, M. A. Gluck, and R. A. Poldrack, "Human midbrain sensitivity to cognitive feedback and uncertainty during classification learning," *Journal of Neurophysiology*, vol. 92, no. 2, pp. 1144–1152, 2004.

[54] C.-H. Ko, T.-J. Hsieh, C.-Y. Chen et al., "Altered brain activation during response inhibition and error processing in subjects with Internet gaming disorder: a functional magnetic imaging study," *European Archives of Psychiatry and Clinical Neuroscience*, 2014.

[55] S. L. Fryer, S. F. Tapert, S. N. Mattson, M. P. Paulus, A. D. Spadoni, and E. P. Riley, "Prenatal alcohol exposure affects frontal-striatal BOLD response during inhibitory control," *Alcoholism: Clinical and Experimental Research*, vol. 31, no. 8, pp. 1415–1424, 2007.

[56] G. Dong, E. E. DeVito, X. Du, and Z. Cui, "Impaired inhibitory control in "internet addiction disorder": a functional magnetic resonance imaging study," *Psychiatry Research—Neuroimaging*, vol. 203, no. 2-3, pp. 153–158, 2012.

[57] M. M. Botvinick, J. D. Cohen, and C. S. Carter, "Conflict monitoring and anterior cingulate cortex: an update," *Trends in Cognitive Sciences*, vol. 8, no. 12, pp. 539–546, 2004.

[58] C. S. Carter and V. Van Veen, "Anterior cingulate cortex and conflict detection: an update of theory and data," *Cognitive, Affective and Behavioral Neuroscience*, vol. 7, no. 4, pp. 367–379, 2007.

[59] R. Leech and D. J. Sharp, "The role of the posterior cingulate cortex in cognition and disease," *Brain*, vol. 137, no. 1, pp. 12–32, 2014.

[60] Y. Zang, T. Jiang, Y. Lu, Y. He, and L. Tian, "Regional homogeneity approach to fMRI data analysis," *NeuroImage*, vol. 22, no. 1, pp. 394–400, 2004.

[61] G. Dong, J. Huang, and X. Du, "Alterations in regional homogeneity of resting-state brain activity in internet gaming addicts," *Behavioral and Brain Functions*, vol. 8, article 41, 2012.

[62] C.-H. Ko, G.-C. Liu, S. Hsiao et al., "Brain activities associated with gaming urge of online gaming addiction," *Journal of Psychiatric Research*, vol. 43, no. 7, pp. 739–747, 2009.

[63] Y. Sun, H. Ying, R. M. Seetohul et al., "Brain fMRI study of crave induced by cue pictures in online game addicts (male adolescents)," *Behavioural Brain Research*, vol. 233, no. 2, pp. 563–576, 2012.

[64] C.-H. Ko, G.-C. Liu, J.-Y. Yen, C.-F. Yen, C.-S. Chen, and W.-C. Lin, "The brain activations for both cue-induced gaming urge and smoking craving among subjects comorbid with Internet gaming addiction and nicotine dependence," *Journal of Psychiatric Research*, vol. 47, no. 4, pp. 486–493, 2013.

[65] D. H. Han, Y. S. Kim, Y. S. Lee, K. J. Min, and P. F. Renshaw, "Changes in cue-induced, prefrontal cortex activity with videogame play," *Cyberpsychology, Behavior, and Social Networking*, vol. 13, no. 6, pp. 655–661, 2010.

[66] N. D. Volkow, G.-J. Wang, J. S. Fowler, and D. Tomasi, "Addiction circuitry in the human brain," *Annual Review of Pharmacology and Toxicology*, vol. 52, pp. 321–336, 2012.

[67] C.-H. Ko, G.-C. Liu, J.-Y. Yen, C.-Y. Chen, C.-F. Yen, and C.-S. Chen, "Brain correlates of craving for online gaming under cue exposure in subjects with Internet gaming addiction and in remitted subjects," *Addiction Biology*, vol. 18, no. 3, pp. 559–569, 2013.

[68] D. H. Han, J. W. Hwang, and P. F. Renshaw, "Bupropion sustained release treatment decreases craving for video games and cue-induced brain activity in patients with internet video game addiction," *Experimental and Clinical Psychopharmacology*, vol. 18, no. 4, pp. 297–304, 2010.

[69] M. Tian, Q. Chen, Y. Zhang et al., "PET imaging reveals brain functional changes in internet gaming disorder," *European Journal of Nuclear Medicine and Molecular Imaging*, vol. 41, no. 7, pp. 1388–1397, 2014.

[70] T. Jones and E. A. Rabiner, "The development, past achievements, and future directions of brain PET," *Journal of Cerebral Blood Flow and Metabolism*, vol. 32, no. 7, pp. 1426–1454, 2012.

[71] M. E. Phelps, "Positron emission tomography provides molecular imaging of biological processes," *Proceedings of the National Academy of Sciences of the United States of America*, vol. 97, no. 16, pp. 9226–9233, 2000.

[72] M. Laruelle, "Imaging synaptic neurotransmission with in vivo binding competition techniques: a critical review," *Journal of Cerebral Blood Flow and Metabolism*, vol. 20, no. 3, pp. 423–451, 2000.

[73] H. S. Park, S. H. Kim, S. A. Bang, E. J. Yoon, S. S. Cho, and S. E. Kim, "Altered regional cerebral glucose metabolism in internet game overusers: a 18F-fluorodeoxyglucose positron emission tomography study," *CNS Spectrums*, vol. 15, no. 3, pp. 159–166, 2010.

[74] J. D. Berke and S. E. Hyman, "Addiction, dopamine, and the molecular mechanisms of memory," *Neuron*, vol. 25, no. 3, pp. 515–532, 2000.

[75] N. D. Volkow, J. S. Fowler, G.-J. Wang, J. M. Swanson, and F. Telang, "Dopamine in drug abuse and addiction: results of imaging studies and treatment implications," *Archives of Neurology*, vol. 64, no. 11, pp. 1575–1579, 2007.

[76] M. J. Koepp, R. N. Gunn, A. D. Lawrence et al., "Evidence for striatal dopamine release during a video game," *Nature*, vol. 393, no. 6682, pp. 266–268, 1998.

[77] S. H. Kim, S.-H. Baik, C. S. Park, S. J. Kim, S. W. Choi, and S. E. Kim, "Reduced striatal dopamine D2 receptors in people with Internet addiction," *NeuroReport*, vol. 22, no. 8, pp. 407–411, 2011.

[78] D. H. Han, Y. S. Lee, K. C. Yang, E. Y. Kim, I. K. Lyoo, and P. F. Renshaw, "Dopamine genes and reward dependence in adolescents with excessive internet video game play," *Journal of Addiction Medicine*, vol. 1, no. 3, pp. 133–138, 2007.

[79] R. A. Vaughan and J. D. Foster, "Mechanisms of dopamine transporter regulation in normal and disease states," *Trends in Pharmacological Sciences*, vol. 34, no. 9, pp. 489–496, 2013.

[80] B. K. Gorentla and R. A. Vaughan, "Differential effects of dopamine and psychoactive drugs on dopamine transporter phosphorylation and regulation," *Neuropharmacology*, vol. 49, no. 6, pp. 759–768, 2005.

[81] K. C. Schmitt and M. E. A. Reith, "Regulation of the dopamine transporter: aspects relevant to psychostimulant drugs of abuse," *Annals of the New York Academy of Sciences*, vol. 1187, pp. 316–340, 2010.

[82] H. Hou, S. Jia, S. Hu et al., "Reduced striatal dopamine transporters in people with internet addiction disorder," *Journal of Biomedicine and Biotechnology*, vol. 2012, Article ID 854524, 5 pages, 2012.

[83] A. Badiani, D. Belin, D. Epstein, D. Calu, and Y. Shaham, "Opiate versus psychostimulant addiction: the differences do matter," *Nature Reviews Neuroscience*, vol. 12, no. 11, pp. 685–700, 2011.

[84] A. M. Przepiorka, A. Blachnio, B. Miziak, and S. J. Czuczwar, "Clinical approaches to treatment of Internet addiction," *Pharmacological Reports*, vol. 66, no. 2, pp. 187–191, 2014.

[85] L. Dutra, G. Stathopoulou, S. L. Basden, T. M. Leyro, M. B. Powers, and M. W. Otto, "A meta-analytic review of psychosocial interventions for substance use disorders," *The American Journal of Psychiatry*, vol. 165, no. 2, pp. 179–187, 2008.

[86] K. S. Young, "Cognitive behavior therapy with internet addicts: treatment outcomes and implications," *Cyberpsychology and Behavior*, vol. 10, no. 5, pp. 671–679, 2007.

Hindawi Publishing Corporation
BioMed Research International
Volume 2015, Article ID 858349, 12 pages
http://dx.doi.org/10.1155/2015/858349

Research Article

Ghrelin Improves Functional Survival of Engrafted Adipose-Derived Mesenchymal Stem Cells in Ischemic Heart through PI3K/Akt Signaling Pathway

Dong Han,[1] Wei Huang,[1] Sai Ma,[1] Jiangwei Chen,[1] Lina Gao,[1] Tong Liu,[1] Rongqing Zhang,[1] Xiujuan Li,[1] Congye Li,[1] Miaomiao Fan,[1] Yundai Chen,[2] and Feng Cao[1,2]

[1]*Department of Cardiology, Xijing Hospital, Fourth Military Medical University, Xi'an 710032, China*
[2]*Department of Cardiology, Chinese PLA General Hospital, Beijing 100853, China*

Correspondence should be addressed to Yundai Chen; cyundai@126.com and Feng Cao; wind8828@gmail.com

Received 15 September 2014; Revised 26 January 2015; Accepted 27 January 2015

Academic Editor: Ignasi Carrio

Mesenchymal stem cells (MSCs) have been proposed as a promising cell population for cell therapy and regenerative medicine applications. However, the low retention and poor survival of engrafted cells hampered the therapeutic efficacy of engrafted MSCs. Ghrelin is a 28-amino-acid peptide hormone and is proved to exert a protective effect on the cardiovascular system. This study is designed to investigate the protective effects of ghrelin on engrafted adipose-derived mesenchymal stem cells (ADMSCs) and its beneficial effects with cellular therapy in mice myocardial infarction (MI). Results showed that intramyocardial injection of ADMSCs combining with ghrelin administration inhibited host cardiomyocyte apoptosis, reduced fibrosis, and improved cardiac function. To reveal possible mechanisms, ADMSCs were subjected to hypoxia/serum deprivation (H/SD) injury to simulate ischemic conditions *in vivo*. Ghrelin (10^{-8} M, 33712 pg/ml) improved ADMSCs survival under H/SD condition. Western blot assay revealed that ghrelin increased AKT phosphorylation both *in vivo* and *in vitro*, decreased the proapoptotic protein Bax, and increased the antiapoptotic protein Bcl-2 *in vitro*, while these effects were abolished by PI3K inhibitor LY294002. These revealed that ghrelin may serve as a promising candidate for hormone-driven approaches to improve the efficacy of mesenchymal stem cell-based therapy for cardiac ischemic disease *via* PI3K/AKT pathway.

1. Introduction

Ischemic heart disease (IHD) is the leading cause of cardiovascular morbidity and mortality worldwide. In past decades, stem cell therapy provides a promising therapy for tissue regeneration and functional recovery for IHD [1]. However, as was revealed by recent studies, one major challenge for stem cell therapy is the limited survival of engrafted stem cells and its residence in ischemic tissues [2, 3]. This limitation is usually associated with the cells' unconvincing therapeutic efficacy [4]. Accordingly, the need to improve the survival and function of transplanted stem cells should be further stressed.

Ghrelin is a 28-amino-acid peptide hormone which exerts independent cardiovascular protective actions, such as promoting angiogenesis, reducing myocardial ischemic reperfusion injury, enhancing vasodilation, and alleviating heart failure [5–7]. In particular, ghrelin could inhibit inflammatory response and apoptosis in endothelial cells [8]. Our previous study also revealed that ghrelin promoted the proliferation, migration, and nitric oxide (NO) secretion of cardiac microvascular endothelial cells (CMECs) [9].

However, the effects of ghrelin on ADMSC engraftment in ischemic microenvironment have remained unclear. In present study, we imitated hypoxic and ischemic injury with hypoxia/serum deprivation (H/SD) cell model *in vitro* and also utilized a mouse myocardial infarction (MI) model *in vivo* to investigate the effects of ghrelin on ADMSCs in an ischemic setting. Moreover, by establishing ADMSCs which stably expressed molecular imaging reporter genes—firefly luciferase (Fluc) and green fluorescence protein (GFP),

we monitored ghrelin's effect on the viability of engrafted ADMSC and *in vivo* possible mechanisms of ghrelin in promoting ADMSC survival.

2. Materials and Methods

2.1. Animals. Fluc$^+$-eGFP$^+$ transgenic mice (Tg [Fluc-egfp]) were bred on a FVB/N background, which could constitutively express firefly luciferase (Fluc) and enhanced green fluorescence protein (eGFP) in all tissues and organs, and were used for ADMSCs isolation. Syngeneic female FVB mice with the same genetic background as Fluc$^+$-eGFP$^+$ transgenic mice (8 weeks old, 20 to 25 g) underwent LAD ligation for the MI model and served as hosts for cellular therapy. All procedures were performed in accordance with the National Institutes of Health Guidelines on the Use of Laboratory Animal. Experimental protocols and animal care methods were approved by the Fourth Military Medical University Committee on Animal Care.

2.2. MI Model and Stem Cell Injection. FVB mice ($n = 80$) were divided into 4 groups: (1) sham group ($n = 20$); (2) MI group (MI, $n = 20$); (3) MI + ADMSCs-vector group (ADMSC, $n = 20$); (4) MI + ADMSCs + ghrelin group (ADMSC-ghrelin, $n = 20$). MI was accomplished by ligation of the left anterior descending (LAD) artery with 6-0 silk sutures after left thoracotomy as described before [10]. Ventricle blanching indicated successful occlusion of the vessel. Sham-operated animals served as surgical controls and were subjected to the same procedures as the experimental animals with the exception that the LAD was not ligated. Mortality rates during and after surgery were less than 5% in all groups. 30 minutes later, cell suspensions were directly injected into the ischemic border zone of the myocardium at four different sites (5 μL to each site) with a total volume of 20 μL containing 7×10^5 cells using a Hamilton syringe with a 29-gauge needle. ADMSCs in ADMSC-ghrelin group were pretreated with ghrelin (10^{-8}, Phoenix Pharmaceuticals). All surgical procedures were performed blindly by an expert with several years of experience on myocardial model.

2.3. Isolation, Cultivation, and Identification of ADMSCs. ADMSCs were isolated with modified procedures described previously [2]. Briefly, adipose tissue was aseptically harvested from Fluc$^+$-eGFP$^+$ transgenic mice and digested by 0.02% collagenase type I solution for 1 h at 37°C. Then cell suspensions were centrifuged at 200 g for 10 min to separate the stromal cell fraction from adipocytes, the cell pellet was resuspended in DMEM supplemented with 15% fetal bovine serum (FBS). Fresh culture media were changed every 3 days. When MSCs reached 80% of confluence, they were passaged and replated at a concentration of $5 \times 10^4/\text{cm}^2$ in cell culture flasks. Cells between third and fifth passage were utilized for further experiments. Cultured ADMSCs were identified by flow cytometry as previously described with minor modifications [2].

2.4. Reporter Gene Imaging of ADMSCs$^{\text{Fluc}^+\text{-eGFP}^+}$. Bioluminescence imaging of firefly luciferase reporter gene (Fluc) was performed to determine the correlation between ADMSCs number and Fluc activity *in vitro*. Briefly, ADMSCs of different quantities ranging from 0.1×10^5 to 10×10^5 were seeded into 96-well plates for 3 wells each group, suspended in 500 μL phosphate-buffered saline (PBS), and incubated with reporter probe D-luciferin (2.25 ng/μL, Invitrogen), followed by imaging with Xenogen Kinetic *In vivo* Imaging System (IVIS, Caliper Life Sciences. CA, USA). For *in vitro* cell viability, ADMSCs were plated in 12-well plates. 24 h later, ADMSCs were administered ghrelin (10^{-9}, 10^{-8}, and 10^{-7} mol/L, resp., equal to 3371.2, 33712, and 337120 pg/mL) or ghrelin with PI3K inhibitor LY294002 (30 μM). After 6 h of either H/SD or normal conditions, cell media were removed from all wells. Cells were incubated with D-luciferin reporter probe (2.25 ng/μL, Invitrogen) and then measured using the IVIS Xenogen Kinetic System (Caliper Life Sciences, USA), using the following imaging parameters: binning at 4, *F*/stop at 1; exposure time with 1 min. For *in vivo* cell viability, engrafted cell was detected using Xenogen *In vivo* Imaging System (IVIS, Caliper Life Sciences, USA) as described previously [11]. Briefly, recipient mice were injected with D-luciferin (150 mg/kg body weight, Caliper, MA, USA) intraperitoneally. Ten minutes later, mice were anesthetized with 2% isoflurane and placed in the imaging chamber. Mice were imaged for 10 min with 1 min acquisition intervals on days 1, 7, 14, and 21 after cell injections. Bioluminescent data were analyzed using Living Image 4.0 software (Caliper, MA, USA) and were quantified as average radiance in photons/s/cm^2/sr.

2.5. ADMSCs *Hypoxia/Serum Deprivation Injury.* Primary ADMSCs were isolated and cultured as described above. ADMSCs were divided into four groups as follows: control group, H/SD group (H/SD), H/SD + ghrelin (10^{-8} M, 33712 pg/mL) group (Ghrelin), and H/SD + ghrelin (10^{-8} M) + PI3K inhibitor LY294002 (30 μM) group (ghrelin/LY). ADMSCs of the group of ghrelin and ghrelin/LY groups were pretreated with ghrelin (10^{-8} M) before H/SD injury. ADMSCs were stimulated with hypoxia/serum deprivation injury as described previously. Briefly, ADMSCs were exposed to hypoxia (94% N_2, 5% CO_2, and 1% O_2) in an anaerobic system (Thermo Forma) at 37°C for 6 h. In the control group, ADMSCs were maintained at normoxia (95% air, 5% CO_2) for equivalent periods.

2.6. Echocardiography. Transthoracic echocardiography (VEVO 2100, VisualSonic, USA) was performed at 24 hours, 1 week, and 4 weeks after infarction in each group. Left ventricular ejection fraction (LVEF) and fractional shortening (FS) were measured as previously described [12]. All measurements (VEVO 2100, VisualSonic, USA) were averaged for three consecutive cardiac cycles and performed by a blinded investigator.

2.7. Histological Assessment of Myocardial Infarction Size. 28 days after cell transplantation, myocardial fibrosis was

examined by Masson's trichrome staining to indicate infarction area within the left ventricle (LV). Briefly, mice were euthanized and hearts were harvested for histological staining at 5 weeks after cell transplantation. Hearts were prepared in 4% paraformaldehyde and embedded in paraffin before staining. Then heart sections (5 μm) were stained with Masson's trichrome (Sigma-Aldrich; St. Louis, MO). Fibrosis was determined using computer morphometry (Bioquant 98) the collagen area was calculated as a percentage of the total left ventricular myocardial area.

2.8. Western Blot Analysis and ELISA Assay. Both cells and myocardium tissues were harvested for Western blot following standard protocol as described previously [2]. Proteins were collected and concentrations were determined using the BCA Protein Assay Kit (Thermo Scientific). Proteins (30 μg/lane) were loaded onto 10% SDS-PAGE gels. After electrophoresis, proteins were transferred to a PVDF Western Blotting membrane (Roche, USA). Membranes were blocked with 5% nonfat dried milk (in TBST) for 2 h at room temperature and then incubated with primary antibody overnight at 4°C (dilution at 1 : 2000 for anti-AKT, 1 : 1000 for phospho-AKT, 1 : 1000 for anti-b-actin, 1 : 200 for anti-Bax, and anti-Bcl-2, all from Cell Signaling Technology, Danvers, MA, USA). After washing and further incubation with appropriate secondary antibody conjugated with horseradish peroxidase for 1 h at room temperature (Cell Signaling Technology), Band intensities were visualized using an enhanced chemiluminescence system (ECL; Amersham). Densitometric analysis of Western blots was carried out using ImageJ software (NIH, Bethesda, MD, USA).

The concentrations of VEGF secreted by ADMSCs were determined by enzyme-linked immunosorbent assay (ELISA) according to the manufacturer's instructions (Sen-Xiong Company, Shanghai, China). In accordance with the manufacturer's instructions, all supernatant was collected, stored at −80°C before measurement and both standards and samples were run in triplicate. OD450 was calculated by subtracting background and standard curves were plotted.

2.9. MTT Assay for Cell Viability. The cell viability of ADMSCs was assessed by 3-(4,5-dimethylthiazol-2-yl)-2,5-diphenyltetrazolium bromide (MTT) assay as described [13]. Briefly, ADMSCs were plated in 96-well plates at 1×10^4/well. After H/SD treatment, cells from each group were harvested and incubated with 10 μL MTT (5 g/L) for 4 h. After that, the incubation medium was removed and formazan crystals were dissolved in 150 μL dimethyl sulphoxide (DMSO). The absorbance was determined at a wavelength of 490 nm.

2.10. Assessment of Apoptosis. TUNEL staining was performed on ADMSCs as well as myocardial sections (frozen sections) according to the manufacturer's instructions (MEBSTAIN Apoptosis kit II; Takara). A cell death detection kit (Roche) was used to detect apoptotic cells. For detection of total nuclei, the slides were covered with the mounting medium containing DAPI (49,6-diamidino-2-phenylindole) (Sigama, USA). Digital photographs were taken at high magnification using a fluorescent microscopy (Olympus). Cells in which the nucleus was stained were defined as TUNEL positive. The percentage of apoptotic cells was termed the apoptotic index. Caspase-3 activity was measured using a caspase-3 assay kit (Clontech, Mountain View, CA) according to the manufacturer's instructions.

2.11. Immunohistochemical Staining for CD31. The density of arteriole was examined in the sections by immunohistochemically staining with anti-CD31 antibody (Sigma, USA), incubated with peroxidase-conjugated streptavidin, stained with DAB, and imaged with microscope (Nikon, Tokyo, Japan). Three high magnification fields within the infarcted region of each section were chosen randomly. Arteriole densities were calculated accordingly. Microvessels in each section were confirmed using the following criteria: (a) being positive for vessel endothelium labeling within the infarct scar; (b) having a visible lumen; and (c) having a diameter between 10 and 100 mm. The density of arteriole was expressed as the quantity of arteriole per mm^2. The immunoreactive areas for CD31 were analyzed with Image J software.

2.12. Statistical Analysis. Results are expressed as mean ± standard deviation (SD). SPSS15.0 (SPSS Inc., USA) was used to perform the one-way analysis of variance (ANOVA) for evaluating the differences among different groups and time points within each group. Pairwise multiple comparisons were to identify the parameters differences between the two groups using Tukey test. Data expressed as proportion was assessed with Chi-square testing. A two-tailed P value <0.05 was considered significant. Polynomial regression analysis was performed to evaluate the correlation between cell number and optical radiance *in vitro*.

3. Results

3.1. Morphology and BLI of ADMSCs$^{Fluc^+\text{-}eGFP^+}$. 24 hours after cell isolation, most cells presented a spheroid appearance under (Figure 1(a)). On the sixth day, cells assumed a typical confluent cobblestone morphological appearance (Figure 1(b)). Noninvasive BLI longitudinally revealed the stable expression of firefly luciferase (Fluc) of ADMSCs. Moreover, cells expressed Fluc reporter genes in a number-dependent trend as confirmed by BLI BLI signal intensity of 1.0×10^5 to 1.0×10^6 ADMSCs increase gradually from 1.74×104 photons/s/cm^2/sr to 2.52×10^5 (P/s/cm^2/sr) (Figure 1(c)). In addition, correlation analysis showed a linear correlation between cell quantities and Fluc signal (correlation coefficient $R^2 = 0.99$; linear regression equation: $y = 0.2627x - 0.1007$) (Figure 1(d)). These data indicated that BLI of Fluc was a reliable tool to monitor viable transplanted ADMSC quantitatively *in vivo*.

3.2. Ghrelin Promoted Viability and Proliferation of ADMSCs *under H/SD Injury.* BLI longitudinally revealed the viability of ADMSCs$^{Fluc^+\text{-}eGFP^+}$ under H/SD injury. H/SD injury significantly decreased ADMSCs viability after H/SD injury for

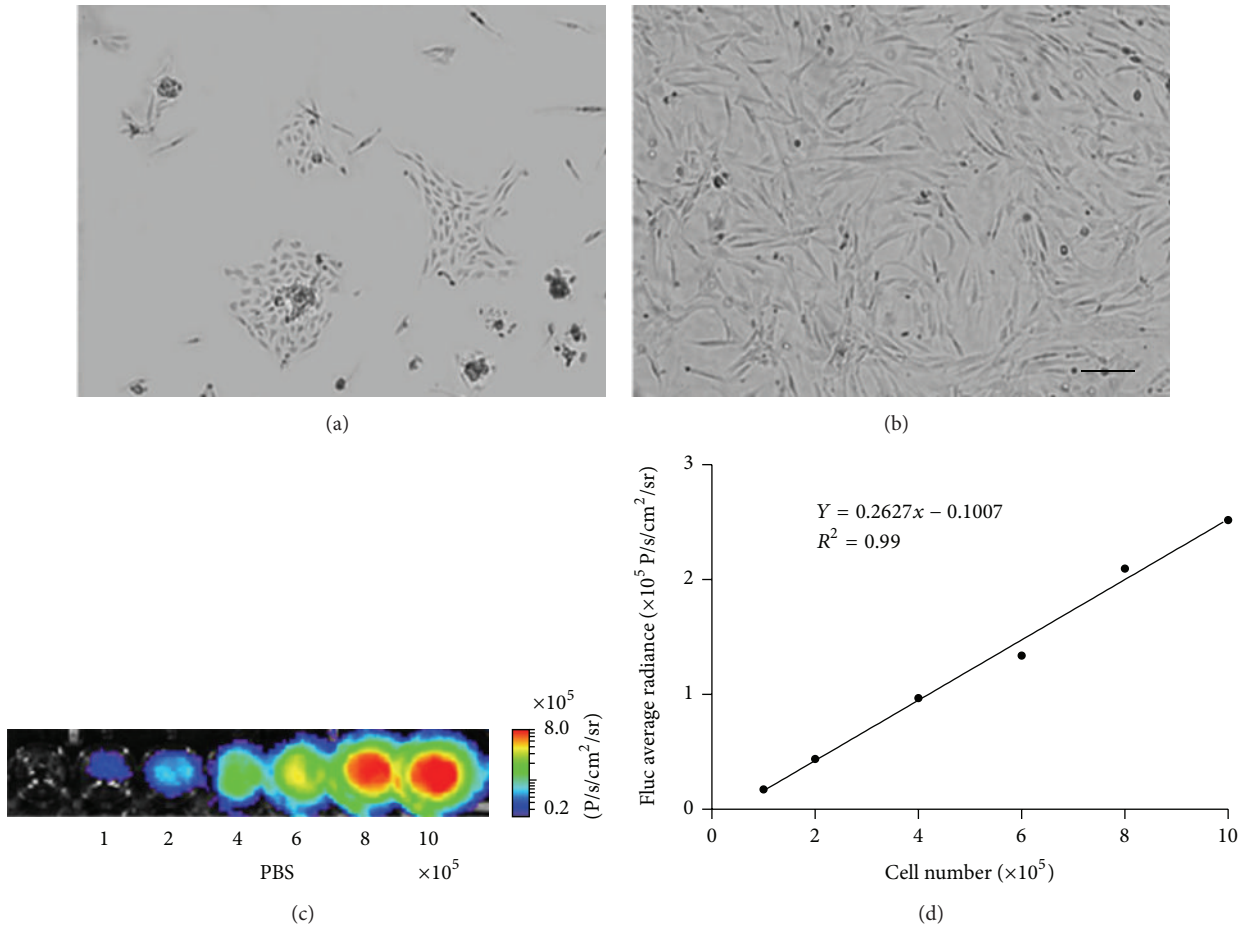

Figure 1: Morphology and bioluminescence imaging (BLI) of ADMSCs$^{Fluc^+\text{-}eGFP^+}$ *in vitro*. (a) The morphology of ADMSCs after culture for 24 hours; (b) the morphology of ADMSCs after culture for five days (scale bar, 100 μm); (c) bioluminescence imaging of ADMSCs with different cell numbers. Colored scale bars represent optical radiance intensity in photons/second/cm^2/steradian (P/s/cm^2/sr); (d) linear correlation of cell quantities with BLI signal was showed.

6 hours ($2.86 \times 10^5 \pm 1.73 \times 10^4$ versus $6.07 \times 10^4 \pm 6.45 \times 10^3$, P/s/cm^2/sr) ($P < 0.05$) and this decrease was significantly reversed (Figure 2(a)) by ghrelin pretreatment at the density of 10^{-8} M ($2.30 \times 10^5 \pm 6.95 \times 10^3$ versus $6.07 \times 10^4 \pm 6.45 \times 10^3$ P/s/cm^2/sr, $P < 0.05$), 10^{-7} M ($1.96 \times 10^5 \pm 1.02 \times 10^4$ versus $6.07 \times 10^4 \pm 6.45 \times 10^3$ P/s/cm^2/sr, $P < 0.05$), while ghrelin pretreatment at the density of 10^{-9} M showed no statistically significant differences, indicating that ghrelin pretreatment at the concentration of 10^{-8} M and 10^{-7} M could increase the viability of ADMSCs under H/SD injury. The protective effect of ghrelin at 10^{-8} mol/L on the viability of ADMSCs after H/SD injury was abolished by addition of the PI3K inhibitor LY294002 (30 μM, Sigma, USA) (Figures 2(a) and 2(b)).

Cell proliferation was assessed by MTT assay. Different concentrations of ghrelin exerted various effects on ADMSCs proliferation capacity in the condition of normoxia, H/SD for 6 hours, H/SD for 12 hours, and H/SD for 24 hours as assessed by MTT assay (Figures 2(c) and 2(d)). Ghrelin significantly enhanced cell proliferation at concentrations of 10^{-8} M in H/SD 6 hours (0.87 ± 0.02 versus 0.67 ± 0.02, $P < 0.05$), H/SD 12 hours (0.66 ± 0.01 versus 0.47 ± 0.03, $P < 0.05$), and H/SD 24 hours group (0.64 ± 0.02 versus 0.42 ± 0.02, $P < 0.05$) compared with respective H/SD groups. This enhanced proliferation by ghrelin at 10^{-8} mol/L on ADMSCs under H/SD injury was abolished by addition of the PI3K inhibitor LY294002.

3.3. Ghrelin Inhibited Apoptosis of ADMSCs. TUNEL assay was used to verify whether H/SD induced ADMSCs apoptosis could be reversed by ghrelin. The percentage of apoptotic ADMSCs in the H/SD group significantly increased compared with the control group ($29.89 \pm 1.98\%$ versus $7.02 + 0.88\%$, $P < 0.05$). In contrast, pretreatment with ghrelin (10^{-8} M) decreased the apoptotic rates of ADMSCs ($14.07 \pm 2.57\%$ versus $29.89 \pm 1.98\%$, $P < 0.05$) compared with the H/SD group. However, coincubation with LY294002 abrogated the antiapoptotic effect of ghrelin on ADMSCs (Figures 3(a) and 3(b)). Concurrently, caspase-3 activity assay confirmed the result of TUNEL assay (Figure 3(c)). These data suggest that ghrelin may prevent H/SD injury-induced apoptosis of ADMSCs *via* the PI3K/AKT signaling pathways.

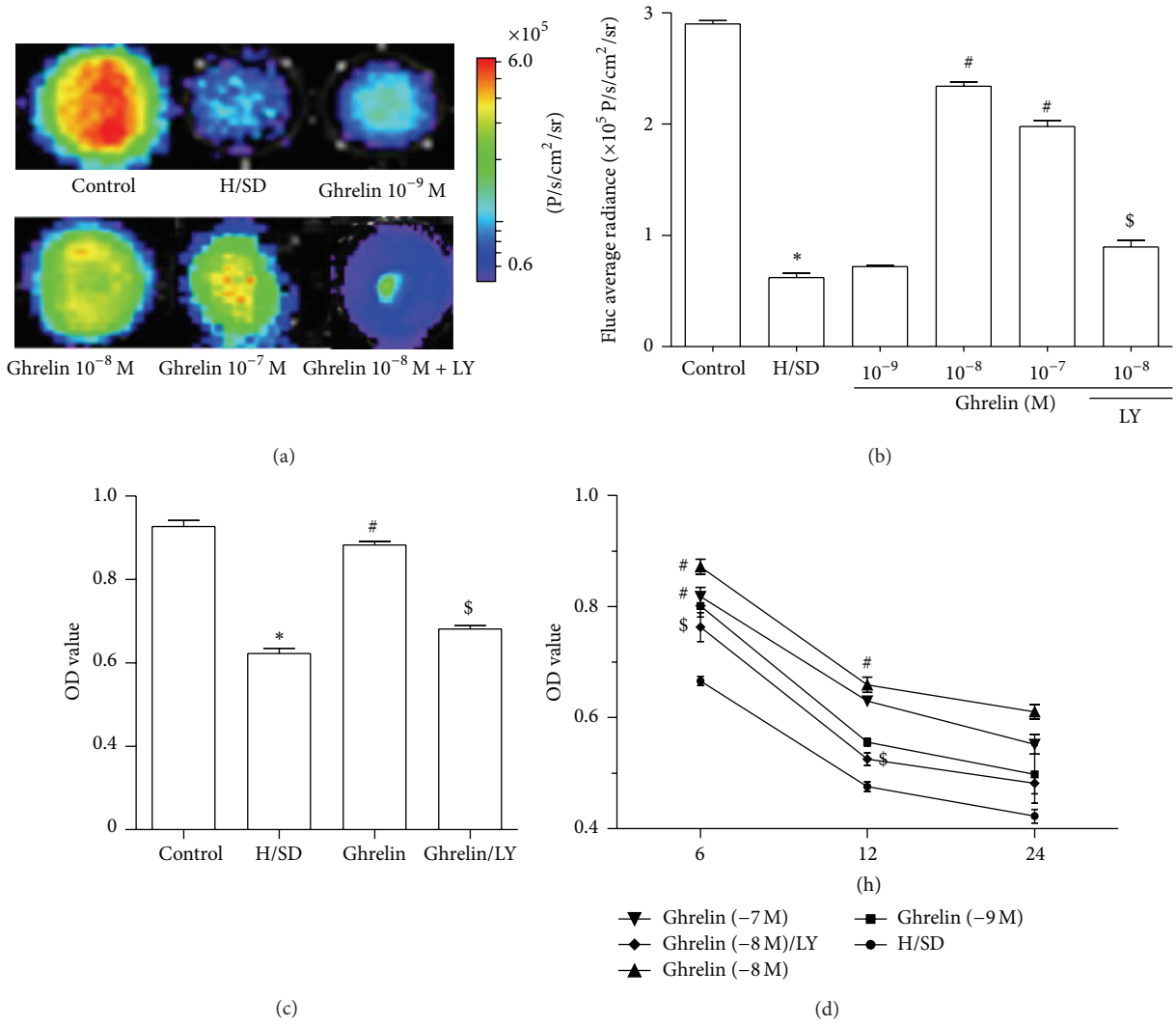

FIGURE 2: Ghrelin reduced ADMSCs apoptosis and promoted ADMSCs proliferation after H/SD injury. ((a), (b)) *In vitro* BLI also confirmed that ghrelin at 10^{-8} mol/L enhanced the impaired viability of ADMSCs after H/SD injury. However, the protective effect of ghrelin was abolished by the PI3K inhibitor LY294002. (c) MTT assay for four groups. (d) MTT assay for H/SD for 6, 12, and 24 hours in different ghrelin pretreatment groups. $^{*}P < 0.05$ versus control group, $^{\#}P < 0.05$ versus H/SD group, and $^{\$}P < 0.05$ versus ghrelin (10^{-8} M) group.

3.4. Ghrelin Pretreated ADMSCs *Significantly Reduced Fibrosis and Apoptosis after MI.* Masson trichrome staining was performed to testify if ghrelin combined ADMSCs influenced fibrosis in infarcted myocardium on day 28 after MI (Figures 4(a) and 4(b)). Masson trichrome staining results showed that severe fibrosis was observed in the post-MI hearts of mice without treatment or treated with ADMSCs. Conversely, fibrosis was markedly alleviated in ADMSC-ghrelin group (23.7 ± 3.2%) compared with MI (9.68 ± 4.69%) and ADMSC group (37.79 ± 4.20%) ($P < 0.05$).

TUNEL assay was used to assess the level of apoptosis of cardiomyocytes in infarcted mouse heart (Figures 4(c)-4(d)). As is shown in representative TUNEL images, a significantly higher apoptosis index (AI) was observed in MI group compared with control group (32.12 ± 3.39% versus 4.91 ± 1.43%, $P < 0.05$). A sharp decrease of AI was noted in ADMSC and ADMSC-ghrelin group compared with MI group (21.89 ± 3.27%, 13.57 ± 2.75% versus 32.12 ± 3.39%, $P < 0.05$), indicating that ghrelin pretreated ADMSCs implantation could suppress MI induced apoptosis. Furthermore, this antiapoptotic effect was more pronounced in ADMSC-ghrelin group compared with ADMSC groups (13.57 ± 2.75% versus 21.89 ± 3.27%, $P < 0.05$). Caspase-3 activity assays confirmed that activation of caspase-3 was attenuated in ADMSC-ghrelin group compared with MI and ADMSC group ($P < 0.05$) (Figure 4(e)).

3.5. Ghrelin Promoted the Viability of Implanted ADMSCs. Longitudinal bioluminescence imaging (BLI) was performed to determine the effect of ghrelin on the viability of ADMSCs transplanted into infarcted hearts. After ADMSCs implantation, BLI signals from both groups decreased gradually to background levels after day 21. At postoperative days (POD) 14 and 21, the BLI signals in ADMSC-ghrelin group were

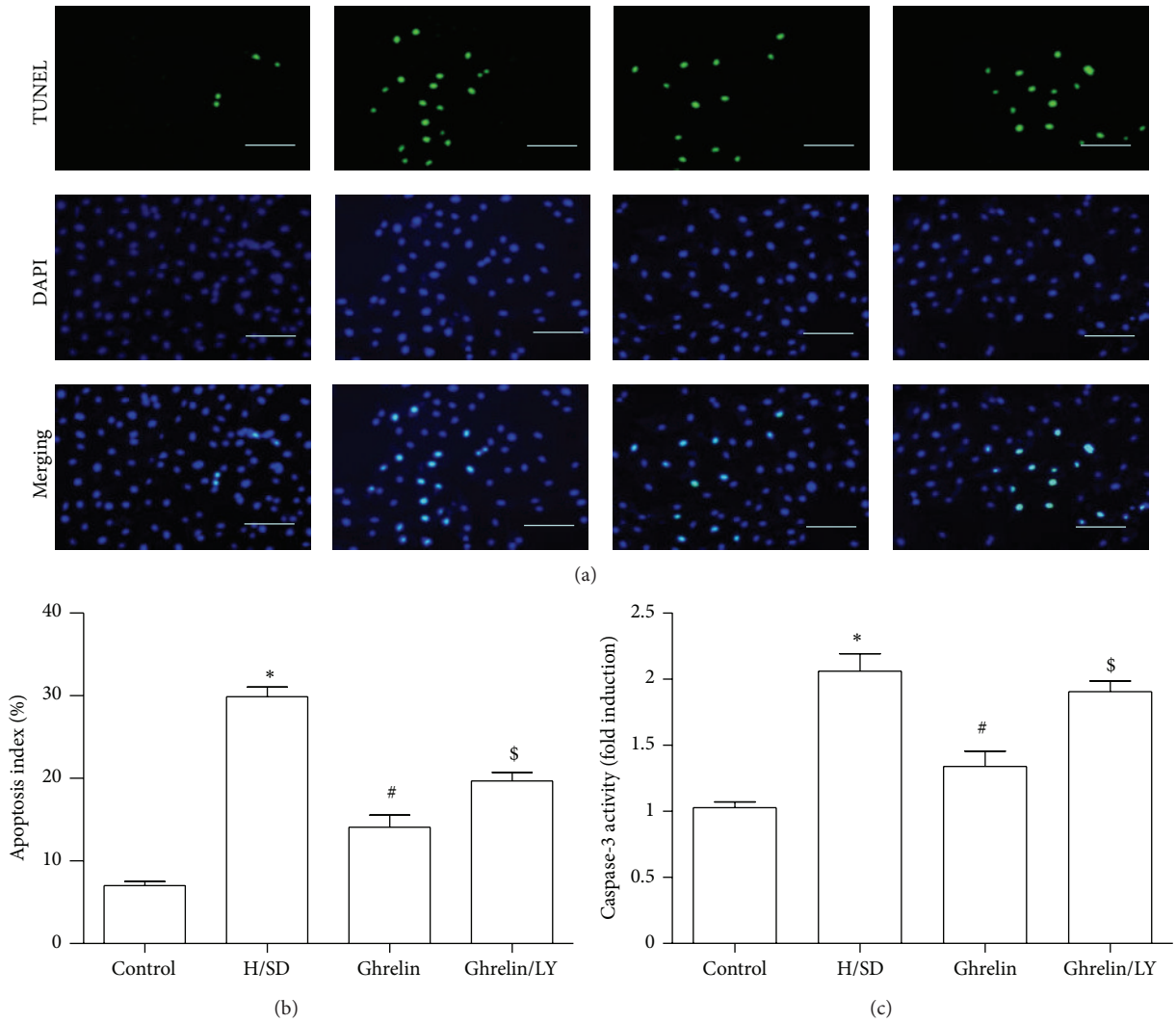

Figure 3: Ghrelin pretreatment reduced ADMSCs apoptosis after H/SD injury. (a) Representative images of TUNEL for apoptotic cells (green, TUNEL; blue, DAPI; scale bar, 100 μm); (b) quantification of TUNEL assay; (c) caspase-3 activity assay confirmed the reduction of ADMSCs apoptosis. $^{*}P < 0.05$ versus control group, $^{\#}P < 0.05$ versus H/SD group, and $^{\$}P < 0.05$ versus ghrelin (10^{-8} M) group.

$1.30 \pm 0.02 \times 10^5$ and $0.70 \pm 0.02 \times 10^5$ photons/s/cm^2/sr, respectively, significantly higher than that in ADMSC group ($0.81 \pm 0.02 \times 10^5$, $0.40 \pm 0.03 \times 10^5$ photons/s/cm^2/sr, $P < 0.05$; Figures 5(a) and 5(b)).

3.6. Ghrelin Combined ADMSCs *Significantly Improved Cardiac Function after MI.* Serial echocardiographic analysis indicated that there was no significant difference in left ventricular ejection fraction (LVEF) and fraction shortening (FS) between all groups at baseline ($P > 0.05$). On POD 7, LVEF decreased significantly in all groups. However, combined therapy of ADMSCs and ghrelin improved cardiac function significantly more than expected. Specifically, by POD 7 and 28 LVEF was improved in the combined therapy group compared to MI groups (POD 7: 46.95 ± 2.92 versus 32.32 ± 2.16% and POD28: 48.924 ± 3.02% versus 28.15 ± 3.92%, Figures 5(c) and 5(d), $P < 0.05$). Similarly, fractional shortening (FS) was significantly improved in the combined therapy group on POD 7 and 28 in contrast to MI groups (POD7: 25.08 ± 2.08 versus 15.84 ± 2.0% and POD28: 27.02 ± 2.20% versus 13.61 ± 2.56%, Figures 5(c) and 5(e), $P < 0.05$).

3.7. Ghrelin Regulated AKT Phosphorylation in ADMSCs *after H/SD Injury.* Western blot assay (Figure 6(a)) showed that ghrelin administration increased PI3K/AKT phosphorylation in ADMSCs after H/SD injury ($P < 0.05$). The effect of promoting AKT phosphorylation by ghrelin on ADMSCs could be attenuated by LY294002 administration.

3.8. Ghrelin Regulated Apoptotic Signaling Pathways. We also analyzed apoptosis associated factors Bcl-2 and Bax protein expression by Western blot assay to figure out whether ghrelin regulated apoptotic signaling pathways (Figures 6(b) and 6(c)). Based on our data, the expression of proapoptotic factor Bax was increased and antiapoptotic factor Bcl-2 was decreased after H/SD injury ($P < 0.05$), while ghrelin

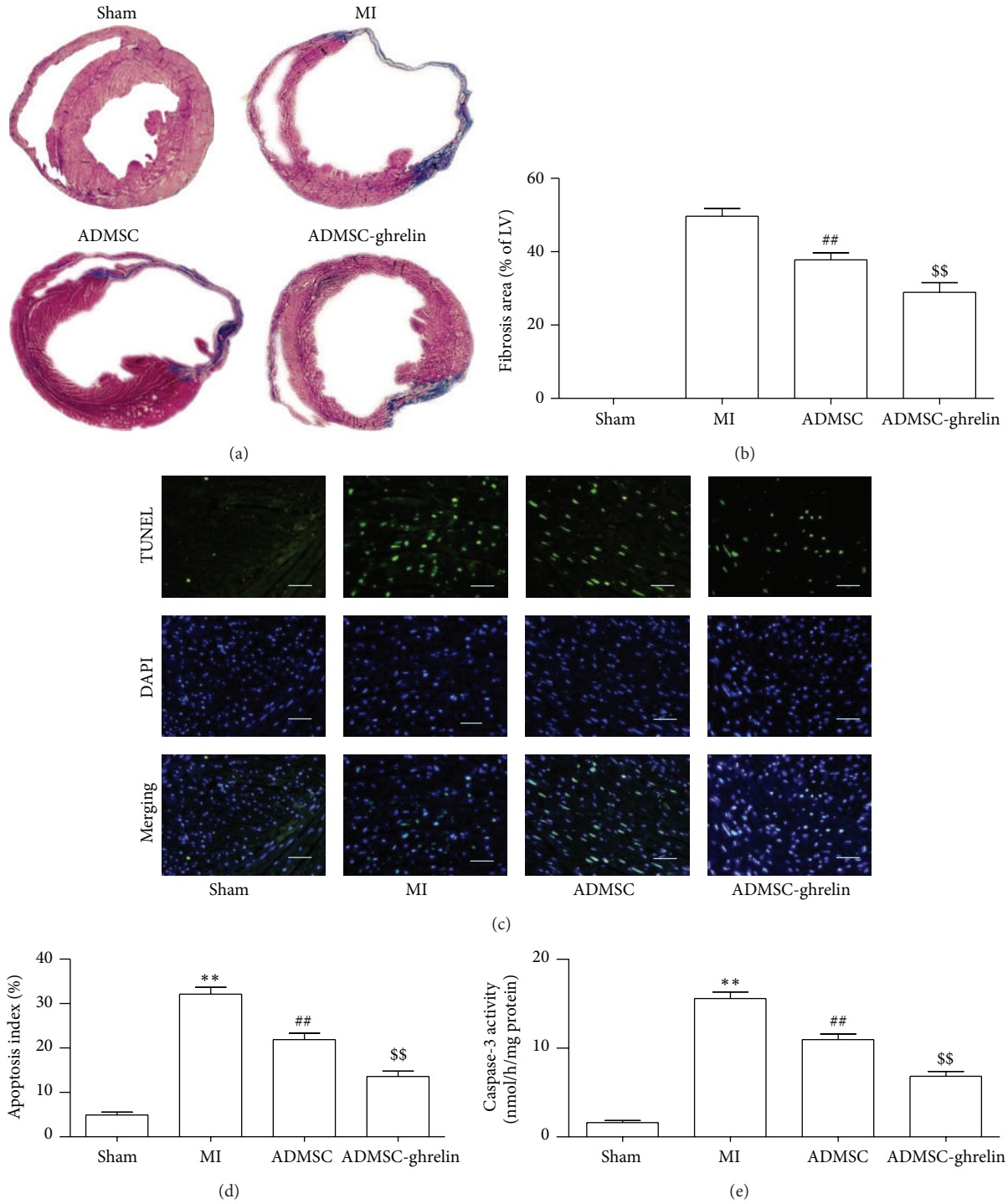

FIGURE 4: Significant reduction of fibrosis and cardiomyocytes apoptosis after ADMSCs implantation. (a) Representative images of Masson's trichrome staining of each group 4 weeks after MI; (b) quantitative analysis of Masson's trichrome staining; (c) representative images of myocardial sections TUNEL (green, TUNEL; blue, DAPI; scale bar, 100 μm); (d) quantification of apoptotic cells; (e) analysis of caspase-3 activity. $^{**}P < 0.05$ versus MI group, $^{\#\#}P < 0.05$ versus MI group, and $^{\$\$}P < 0.05$ versus ADMSC group.

inhibited these changes ($P < 0.05$). However, the antiapoptotic effect of ghrelin was eliminated when LY294002 was used ($P < 0.05$), indicating that the antiapoptotic effect of ghrelin was *via* PI3K/AKT pathways.

3.9. VEGF Secretion Was Increased by Ghrelin Administration. ELISA assays were performed to evaluate the effect of ghrelin on VEGF secretion in ADMSCs (Figure 6(d)). Data showed that H/SD injury increased VEGF secretion in comparison

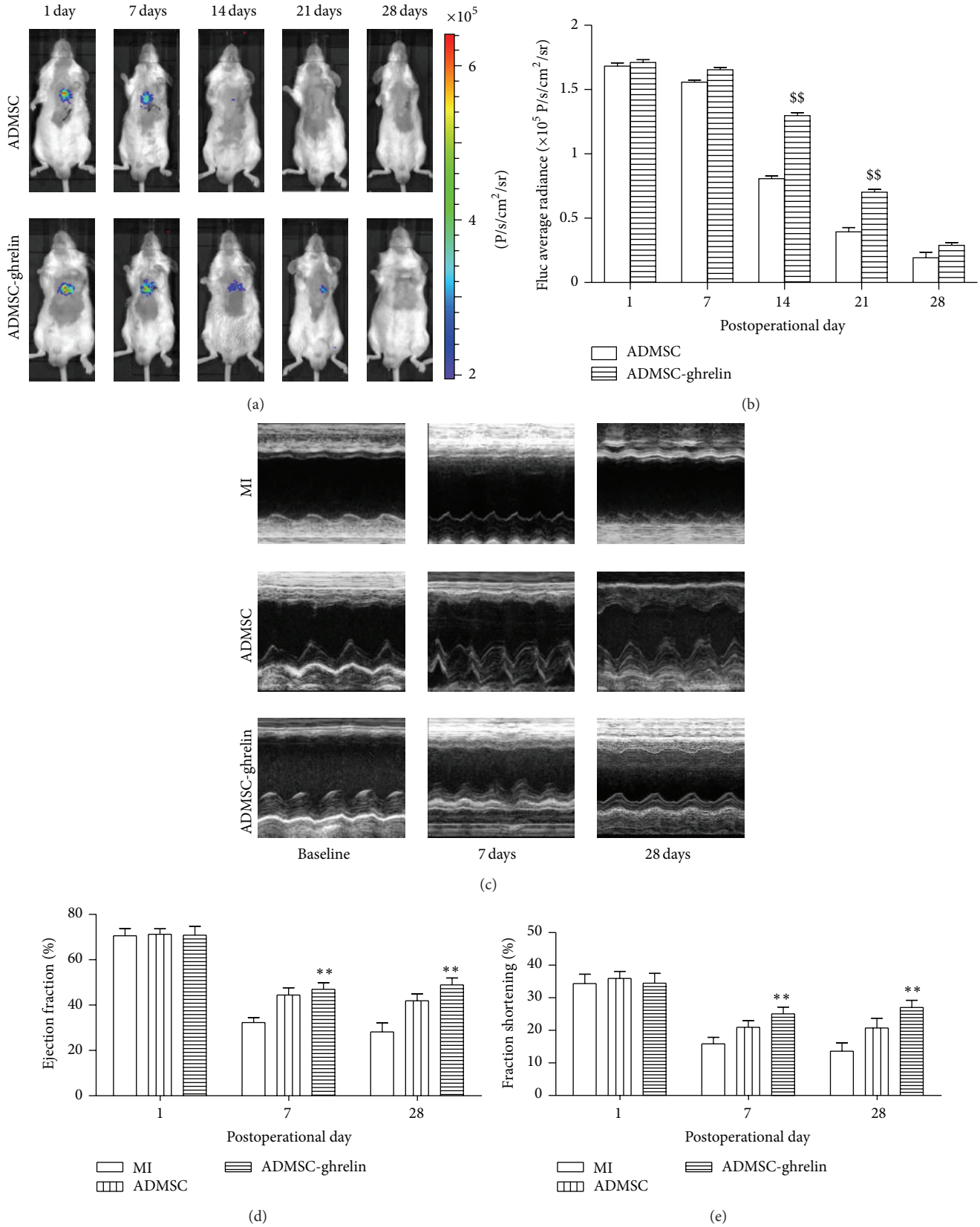

Figure 5: Viability of transplanted ADMSCs and cardiac function after MI. (a) *In vivo* BLI of ADMSCs viability after transplantation; (b) quantitative analysis of BLI. (c) Representative images of M-mode echocardiography. ((d), (e)) Quantitative analysis of cardiac function of ejection fraction (*E*) and fraction shortening (*F*) at baseline and 1 week and 4 weeks after MI. $n = 10$/group, $^{**}P < 0.05$ versus MI group.

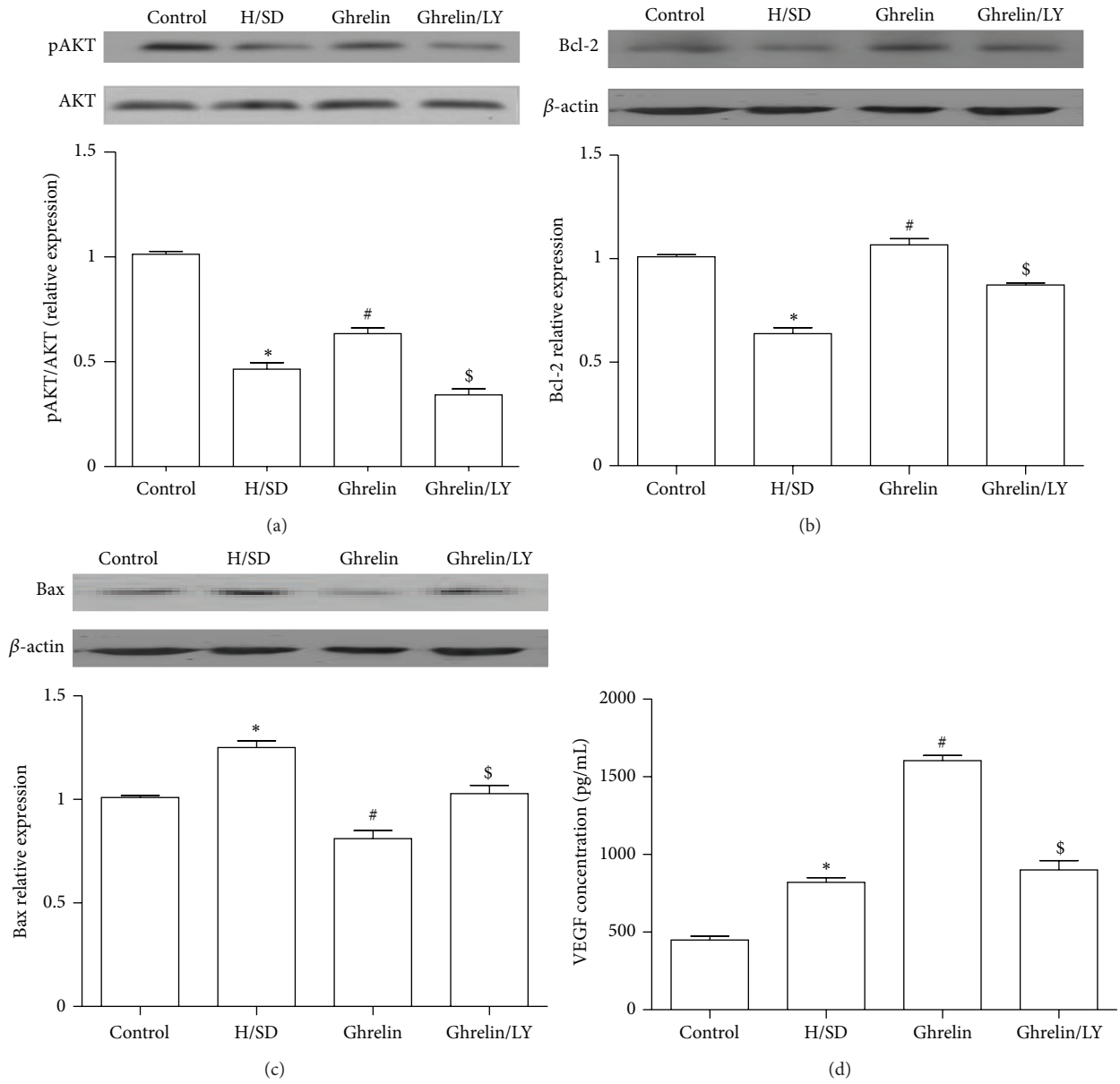

Figure 6: Ghrelin regulated AKT phosphorylation and apoptotic signaling pathways. ((a)–(c)) Western blot and quantification of phosphorylation of AKT (normalized to total AKT), Bcl-2, and Bax respectively (all normalized to control group). (d) Ghrelin increased VEGF secretion in ADMSCs after H/SD injury; $^{*}P < 0.05$ versus control group, $^{\#}P < 0.05$ versus H/SD group, and $^{\$}P < 0.05$ versus ghrelin (10^{-8} M) group.

with the control group (820.90 ± 74.7 versus 449.10 ± 62.50 pg/mL, $P < 0.05$). Furthermore, ghrelin promoted the secretion of VEGF after H/SD, and this effect was abolished by addition of LY294002.

3.10. Ghrelin Pretreated ADMSCs *Regulated AKT Phosphorylation in Mouse Infarcted Heart.* The phosphorylations of AKT in mouse heart of all groups were measured by Western blot assay (Figure 7(a)). Our results showed that ADMSCs implantation increased PI3K/AKT phosphorylation in mouse heart as compared with MI group, and ADMSCs implantation combined ghrelin administration further increased this trend compared with ADMSCs only ($P < 0.05$).

3.11. Ghrelin Pretreated ADMSCs *Promoted Neovasculature Formation.* Arteriole within the infarct was counted to assess the neovascular effect of the different treatments as collateral arterioles are often observed bordering the scar after MI. The results showed that ADMSC (Figure 7(b)-(C), 152.5 ± 25.28/mm^2) and ADMSC-ghrelin (Figure 7(b)-(D), 233.7 ± 36.23/mm^2) all resulted in better arteriole density in scar areas than MI group (Figure 7(b)-(B), 79.97 ± 11.18/mm^2)

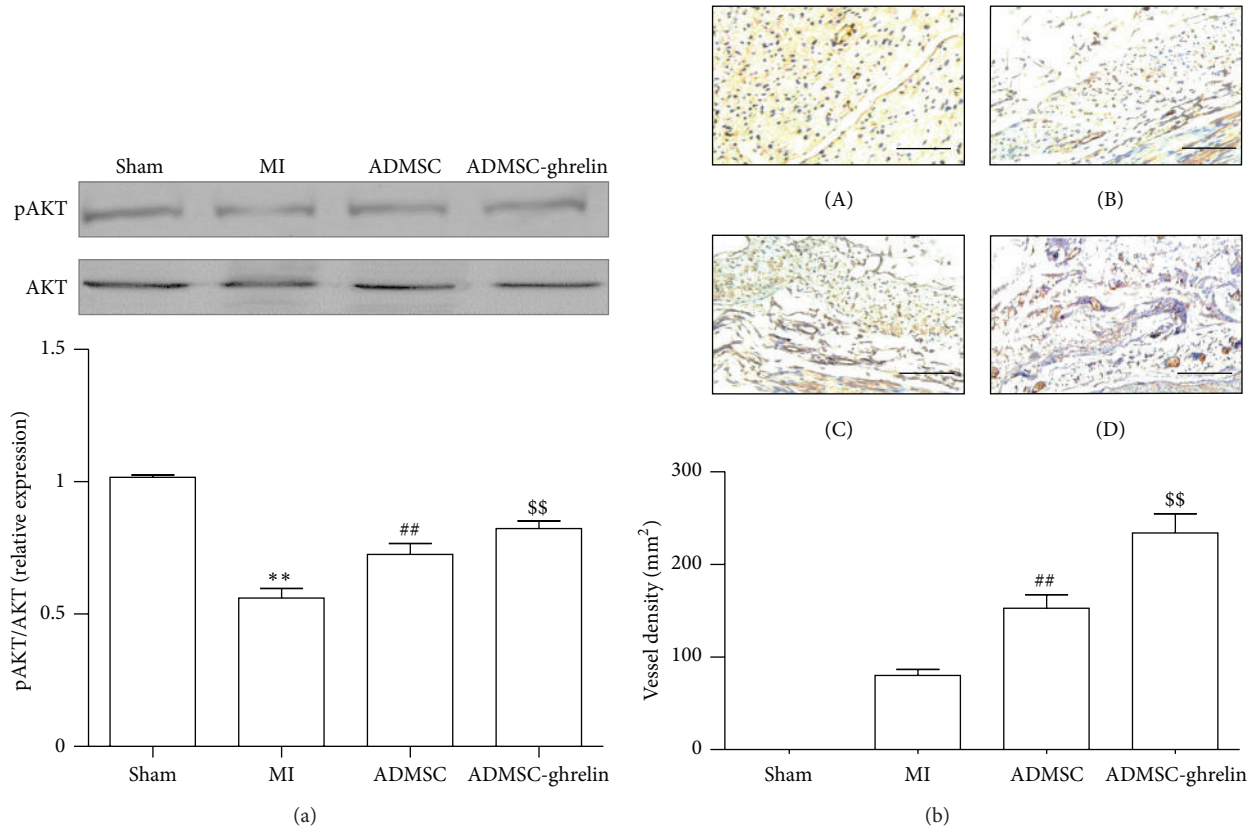

Figure 7: Ghrelin pretreated ADMSCs implantation regulated AKT phosphorylation in mouse infarcted heart and microvessel density in the myocardial infarction sites. (a) ADMSCs implantation regulated AKT phosphorylation in mouse infarcted heart and quantification of phosphorylation of AKT (normalized to total AKT and control group). (b) Microvessel density in the myocardial infarction sites and quantitative analysis. (b) Representative images of myocardial sections from different groups stained with CD31 antibody, (b-A) sham group; (b-B) MI group; (b-C) ADMSC group; and (b-D) ADMSC-ghrelin group. Microvessel densities were statistically compared below between different groups (scale bar = 100 μm). $^{**}P < 0.05$ versus sham group, $^{\#\#}P < 0.05$ versus MI group, and $^{\$\$}P < 0.05$ versus ADMSC group.

($P < 0.01$). The arteriole density of the ADMSC-ghrelin was the highest ($P < 0.05$, resp.).

4. Discussion

Mesenchymal stem cells hold promise for cardiovascular regenerative therapy of ischemic heart diseases (IHD) [14]. The success of stem cell-based IHD therapy needs effective cell engraftment and survival rate [15]. However, when stem cells are injected into the infarcted region, most of the cells encounter acute cell death due to the hypoxic and ischemic microenvironment [16]. Ghrelin has been reported to directly exert a protective effect on the cardiovascular system [17, 18]. Our present study has verified for the first time the beneficial effects of ghrelin on adipose tissue-derived stromal cells (ADMSCs) based IHD therapy. Our results revealed that ADMSC-ghrelin significantly reduced cardiac fibrosis, decreased cardiomyocyte apoptosis, and improved cardiac function after MI injury. Moreover, ghrelin increased the survival of transplanted ADMSCs in the regional myocardial tissue. Furthermore, both *in vivo* and *in vitro* results verified that ghrelin exerts the protective effect on ADMSCs and infarcted heart partly through the activation of PI3K/AKT signaling pathways.

Ghrelin is a 28-amino acid peptide secreted by the stomach, which serves as an endogenous ligand for growth GHSR [5]. Numerous investigations have been done recently suggesting that ghrelin is capable of exerting cardioprotective effects. Ghrelin was reported to have anti-inflammatory effects, specifically *via* suppression of chemotactic factors such as IL-8 and MCP-1 that are normally induced by TNFα-mediated NF-κB activation [8]. Ghrelin also inhibited the adherence of U937 monocytes to HUVECs (human umbilical vein endothelial cells), another mechanism by which ghrelin may suppress the development of early atherosclerosis [19]. Moreover, ghrelin could also inhibit high glucose-induced (33.3 mM, 72 h) apoptosis of HUVECs, possibly by decreasing the concentration of ROS reactive oxygen species [20]. Protective as ghrelin seemed to be, we were curious to know whether ghrelin could also exert a protective effect on ADMSCs in an ischemic setting. In our study, we found that pretreatment with ghrelin could induce ADMSC proliferation, inhibit apoptosis, and increase VEGF secretion under H/SD injury *in vitro*; moreover, ghrelin could exert a protective effect on mesenchymal stem cells (ADMSCs)

in the model of MI in the mouse heart, indicating that ghrelin may be a favorable factor in stem cell-based IHD therapy. Similarly, some previous reports have indicated that ghrelin significantly increased the proliferation of C3H10T1/2 cells at the concentration of 10^{-13} and 10^{-11} M. Ghrelin also exerted an antiapoptotic effect on C3H10T1/2 cells by decreasing caspase-3 activity significantly at concentrations between 10^{-13} and 10^{-7} M [21]. Ghrelin could serve as an autocrine signal regulating skeletal myogenesis, exogenous ghrelin stimulation was shown to regulate myoblast migration and proliferation, and the addition of ghrelin to the differentiation medium increased myogenic differentiation of L6E9 cells [22]. However, other studies have documented that 1 μM ghrelin induced apoptosis in colorectal adenocarcinoma cells by inhibiting the ubiquitin-proteasome system and by activating autophagy, with p53 having an "interactive" role [23]. In addition, ghrelin induced a significant inhibition of cell proliferation in MCF7 cells, at a concentration of 1×10^{-6} M [24]. From our standpoint, ghrelin may act as either antiapoptotic or proapoptotic factor and may enhance or inhibit proliferation in different cells, suggesting that these effects are cell type dependent and are presumably affected by specific cell microenvironment.

Additionally, we found the presence of ghrelin increased the secretion of VEGF of ADMSCs under H/SD injury. VEGF was recognized as a central mediator of angiogenesis [25]. We previously reported that VEGF enhanced the functional survival of donor cells in ischemic myocardium suggesting VEGF secretion is a protective response of ADMSCs to ischemia *in vivo* and hypoxic stimuli *in vitro* [26]. VEGF primarily activates the VEGFR2 (KDR/Flk-1) tyrosine kinase, a key regulator of proangiogenic and antiapoptotic responses [27]. Activation of VEGF/VEGFR2 facilitated the functional survival of ADMSCs. This may be one of the possible mechanisms by which ghrelin enhance proliferation of ADMSCs *in vivo*.

Although previous studies demonstrated that the ADMSC together with its secretome could enhance tissue regeneration in ischemic models, the fate of ADMSCs in ischemic settings could not been fully illuminated using traditional cell tracking techniques. Furthermore, the longitudinal therapeutic efficacy of the engrafted cells was uncertain. Previously, we demonstrated that molecular imaging strategy provided valuable insight into the *in vivo* kinetics of engrafted cells [28]. Namely, BLI is an accurate and sensitive approach for noninvasive stem cell tracking of as few as 500 cells. By BLI, we longitudinally and spatiotemporally visualized the viability of ADMSCs both *in vitro* and *in vivo*, which favorably provided an incremental benefit in monitoring the effects of ghrelin on ADMSCs.

However, there are still some limitations in our present study. Since ghrelin peptides circulate in two distinct forms, AG (acylated ghrelin) and UAG (unacylated ghrelin), they may play different roles in the pathogenesis of specific diseases [29]. In our study we chose mouse UAG (the most abundant form of ghrelin in plasma, amino acids sequence: GSSFLSPEHQKAQQRKESKKPPAKLQRP) as our interesting target according to the previous study [30]. However, we did not compare these two forms of ghrelin in their effects of cellular therapy, which is one of our study limitations. To elucidate systematically this issue, future studies will compare the roles of AG and UAG in ADMSC based mice MI therapy.

5. Conclusions

This study demonstrated that ghrelin pretreatment promoted the proliferation and inhibited apoptosis of ADMSCs under H/SD injury, improving therapeutic efficacy of ADMSC based stem cell therapy for IHD. It is suggested that ghrelin may potentially serve as a potent agent for a hormone-driven strategy to facilitate the progression of stem cell-based transplantation therapy for ischemic disease with clinical perspective.

Conflict of Interests

The authors declare that no competing financial interests exist.

Acknowledgments

This work was supported by the National Funds for Distinguished Young Scientists of China (81325009) and National Nature Science Foundation of China (no. 81270168), (FCao BWS12J037), and Beijing Nature Science Foundation (no. 7152131) National Basic Research Program of China (2012CB518101).

References

[1] J. C. Garbern and R. T. Lee, "Cardiac stem cell therapy and the promise of heart regeneration," *Cell Stem Cell*, vol. 12, no. 6, pp. 689–698, 2013.

[2] W. Fan, K. Cheng, X. Qin et al., "mTORC1 and mTORC2 play different roles in the functional survival of transplanted adipose-derived stromal cells in hind limb ischemic mice via regulating inflammation in vivo," *Stem Cells*, vol. 31, no. 1, pp. 203–214, 2013.

[3] Q. Li, Y. Wang, and Z. Deng, "Pre-conditioned mesenchymal stem cells: a better way for cell-based therapy," *Stem Cell Research and Therapy*, vol. 4, no. 3, article 63, 2013.

[4] A. Leri and P. Anversa, "Stem cells and myocardial regeneration: cooperation wins over competition," *Circulation*, vol. 127, no. 2, pp. 165–168, 2013.

[5] M. Kojima, H. Hosoda, Y. Date, M. Nakazato, H. Matsuo, and K. Kangawa, "Ghrelin is a growth-hormone-releasing acylated peptide from stomach," *Nature*, vol. 402, no. 6762, pp. 656–660, 1999.

[6] M. Kojima and K. Kangawa, "Structure and function of Ghrelin," *Results and Problems in Cell Differentiation*, vol. 46, pp. 89–115, 2008.

[7] T. Tokudome, I. Kishimoto, M. Miyazato, and K. Kangawa, "Ghrelin and the cardiovascular system," *Frontiers of Hormone Research*, vol. 43, pp. 125–133, 2014.

[8] W. G. Li, D. Gavrila, X. Liu et al., "Ghrelin inhibits proinflammatory responses and nuclear factor-kappaB activation in human endothelial cells," *Circulation*, vol. 109, no. 18, pp. 2221–2226, 2004.

[9] Y. Wang, K. Narsinh, L. Zhao et al., "Effects and mechanisms of ghrelin on cardiac microvascular endothelial cells in rats.," *Cell biology international*, vol. 35, no. 2, pp. 135–140, 2011.

[10] E. Gao, Y. H. Lei, X. Shang et al., "A novel and efficient model of coronary artery ligation and myocardial infarction in the mouse," *Circulation Research*, vol. 107, no. 12, pp. 1445–1453, 2010.

[11] F. Cao, S. Lin, X. Xie et al., "In vivo visualization of embryonic stem cell survival, proliferation, and migration after cardiac delivery," *Circulation*, vol. 113, no. 7, pp. 1005–1014, 2006.

[12] Q. Pan, X. Qin, S. Ma et al., "Myocardial protective effect of extracellular superoxide dismutase gene modified bone marrow mesenchymal stromal cells on infarcted mice hearts," *Theranostics*, vol. 4, no. 5, pp. 475–486, 2014.

[13] Z. Zhang, S. Li, M. Cui et al., "Rosuvastatin enhances the therapeutic efficacy of adipose-derived mesenchymal stem cells for myocardial infarction via PI3K/Akt and MEK/ERK pathways," *Basic Research in Cardiology*, vol. 108, no. 2, article 333, 2013.

[14] J. H. Houtgraaf, W. K. den Dekker, B. M. van Dalen et al., "First experience in humans using adipose tissue-derived regenerative cells in the treatment of patients with ST-segment elevation myocardial infarction," *Journal of the American College of Cardiology*, vol. 59, no. 5, pp. 539–540, 2012.

[15] H. Mizuno, M. Tobita, and A. C. Uysal, "Concise review: adipose-derived stem cells as a novel tool for future regenerative medicine," *Stem Cells*, vol. 30, no. 5, pp. 804–810, 2012.

[16] T. E. Robey, M. K. Saiget, H. Reinecke, and C. E. Murry, "Systems approaches to preventing transplanted cell death in cardiac repair," *Journal of Molecular and Cellular Cardiology*, vol. 45, no. 4, pp. 567–581, 2008.

[17] G. Alloatti, E. Arnoletti, E. Bassino et al., "Obestatin affords cardioprotection to the ischemic-reperfused isolated rat heart and inhibits apoptosis in cultures of similarly stressed cardiomyocytes," *The American Journal of Physiology—Heart and Circulatory Physiology*, vol. 299, no. 2, pp. H470–H481, 2010.

[18] E. A. García and M. Korbonits, "Ghrelin and cardiovascular health," *Current Opinion in Pharmacology*, vol. 6, no. 2, pp. 142–147, 2006.

[19] X. Xu, B. S. Jhun, C. H. Ha, and Z. G. Jin, "Molecular mechanisms of ghrelin-mediated endothelial nitric oxide synthase activation," *Endocrinology*, vol. 149, no. 8, pp. 4183–4192, 2008.

[20] K. Isoda, J. L. Young, A. Zirlik et al., "Metformin inhibits proinflammatory responses and nuclear factor-κB in human vascular wall cells," *Arteriosclerosis, Thrombosis, and Vascular Biology*, vol. 26, no. 3, pp. 611–617, 2006.

[21] S. W. Kim, O. K. Choi, J. Y. Jung et al., "Ghrelin inhibits early osteogenic differentiation of C3H10T1/2 cells by suppressing Runx2 expression and enhancing PPARγ and C/EBPα expression," *Journal of Cellular Biochemistry*, vol. 106, no. 4, pp. 626–632, 2009.

[22] U. Gurriarán-Rodríguez, I. Santos-Zas, O. Al-Massadi et al., "The obestatin/GPR39 system is up-regulated by muscle injury and functions as an autocrine regenerative system," *The Journal of Biological Chemistry*, vol. 287, no. 45, pp. 38379–38389, 2012.

[23] L. Bonfili, M. Cuccioloni, V. Cecarini et al., "Ghrelin induces apoptosis in colon adenocarcinoma cells via proteasome inhibition and autophagy induction," *Apoptosis*, vol. 18, no. 10, pp. 1188–1200, 2013.

[24] P. Cassoni, M. Papotti, C. Ghè et al., "Identification, characterization, and biological activity of specific receptors for natural (ghrelin) and synthetic growth hormone secretagogues and analogs in human breast carcinomas and cell lines," *The Journal of Clinical Endocrinology & Metabolism*, vol. 86, no. 4, pp. 1738–1745, 2001.

[25] M. Grunewald, I. Avraham, Y. Dor et al., "VEGF-induced adult neovascularization: recruitment, retention, and role of accessory cells," *Cell*, vol. 124, no. 1, pp. 175–189, 2006.

[26] W. Fan, D. Sun, J. Liu et al., "Adipose stromal cells amplify angiogenic signaling via the VEGF/mTOR/Akt pathway in a murine hindlimb ischemia model: a 3D multimodality imaging study," *PLoS ONE*, vol. 7, no. 9, Article ID e45621, 2012.

[27] A.-K. Olsson, A. Dimberg, J. Kreuger, and L. Claesson-Welsh, "VEGF receptor signalling—in control of vascular function," *Nature Reviews Molecular Cell Biology*, vol. 7, no. 5, pp. 359–371, 2006.

[28] F. Cao, Z. Li, A. Lee et al., "Noninvasive de novo imaging of human embryonic stem cell-derived teratoma formation," *Cancer Research*, vol. 69, no. 7, pp. 2709–2713, 2009.

[29] J. Isgaard, A. Barlind, and I. Johansson, "Cardiovascular effects of ghrelin and growth hormone secretagogues," *Cardiovascular and Hematological Disorders—Drug Targets*, vol. 8, no. 2, pp. 133–137, 2008.

[30] G. Togliatto, A. Trombetta, P. Dentelli et al., "Unacylated ghrelin promotes skeletal muscle regeneration following hindlimb ischemia via SOD-2-mediated miR-221/222 expression," *Journal of the American Heart Association*, vol. 2, no. 6, Article ID e000376, 2013.

Hindawi Publishing Corporation
BioMed Research International
Volume 2015, Article ID 917968, 14 pages
http://dx.doi.org/10.1155/2015/917968

Review Article

Somatostatin Receptor Based Imaging and Radionuclide Therapy

Caiyun Xu[1,2,3,4] and Hong Zhang[1,2,3,4]

[1] *Department of Nuclear Medicine, The Second Affiliated Hospital of Zhejiang University School of Medicine, Hangzhou, Zhejiang 310009, China*
[2] *Zhejiang University Medical PET Center, Zhejiang University, Hangzhou, Zhejiang 310009, China*
[3] *Institute of Nuclear Medicine and Molecular Imaging, Zhejiang University, Hangzhou, Zhejiang 310009, China*
[4] *Key Laboratory of Medical Molecular Imaging of Zhejiang Province, Hangzhou, Zhejiang 310009, China*

Correspondence should be addressed to Hong Zhang; hzhang21@gmail.com

Received 19 September 2014; Revised 15 January 2015; Accepted 20 January 2015

Academic Editor: Enzo Terreno

Somatostatin (SST) receptors (SSTRs) belong to the typical 7-transmembrane domain family of G-protein-coupled receptors. Five distinct subtypes (termed SSTR1-5) have been identified, with SSTR2 showing the highest affinity for natural SST and synthetic SST analogs. Most neuroendocrine tumors (NETs) have high expression levels of SSTRs, which opens the possibility for tumor imaging and therapy with radiolabeled SST analogs. A number of tracers have been developed for the diagnosis, staging, and treatment of NETs with impressive results, which facilitates the applications of human SSTR subtype 2 (hSSTr2) reporter gene based imaging and therapy in SSTR negative or weakly positive tumors to provide a novel approach for the management of tumors. The hSSTr2 gene can act as not only a reporter gene for *in vivo* imaging, but also a therapeutic gene for local radionuclide therapy. Even a second therapeutic gene can be transfected into the same tumor cells together with hSSTr2 reporter gene to obtain a synergistic therapeutic effect. However, additional preclinical and especially translational and clinical researches are needed to confirm the value of hSSTr2 reporter gene based imaging and therapy in tumors.

1. Introduction

Somatostatin receptors belong to the typical 7-transmembrane domain family of G-protein-coupled receptors [1]. Five distinct subtypes (termed SSTR1-5) have been identified, with SSTR2 showing the highest affinity for natural SST and synthetic SST analogs [2]. Most NETs, including pituitary adenoma, gastroenteropancreatic tumor (GEP-NET), pheochromocytoma, neuroblastoma, paraganglioma [3, 4], medulloblastoma [5], and medullary thyroid carcinoma [6], have relatively high expression levels of SSTRs, which opens the possibility for tumor imaging and therapy with radiolabeled SST analogs. A number of tracers have been produced due to encouraging initial results from the applications of radiolabeled ligand-receptor systems [7, 8]. The most commonly used radiopharmaceutical for somatostatin receptor scintigraphy (SRS) is [^{111}In-DTPA^{0}]octreotide, which has proven its role in the diagnosis and staging of NETs [9]. Favorable results also have been observed in NET imaging using other γ-emitting tracers like ^{99m}Tc-Depreotide and [^{111}In-DOTA]lanreotide [10, 11]. More recently, positron-emitting radiotracers have been developed and seem to be more promising. ^{68}Ga-DOTA-peptides used for positron emission tomography (PET) or positron emission tomography/computed tomography (PET/CT) imaging of NETs have been reported by various research groups with higher sensitivity and specificity compared to SRS and conventional imaging modalities [12–14]. In addition, SST analogs labeled with therapeutic radionuclides, such as ^{111}In, ^{90}Y, ^{177}Lu, and ^{213}Bi, have been applied in peptide receptor radionuclide therapy (PRRT) for patients with inoperable and/or metastatic NETs [15]. The results that were obtained with [^{90}Y-DOTA^{0}-Tyr^{3}]octreotide (^{90}Y-DOTATOC) and [^{177}Lu-DOTA^{0}-Tyr^{3}]octreotate (^{177}Lu-DOTATATE) are particularly promising in terms of tumor regression, overall survival, and quality of life, if adequate renal protection is used [16, 17].

However, SSTR based imaging and therapy are only available in SSTR positive tumors. Many malignant human cancers were poorly or not detected to express SSTR subtypes [18, 19]. Surgery, chemotherapy, and radiotherapy have limited effects on improving survival for patients diagnosed with these cancers [20]. Therefore, some studies [21, 22] have tried to explore the applications of hSSTr2 reporter gene based imaging and therapy in SSTR negative or weakly positive tumors to provide a new strategy for the management of these tumors. To this end, the target gene hSSTr2 should be inserted into gene transfer vectors to induce transfected tumors to express SSTR2 [23–25] and assure that hSSTr2 expression could occur on tumor cell membranes. Optical imaging and biopsy have been taken to identify whether gene transfer succeeds or not. However, poor tissue penetration of light-based reporter systems, such as green fluorescent protein [23, 26] and luciferase [27], hampers a comprehensive assessment of whole organism or targeted tumors [20]. On the other hand, biopsy is an invasive technique and can only evaluate the outcome of gene expression [28]. Nuclear imaging can avoid the unclear images in deep tissues and the need of tissue sampling for histological analysis of gene expression. Tumors transfected with hSSTr2 gene can be monitored by external gamma camera, single photon computed emission tomography (SPECT), or PET imaging techniques with radiolabeled SST analogs [29]. These *in vivo* hSSTr2 based imaging methods have several advantages: repetitively observing the expression levels of hSSTr2 or other genes within transfected tumors [30], studying the biodistribution of gene transfer vectors [25], predicting the effects of PRRT, and monitoring the time course of tumor growth and the efficacy of antitumor gene therapy [21]. The hSSTr2 gene transfer not only allows for some SSTR negative tumors to be imaged *in vivo*, but also can be useful for antitumor radionuclide therapy. SST analogs labeled with therapeutic radionuclides can be delivered to the cell receptor targeting site and are able to induce the internalization of ligand-receptor complexes [31–33]. The trapped radiopeptides in transfected tumor cells have been considered to be necessary for internal local irradiation, which offers an alternative approach to conventional therapeutics for SSTR negative tumors [22]. Furthermore, by the simultaneous inclusion of a second therapeutic gene like thymidine kinase (TK) or cytosine deaminase (CD), it is possible to obtain a dual gene vector that includes hSSTr2 working as a reporter gene for *in vivo* imaging as well as a therapeutic gene for radionuclide therapy. Preliminary studies suggested that a synergistic therapeutic effect could be achieved following dual gene transfer with one vector encoding both hSSTr2 reporter gene and a second therapeutic gene [21, 34].

In this review, we summarize the performances of SSTR based imaging and radionuclide therapy in NETs and introduce the applications of hSSTr2 reporter gene based imaging and therapy with radiolabeled SST analogs in SSTR negative or weakly positive tumors.

2. Somatostatin Receptor Based Imaging

Computed tomography (CT) and magnetic resonance imaging (MRI) are commonly used to detect NETs and have sensitivity between 50 and 80% based on anatomic characteristics [37]. In comparison, functional imaging modalities, that is, PET, SPECT, or scintigraphy, have shown higher sensitivity and specificity in visualizing primary tumors and their metastases. During the past two decades, SRS has been widely used for the diagnosis and staging of NETs. [^{123}I, Tyr^3]octreotide was the first radiolabeled SST analog utilized for *in vivo* imaging [38]. Unfortunately, high nonspecific accumulation was observed in the liver and intestine, which has limited its ability to locate early primary tumors [39]. Soon a new radiotracer consisting of octreotide, the chelator DTPA, and the radionuclide ^{111}In was developed as [^{111}In-DTPA^0]octreotide (OctreoScan). It has been approved by the Food and Drug Administration and was commercially available as ^{111}In-pentetreotide [40]. An early study [41] tried to evaluate the potential of [^{111}In-DTPA^0]octreotide in the visualization of NETs. Patients (n = 6) with proven tumors (three carcinoids, three insulinomas) were scanned using both [^{111}In-DTPA^0]octreotide and [^{123}I, Tyr^3]octreotide, obtaining the same results in 4 patients. Nevertheless, [^{111}In-DTPA^0]octreotide images showed higher resolution at 21 hours after injection with a more satisfactory tumor-background ratio. Several papers [42–44] reported high sensitivity, varying between 67 and 100%, in NET imaging with [^{111}In-DTPA^0]octreotide. In the management of patients with NETs, [^{111}In-DTPA^0]octreotide scintigraphy can be used not only to detect primary NETs and their metastases, but also to follow up patients with known tumors, monitor tumor response to therapy, and predict the efficacy of PRRT for patients with inoperable and/or metastatic NETs [41, 45, 46]. These good qualities lay the foundation for [^{111}In-DTPA^0]octreotide becoming the gold standard for NET imaging [40]. From 2012, SPECT/CT scanning using [^{111}In-DTPA^0]octreotide is an important part of the diagnostic work-up of patients with NETs in the consensus guidelines of European Neuroendocrine Tumor Society [47, 48]. However, some NETs, like primary sympathetic paragangliomas, show low uptake of [^{111}In-DTPA^0]octreotide in tumor regions [49] while other NETs may become OctreoScan negative with time due to tumor dedifferentiation [10]. Efforts are therefore spent on developing radiolabeled SST analogs to be capable of imaging SSTR positive tumors with higher sensitivity, specificity, and accuracy. The ^{99m}Tc-labeled agent, ^{99m}Tc-Depreotide, has received regulatory approval in the United States and Europe for use in the detection of lung cancer [50]. It binds to a wide range of SSTR subtypes (SSTR2, SSTR3, and SSTR5) and has shown promise in diagnosing a variety of tumor types [51–53], including some OctreoScan negative NETs [10]. ^{111}In-DOTA-lanreotide is another γ-emitting tracer with different affinity for SSTR subtypes compared to [^{111}In-DTPA^0]octreotide. Tumors expressing mainly SSTR3 and/or SSTR4, for example, intestinal adenocarcinomas, may be well visualized by ^{111}In-DOTA-lanreotide [11, 54].

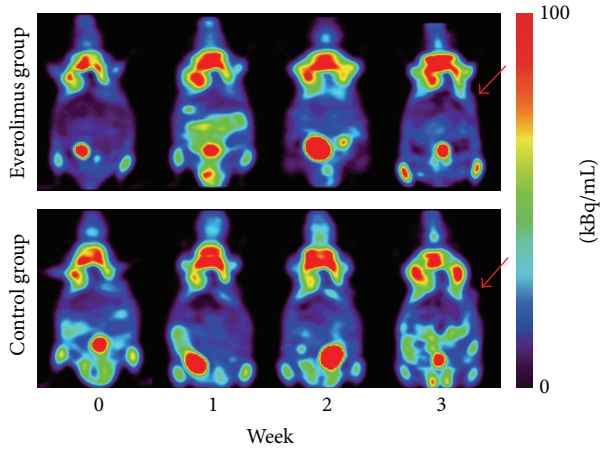

Figure 1: Serial PET images demonstrating glucose metabolism changes before (week 0) and after everolimus treatment (week 1, week 2, and week 3) in nude mice bearing Bon-1 pancreatic tumor xenografts (red arrows). The two groups are presented as the everolimus treatment group and the control group. Images are shown in axial view. No significant difference of the tumor uptake was found between the two groups at each time point after everolimus treatment.

With the emerging of PET scanning, a variety of positron-emitting tracers have been produced. [^{18}F]fluorodeoxyglucose (^{18}F-FDG) is the most widely used radiotracer for tumor staging and treatment response surveillance in a number of tumor types. The trapped ^{18}F-FDG in cells can reflect glucose metabolism profile of normal tissues and lesions [40]. In general, malignant tumors demonstrate increased uptake of ^{18}F-FDG and can be distinguished from normal tissues. It has been demonstrated in patients affected by NET that ^{18}F-FDG PET has a high accuracy for poorly differentiated tumors [55, 56]. However, ^{18}F-FDG is not indicated primarily for NET imaging since most NETs present low proliferative activity and well differentiation. We attempted to use ^{18}F-FDG imaging to monitor everolimus effect on tumor growth in Bon-1 pancreatic NETs. The results showed that *in vivo* tumor volumes measured relative to baseline were significantly lower in the everolimus group compared to the control group, whereas the uptake of ^{18}F-FDG was quite low in tumor regions and showed no significant difference between the two groups at any time point after everolimus treatment (Figure 1).

Positron-emitter ^{68}Ga can be produced just depending on ^{68}Ge-^{68}Ga generator, so it is available in departments without a cyclotron. ^{68}Ga-labeled SST analogs with a quite short half-life (68 min) have exhibited great potential for PET imaging of NETs and their metastases [12, 42, 57]. Some [38, 58] predicted that ^{68}Ga-labeled peptides are the most likely candidates for such a universal tracer applied in the diagnosis, staging, and restaging of patients with NETs instead of ^{111}In-DTPA-octreotide. [^{68}Ga-DOTA^0-Tyr^3]octreotide (^{68}Ga-DOTATOC), [^{68}Ga-DOTA^0,1NaI^3]octreotide (^{68}Ga-DOTANOC), and [^{68}Ga-DOTA^0-Tyr^3]octreotate (^{68}Ga-DOTATATE) are three main ^{68}Ga-labeled SST analogs widely utilized to NET imaging and patient selection for PRRT [59]. They demonstrate slightly different affinities for the five SSTR subtypes. ^{68}Ga-DOTATATE is SSTR2 selective, presenting 10-fold higher affinity for SSTR2 *in vitro* than that of ^{68}Ga-DOTATOC [60], which has high affinity for SSTR2 and SSTR5. In comparison, ^{68}Ga-DOTANOC has a wider receptor binding profile, able to specifically bind to SSTR2, SSTR3, and SSTR5 [61]. These differences may affect their efficiency in the detection of NET lesions. A study [60] explored 40 patients with metastatic NETs, who underwent both ^{68}Ga-DOTATOC and ^{68}Ga-DOTATATE PET/CT. The diagnostic accuracy was almost the same between the two ^{68}Ga-DOTA-conjugated peptides. However, tumor uptake varied considerably both within and between patients. Eighteen patients displayed only lesions with higher uptake of ^{68}Ga-DOTATOC than ^{68}Ga-DOTATATE and the reverse situation was found in 4 patients. The other 18 patients displayed a mixture of lesions with higher uptake of either ^{68}Ga-DOTATATE or ^{68}Ga-DOTATOC. These differences in tumor uptake of the two radiopeptides were also reported by a latest study [35] (Figure 2). The possible reasons for such a variation could be the extensive difference in the SSTR subtype profile and the nonstandardized examination conditions. For tumors expressing broader SSTR subtypes, ^{68}Ga-DOTANOC may be more efficient to detect NET lesions; Wild et al. conducted a study [61] in which 18 patients with clearly diagnostic GEP-NETs were imaged with ^{68}Ga-DOTANOC and ^{68}Ga-DOTATATE. Consequently, the SSTR2, 3, 5 specific radiotracer ^{68}Ga-DOTANOC detected significantly more lesions than the SSTR2 selective radiotracer ^{68}Ga-DOTATATE. Although the diagnostic efficacy varies among the three radiopeptides, PET imaging with ^{68}Ga-DOTA-conjugated peptides offers higher sensitivity and specificity compared with SRS and conventional imaging modalities. In an early study [12], ^{68}Ga-DOTATOC PET was compared with SRS and CT in the visualization of known or suspected NETs (n = 84 patients). As a consequence, ^{68}Ga-DOTATOC PET had a significantly higher diagnostic efficacy than SRS and CT in various clinical situations (initial diagnosis, staging, and follow-up), which have affected clinical management in a considerable number of patients, especially when compared with CT. A latest study [13] aimed to compare NET lesion detectability among SPECT/CT, ^{68}Ga-DOTATATE PET/CT, and whole-body diffusion-weighted MR imaging (WB DWI). The results showed that ^{68}Ga-DOTATATE PET/CT seemed to be more sensitive for detection of NET lesions, especially for bone and unknown primary lesions (Figure 3). Comparison of ^{68}Ga-DOTANOC PET/CT and conventional imaging (mainly CT and MRI) was undertaken in a clinical study [14]. Conventional imaging was available in included patients (n = 111) with 93 patients suspected of NETs; ^{68}Ga-DOTANOC PET/CT was superior for detection of NETs with high sensitivity, specificity, positive predictive value, negative predictive value, and accuracy.

NETs were formerly described as APUDomas (amine precursor uptake and decarboxylation). Amine

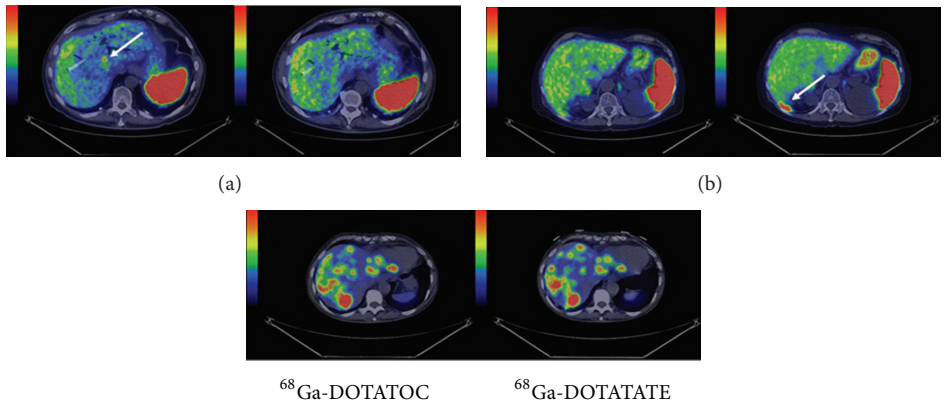

Figure 2: Transaxial images of liver metastases demonstrating cases of higher detection rate for ^{68}Ga-DOTATOC ((a): patient 6, PET/CT fusion); higher detection rate for ^{68}Ga-DOTATATE ((b): patient 8, PET/CT fusion); and equal detection rate ((c): patient 1, PET/CT fusion). Whole-body scans were conducted at 1 hour after injection. Arrows point toward hepatic metastases [35].

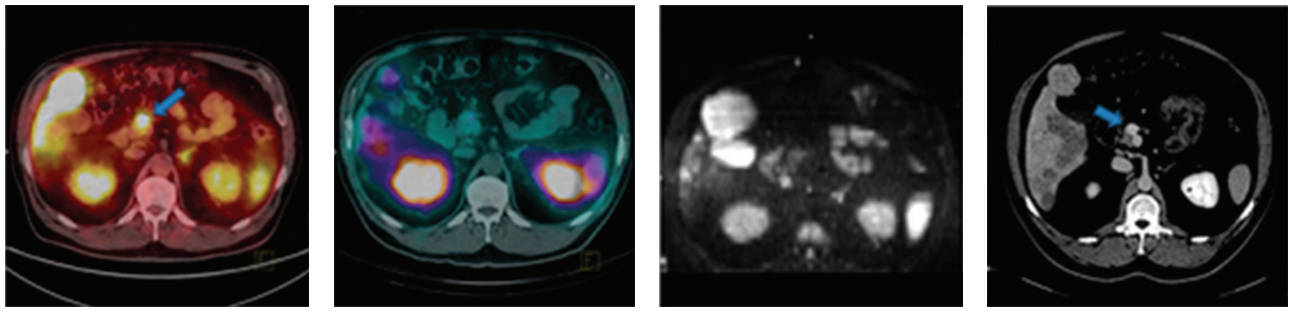

Figure 3: A 49-year-old man with NET of unknown origin for over 4 years. ^{68}Ga-DOTATATE PET/CT (a) identified primary pancreatic lesion (arrow), whereas SPECT/CT (b) and WB DWI (c) did not. This lesion was noted only retrospectively (arrow) on dedicated abdominal CT (d) performed 4 years previously [13].

precursor such as 5-hydroxy-L-tryptophan (5-HTP) and L-dihydroxyphenylalanine (L-DOPA) may be absorbed into tumor cells and turned into their corresponding amines, dopamine and serotonin. Based on these characteristics of APUD system, ^{11}C-labelled and ^{18}F-labelled L-DOPA (^{11}C-L-DOPA, ^{18}F-L-DOPA) as well as 5-HTP (^{11}C-5-HTP, ^{18}F-5-HTP) have been developed to visualize NETs [62–64]. Their imaging performances are quite good and they can provide additional information for the diagnosis, staging, and management of NETs. One shortage is that nonfunctioning NETs cannot be detected using these tracers. Now they are employed as problem solving tools when other imaging technique results are negative or contradictory [29].

3. Somatostatin Receptor Based Therapy

Surgical treatment suffices for the majority of NETs, but malignant, recurrent, and metastatic tumors need further treatment in order to gain a lengthening of time to progression [65]. Systemic chemotherapy is currently used for patients with poorly differentiated NETs, whereas tumor response is difficult to be assessed as these tumors are not highly chemosensitive and spontaneous standstill or regression is noticed in the time course of tumor growth [66]. A limited number of studies have explored the role for the therapeutic use of external beam radiation therapy in malignant NETs [67]. SST analogs, predominantly octreotide and octreotate, suppressing hormone production, have improved symptoms as well as prognosis in tumors. But the employment of SST analogs must be weighed against the tachyphylaxis and the limited antitumor effects [68]. PRRT using radiolabeled SST analogs has proven to be an effective therapeutic option for NET patients with inoperable and/or metastasized diseases. SST analogs labeled with therapeutic radionuclides, such as ^{111}In, ^{90}Y, ^{177}Lu, and ^{213}Bi, are able to specifically bind to SSTRs on tumor cells and deliver an effective radiation dose to tumors with minimal damage to normal tissues [69].

3.1. Studies with [^{111}In-DTPA^{0}]octreotide. ^{111}In not only emits γ-radiation, which penetrates tissues easily and can be imaged by a γ-scanner, but also emits therapeutic Auger and conversion electrons that play an antiproliferative role in malignant tumors with a short to medium tissue penetration

Table 1: Tumor responses in patients with various NETs, treated with different radiolabeled SST analogs.

Ligand	Patient number	Tumor response				References
		CR	PR	SD	PD	
[^{111}In-DTPA^{0}]octreotide	26	0	2 (8%)	21 (81%)	3 (11%)	[71]
[^{111}In-DTPA^{0}]octreotide	18	0	2 (11%)	16 (89%)	0	[72]
^{90}Y-DOTATOC	116	5 (4%)	26 (22%)	72 (62%)	13 (11%)	[79]
^{90}Y-DOTATOC	41	1 (2%)	9 (22%)	25 (61%)	6 (15%)	[80]
^{177}Lu-DOTATATE	310	5 (2%)	86 (28%)	158 (51%)	61 (20%)	[81]
^{177}Lu-DOTATATE	26	3 (12%)	7 (27%)	12 (46%)	4 (15%)	[82]
^{90}Y-DOTATATE and ^{177}Lu-DOTATATE	26	2 (7.7%)	9 (34.6%)	11 (42.3%)	4 (15.4%)	[83]
^{213}Bi-DOTATOC	7	1 (14%)	2 (28%)	3 (44%)	n.a.	[36]

CR: complete remission; PR: partial remission; SD: stable disease; PD: progressive disease; n.a. not available.

[70]. Initial therapeutic studies [71, 72] performed with high radioactivity doses of [^{111}In-DTPA^{0}]octreotide in patients with metastatic NETs resulted in significant symptom relief but relatively few and short-lived objective tumor responses. These results are not unexpected since [^{111}In-DTPA^{0}]octreotide is not an ideal option for PRRT due to their small particle range of Auger electrons [73]. It has been recommended that SST analogs labeled with higher energy β-emitters, which, in reality, have obtained better response rates in various studies [74, 75], should be employed to treat SSTR positive tumors.

3.2. Studies with [^{90}Y-DOTA^{0}, Tyr^{3}]octreotide. ^{90}Yttrium (^{90}Y) is a β-particle emitter with a maximum energy of 2.3 MeV and a maximum range of 12 mm in tissue [76]. It is combined with a more stable chelator DOTA instead of DTPA and a modified SST analog octreotide to get a conjunction ^{90}Y-DOTATOC. This tracer has superior therapeutic efficacy since adequate dose of radiation can be delivered to tumors, especially larger tumor masses, to cause cell damage [77]. After 15 years of experience, PRRT with ^{90}Y-DOTATOC is generally well tolerated [78].

Forrer et al. selected 116 patients with metastatic NETs, who underwent PRRT with ^{90}Y-DOTATOC (5994–7400 MBq/m^2 body surface). All cases were positive in the scintigraphy. After the last administration, each patient was evaluated with respect to the therapeutic effects on tumor size. The objective response rate was found in 31 patients (26%), including 4% complete remission (CR) and 22% partial remission (PR). 72 patients (62%) showed stabilization of their diseases and the remaining patients (11%) were still progressive (Table 1). No serious side effects occurred and the toxicity was well tolerated [79]. A similar tumor response rate (24%, 2% of which were CR and 22% were PR) was found in a phase II study of 41 patients with GEP-NETs and bronchial tumors who were given intravenously four injections of a total of 6000 MBq ^{90}Y-DOTATOC (Table 1). Grade III pancytopenia was the most severe adverse event occurring in 5% patients [80]. It is not possible to state that ^{90}Y-DOTATOC is of great use for the management of inoperable and/or metastatic NETs when drawing conclusion from a relatively small sample. A study [84] conducted in a larger group of patients with a wide spectrum of NETs supplied more meaningful results. 1109 patients from 29 countries were treated with repeated cycles of ^{90}Y-DOTATOC. Morphologic response was found in 378 patients (34.1%) and stable disease (SD) in 58 patients (5.2%). The median survival from diagnosis was 94.6 months, which was longer than the expected 33-month survival. Longer survival was associated with morphologic, biochemical, and clinical response as well as high tumor uptake in pretherapeutic SRS. Among all the patients, 143 were subjected to severe hematologic toxicities and 102 to permanent renal toxicity.

Except mentioned studies, there are a large number of reported articles assessing the therapeutic effects of ^{90}Y-DOTATOC. Despite differences in protocols, the objective tumor responses in most of the studies with ^{90}Y-DOTATOC are in the same range, approximately 20–28% in patients with NETs and for patients with GEP-NETs in the range of 28–38% [85].

3.3. Studies with [^{177}Lu-DOTA^{0}-Tyr^{3}]octreotate. ^{177}Lutetium (^{177}Lu) is a median energy β-emitter (0.5 MeV) with small particle range [86]. This allows for higher radiation dose delivered to smaller tumors and less damage to surrounding tissues than the radionuclide ^{90}Y [87]. ^{177}Lu also emits γ rays; thus ^{177}Lu-labeled peptides can be used for treatment as well as for dosimetry and monitoring of tumor response. [DOTA^{0}, Tyr^{3}]octreotate (DOTATATE), which presents a ninefold increase in the affinity for SSTR2 compared with [DOTA^{0}, Tyr^{3}]octreotide [88], usually labeled with the radionuclide ^{177}Lu, has been widely used in PRRT. The results that were obtained with ^{177}Lu-DOTATATE are impressive in terms of tumor suppression and patient survival [17, 89].

An early clinical study [75] compared the therapeutic effects of ^{177}Lu-DOTATATE with [^{111}In-DTPA^{0}]octreotide in 6 patients with SSTR positive tumors. After 24 hours, the uptake of ^{177}Lu-DOTATATE was almost equal to that of [^{111}In-DTPA^{0}]octreotide for kidneys but was three- to fourfold higher for 4 of the analyzed tumors. Thus, ^{177}Lu-DOTATATE potentially represents an important improvement since the higher radiation doses can be delivered to

tumors with about equal doses to dose-limiting organs, especially kidneys. Latest data illustrated that, even with low radiation doses, ^{177}Lu-DOTATATE could have antitumor effects in advanced pancreatic NETs [82]. Fifty-two patients were assigned to the following two groups: full dosage (FD) group (25.5 GBq, $n = 26$) and reduced dosage (RD) group (17.8 GBq, $n = 26$). Both groups showed antitumor activity, with 12% CR, 27% PR, and 46% SD in the FD group (Table 1), while 4% CR, 15% PR, and 58% SD in the RD group. Although response rate was higher in FD, no significant difference was found. However, progression-free survival was significantly longer after injection of a total dose of 25.5 GBq, which is the preferential dosage in tolerated patients.

Since the physical properties of ^{90}Y suggest that this radionuclide will be more effective in larger tumor masses and ^{177}Lu in smaller tumor masses and metastases, the combination treatment of ^{90}Y- and ^{177}Lu-labeled SST analogs seems a reasonable option for managing tumors of varying sizes and SSTR subtypes. As expected, both preclinical and clinical researches have found higher tumor response rate through the combined therapy [83, 86]. Nevertheless, the optimal combination of two radiopharmaceuticals should be determined on a patient-specific basis. As discussed by a recent article [90], the absorbed dose to tumors shows huge interpatient variance, and renal toxicity should be particularly considered since the biologically effective dose to the kidneys of ^{177}Lu was lower compared with ^{90}Y.

3.4. Studies with α-Emitters. The application of α-emitters such as ^{213}Bi or its mother radionuclide ^{225}Ac is arousing immense interest in PRRT. These radionuclides emit higher energy (8.32 MeV for ^{213}Bi and 27.5 MeV for ^{225}Ac) compared with β-emitters and had a short path-length of only 40–50 μm, which increases the local antitumor effect without affecting untargeted tissues [90]. Alpha radiation can cause double-strand DNA breaks, independent of the cell cycle phase and oxygen concentration [91, 92]. Although PRRT with ^{90}Y- and ^{177}Lu-labeled SST analogs has been promising for NET therapy, some tumors are not radiosensitive to this treatment. SST analogs labeled with α-emitting isotopes may provide an alternative therapy for metastatic, chemoresistant, and hypoxic NETs, which are known to be resistant to PRRT with β-emitting radionuclides. A number of preclinical studies [93–95] have shown the potency and limited toxicity of targeted α therapy in NETs, while clinical trials were seldom studied. Recently, for the first time ^{213}Bi-DOTATOC was used to treat patients with metastatic NETs refractory to therapy with ^{90}Y/^{177}Lu-DOTATOC [36]. Enduring responses were observed in all treated patients during follow-up for more than 2 years (Figure 4; Table 1). The side effects only include moderate chronic kidneys toxicity and favorable acute haematotoxicity. Nevertheless, α radiation with high linear energy transfer may lead to various and less repairable clustered damage, which may further induce secondary neoplasm formation [96]. Also it is unclear whether α-emitting radionuclides are superior to β-emitting radionuclides. Therefore, the therapeutic effects and safety should be further confirmed before α therapy can be well translated to clinical application.

4. Gene Transfection with hSSTr2

As previously presented, SSTR based imaging and therapy have made a great contribution to the diagnosis and treatment of NETs. However, many SSTR negative or weakly positive tumors, like non-small-cell lung cancer (NSCLC) [20], ovarian cancer [97], malignant glioma [98], and pancreatic cancer [18], are facing a big challenge in therapy. Surgery, chemotherapy, radiotherapy, or the combined therapy modalities have limited effects on improving overall survival. Most patients diagnosed with these tumors will ultimately suffer from recurrent diseases, resist further treatment, and eventually die of their diseases [99].

Over the past two decades, gene therapy has been applied in a number of malignant tumors and appears to be a safe and effective method for treatment. The TK gene, which is a suicide gene from herpes simplex virus (HSV), was widely studied. When HSV-TK is transfected into tumor cells in combination with intravenous ganciclovir, the antitumor efficacy is achieved through converting ganciclovir into a triphosphate configuration, which inhibits DNA synthesis and induces cell apoptosis [100]. Although noninvasive imaging of transferred gene expression has proven available following vector-mediated transfer of the HSV-TK using radiolabeled tracers, some studies [98, 101] found that hSSTr2 reporter based imaging was more sensitive and the uptake of radiolabeled SST analogs well correlated with recombinant vector dose. Moreover, SST analogs labeled with therapeutic radionuclides can be specifically delivered to transfected tumors, which provides an alternative approach to conventional therapeutics for SSTR negative or weakly positive tumors [102]. Since SSTR2 has been known to be most commonly expressed in various NETs and possesses the highest affinity for natural SST and synthetic SST analogs, most experiments utilize hSSTr2 reporter gene to transfect targeted tumor cells alone or together with other therapeutic genes.

In order to improve hSSTr2 gene transfer efficiency, it is critical to choose a vector with powerful infectivity. So far, different vector systems, mainly including adenovirus (Ad), retrovirus, adenoassociated virus, and vaccinia virus, have been employed in various tumor models [98, 109]. Ad remains the most frequently used and most promising virus for gene delivery because it has many advantageous features such as keeping itself stability, acquiring high titers, infecting a wide range of dividing cells as well as nondividing cells, permitting the high level expression of transferred gene, and maintaining a clear separation between viral genome and host chromosomes [103, 111]. Yet, a shortage that Ad depends on the coxsackie Ad receptor (CAR) to enter cells dramatically affects the transfection efficiency because many primary tumors do not express CAR [112]. Various approaches like genetic, chemical, and nonchemical modifications have been taken to retarget Ad vectors to other receptors [104]. The advantages and disadvantages of other main viral vectors used to transfer hSSTr2 are presented in Table 2.

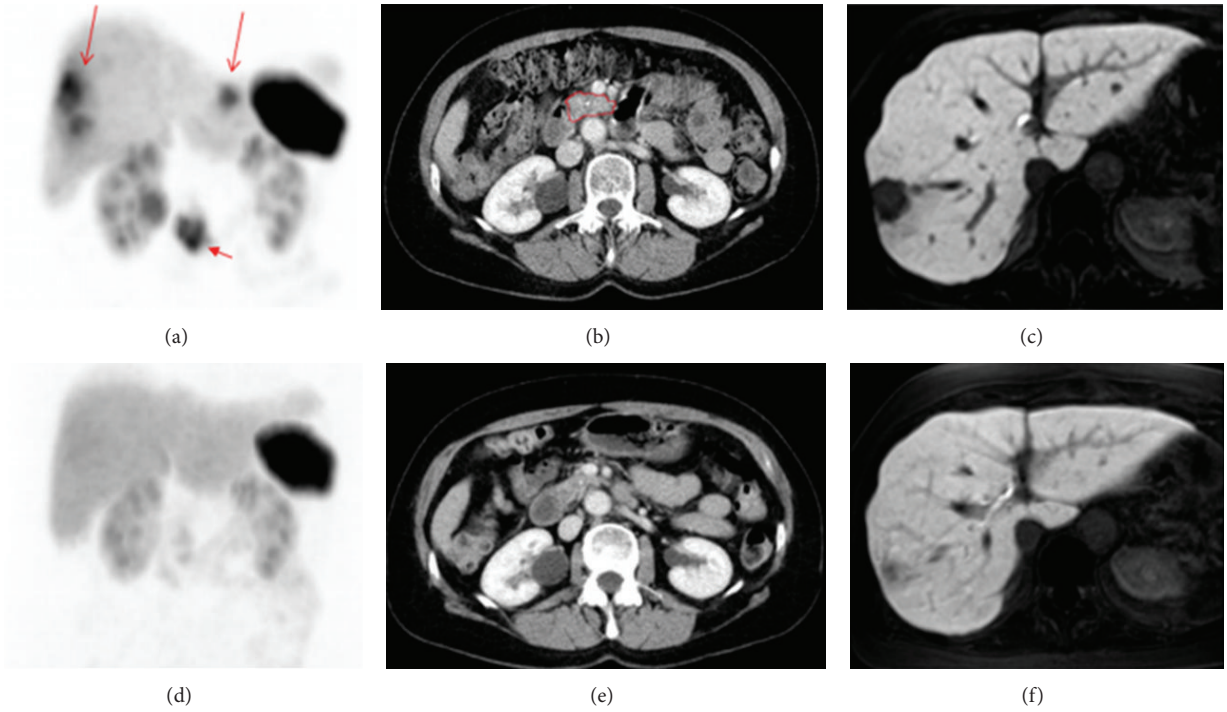

FIGURE 4: Patient 5 before therapy ((a)–(c)) and after three cycles of ^{213}Bi-DOTATOC ((d)–(f)) to a dose of 4 GBq. (a) Beta-resistant residuals in the liver (long arrows) and primary tumor (short arrow) are present in the ^{68}Ga-DOTATOC PET maximum intensity projection image. (b) Contrast enhanced CT image with the primary tumor outlined in red. (c) In the MR image with hepatocyte-specific contrast medium, the liver metastases appear as black cavities against the enhancing normal liver parenchyma. ((d)–(f)) After three cycles of ^{213}Bi-DOTATOC to a dose of 4 GBq, the lesions have diminished on the PET image (d) and CT image (e). Also on the MR image (f), the residual lesion has almost disappeared as shown by the growth of normal hepatocytes demonstrated by the uptake of the hepatocyte-specific contrast medium [36].

5. Somatostatin Receptor Based Reporter Gene Imaging

Although gene therapy in various animal models has acquired encouraging results, many obstacles should be overcome before gene therapy can be well translated to clinical trials [113]. One obstacle is how to make sure that gene transfer occurs in targeted tissues. Some studies have tried to use optical imaging and biopsy to detect the expression levels of transferred genes. However, poor tissue penetration of light-based reporter systems [20] and invasive damage of biopsies [28] hamper a comprehensive assessment of the magnitude and time course of gene expression. Nuclear imaging based on hSSTr2 reporter gene transfer can get rid of these limitations. The hSSTr2 based reporter system has been utilized in a variety of tumor studies both *in vitro* and *in vivo* to estimate its ability to image gene transfer. A study [20] hoped to assess whether hSSTr2 is competent to act as a reporter of gene transfer. It used Ad encoding hemagglutinin A and SSTR2 (Ad-CMV-HA-hSSTr2) or control virus to transfect NSCLC cell lines and tumors bearing nude mice. As a result, the radiopeptide [^{111}In-DTPA^{0}]octreotide could specifically bind to tumor cells after Ad-CMV-HA-hSSTr2 transfection and the uptake of tracers in Ad-CMV-HA-hSSTr2 transfected tumors was higher than that of control groups. Similar results were reported by an article [19] which observed the expression of hSSTr2 originating from Ad5-mediated gene transfer to non-small-cell lung tumors with ^{99m}Tc- or ^{88}Re-labeled peptides (Figure 5). The article even calculated the approximate number of SSTR2 expressed per Ad5-transfected cell through the uptake of radiolabeled peptides, which provided more accurate information of gene expression. Except NSCLC, hSSTr2 reporter system was adopted to monitor the duration and time course of gene expression in other transfected tumors, including ovarian cancer [24], malignant glioma [98], and fibroblastoma [114], as well as normal tissues like muscle and liver [30]. All these laboratory results were so encouraging that hSSTr2 reporter gene system was applied to clinical trials. Kim et al. conducted a phase I clinical trial of Ad5.SSTR/TK.RGD in patients with recurrent gynecologic cancer [99]. The Ad vector not only contains the therapeutic gene TK but also contains the hSSTr2 reporter gene which allows for noninvasive and repetitive gene transfer imaging with [^{111}In-DTPA^{0}]octreotide. Compared to imaging before Ad-mediated gene therapy, significantly increased uptake of [^{111}In-DTPA^{0}]octreotide was found in patients after the last administration in the highest Ad dose group. All these studies indicate that the hSSTr2 reporter based imaging is a promising method to track gene delivery and expression. The detailed functions of hSSTr2 reporter gene based imaging are demonstrated below: repetitively observing the magnitude,

Table 2: The advantages and disadvantages of main viral vectors used to transfer hSSTr2.

Vectors	Advantages	Disadvantages	References
Adenovirus	(1) Stability (2) High titers (3) Infecting dividing and nondividing cells (4) High level expression of transgene (5) Not integrating into host chromosome	(1) Strong immune response (2) Potential replication competence (3) Short-term expression (4) Demanding packaging cell line (5) Small insert size (6) No targeting	[103–105]
Adenoassociated virus	(1) No associated disease (2) Long-term gene expression (3) Integrating into human chromosome 19	(1) Extensive antiviral immunity (2) Helper-dependent replication (3) Poor host tropism (4) Small insert size: about 5 kb	[106]
Retrovirus	(1) Integrating into host cell genome (2) Reverse transcription of the RNA genome (3) Infecting dividing cells (4) Long-term expression (5) Fairly high titers	(1) Immune-related toxicity (2) Infecting dividing cells (3) Potential replication competence (4) Insertion mutation (5) No targeting	[107, 108]
Vaccinia virus	(1) Cytolytic viral vector (2) Preferentially infecting rapid dividing cells (3) Difficult to leak from normal vasculature (4) The vector itself serving as a therapeutic method (5) Large insert size: ≥25 kb DNA	(1) Live infectious lytic virus (2) Replication competence (3) Short-term gene expression (4) Postvaccinal encephalitis and progressive complications (5) No targeting	[109, 110]

duration, and time variation of gene expression both *in vitro* and *in vivo* [30], studying the biodistribution of gene transfer vector in mice or patients [25], optimizing the administration dose of vector encoding hSSTr2 reporter gene and/or other therapeutic genes [24], predicting treatment response of transfected tumor to PRRT [21], and monitoring antitumor effects of various treatments including hSSTr2 gene or another therapeutic gene based therapy [21, 99].

6. Somatostatin Receptor Based Reporter Gene Therapy

In addition to reporter based imaging, the hSSTr2 can serve as a therapeutic gene to cause tumor regression alone or together with other treatments [115]. As mentioned above, the prognosis of many malignant tumors is poor no matter what therapeutic methods are given. It is badly in need of new therapeutic approaches to treating these tumors. Impressive response of NET leading to improved survival has been observed with PRRT [116], which, however, is only suitable for tumors showing SSTR expression, but not for SSTR negative tumors. Fortunately, it is feasible to induce SSTR negative tumors to express SSTRs by means of gene transfer technology, which provides a novel therapy for some malignant tumors [22, 98, 117].

6.1. Therapy Studies with the Vector Encoding the Single hSSTr2 Gene. In a therapeutic study [22], Zhao et al. evaluated the antitumor effects of ^{188}Re-RC-160 (^{188}Re-labeled SST analog) on A549 tumor, which is one kind of lung adenocarcinomas, transfected with plasmid pcDNA3 encoding hSSTr2 reporter gene. Nude mice bearing pcDNA3-hSSTr2 transfected tumors were divided into five groups according to different therapeutic protocols. Finally, the tumor growth inhibition in the single dose treatment group (7.4 MBq, ^{188}Re-RC-160) was significantly higher than that in ^{188}Re group (2 × 7.4 MBq), RC-160 group, and saline control group. Moreover, two-injection group (2 × 7.4 MBq, ^{188}Re-RC-160) led to significantly increased tumor growth inhibition compared with the single dose treatment group. These results provided a preliminary proof that SSTR negative tumor could be transfected with hSSTr2 reporter gene for radionuclide therapy. One problem observed in the present study was the low transfection efficiency. In fact, viral vectors have become the major vehicle to deliver hSSTr2 reporter gene. Although the drawbacks of viral vectors, especially immune response, are inevitable, transfection rate is fairly higher than that of nonviral vehicles and gene expression within tumors is relatively stable [118].

Reconstructed Ad encoding hSSTr2 gene (Ad-hSSTr2) was utilized in a study [119] to explore the therapeutic effects of [^{90}Y]-SMT 487 ([^{90}Y]-DOTA-$_{D}$-Phe^{1}-Tyr^{3}-octreotide) on transfected tumors. Mice bearing non-small-cell lung tumors were intratumorally injected two doses of Ad-hSSTr2 (1 week apart) and intravenously administrated four doses of 14.8 MBq [^{90}Y]-SMT 487 or four doses of 18.5 MBq [^{90}Y]-SMT 487 with median tumor quadrupling times of respective 40 and 44 days, while in untreated group and the group that received only four doses of 18.5 MBq [^{90}Y]-SMT 487 without virus, the median tumor quadrupling times were 16 and 25 days, respectively. Significant difference in time to tumor quadrupling between the groups that received Ad-CMV-hSSTr2 plus [^{90}Y]-SMT 487 and the control groups was revealed by the log-rank test. The hSSTr2/[^{90}Y]-SMT 487 system is a potential approach for clinical application, since both Ad vector encoding hSSTr2 gene and [^{90}Y]-SMT 487 have been used for cancer therapy in clinical trials.

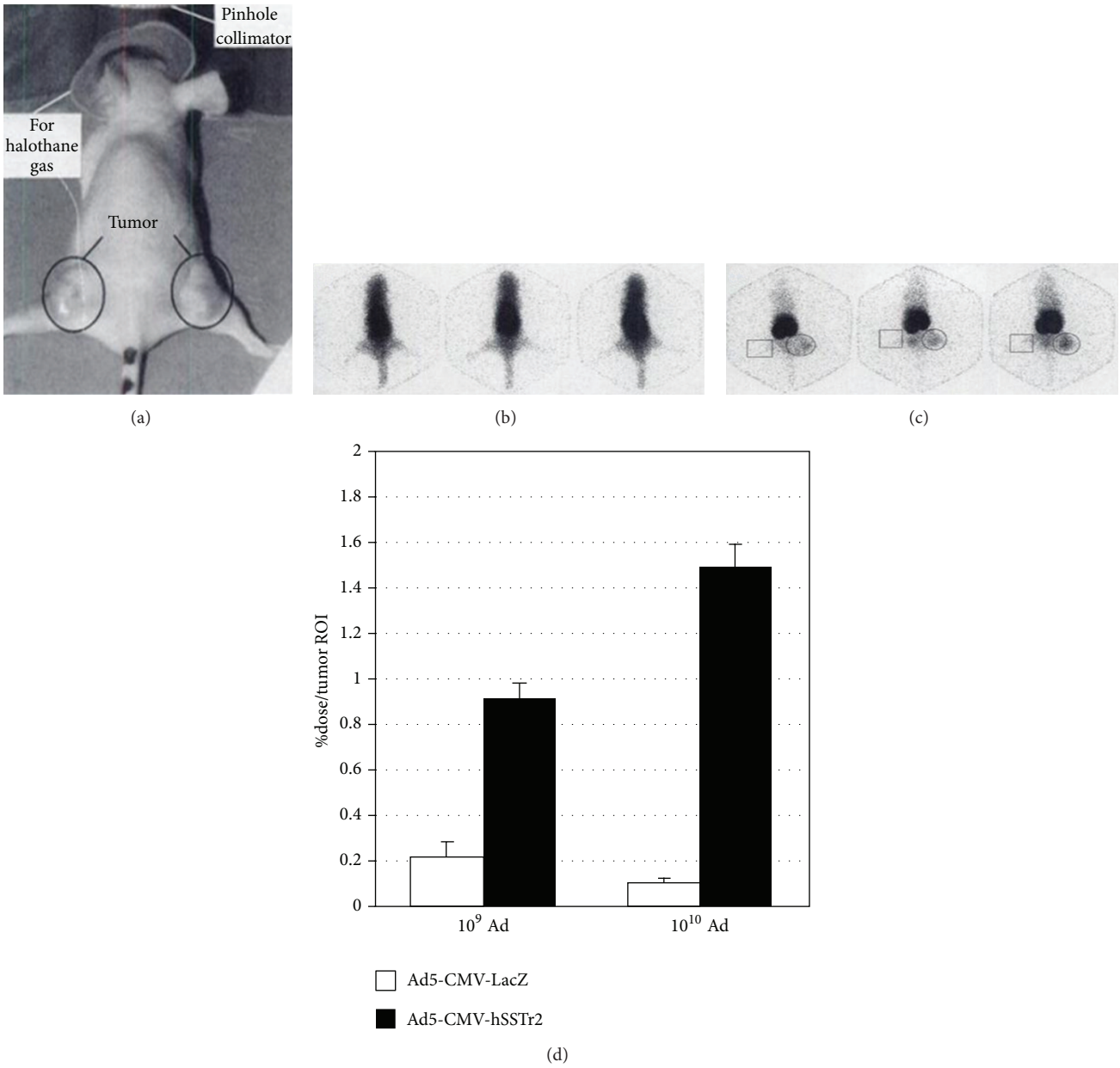

FIGURE 5: γ camera imaging of mice injected with ^{99m}Tc-labeled SST analogs. Imaging position is shown in (a), with 3 representative images of mice at 3 minutes (b) and 3 hours (c) after intravenous injection. Circles in (c) indicate location of human A427 tumors injected 48 h earlier with Ad5-CMV-hSSTr2, and squares indicate human A427 tumors injected 48 h earlier with Ad5-CMV-LacZ. (d) Results of region of interest analyses [19]. A427 tumors: human non-small-cell lung cancer, hSSTr2 negative Ad5-CMV-LacZ: Ad encoding *Escherichia coli* β-galactosidase under control of the CMV promoter element.

6.2. Therapy Studies with the Bicistronic Vector Encoding Both hSSTr2 and CD Genes. Gene therapy vectors containing both hSSTr2 reporter gene and a second therapeutic gene encoding TK or CD have been investigated [21, 99]. The hSSTr2 is available not only for noninvasive imaging of the expression of transferred gene, but also for radionuclide therapy [21]. A synergistic therapeutic effect may be achieved through the combined gene therapy. In view of the toxicity that resulted from the combination treatment of radiolabeled peptide and TK gene [34], the hSSTr2/CD system received considerable attention. Mechanisms of CD gene based therapy are that CD specifically converts the prodrug 5-FC to the highly toxic 5-FU, which disturbs DNA synthesis and induces cell death [120].

NSCLC A549 cells transfected by the bicistronic plasmid pCD-IRES-hSSTR2 (pCIS) were induced to express both SSTR2 and CD. Then 3×10^6 pCIS-A549 cells were injected subcutaneously into each nude mouse on the right axilla and the same number of control A549 cells on the contralateral axillary regions of the same mouse to establish a xenograft

tumor model. When tumors grew to an average diameter of 1cm, mice ($n = 6$) were intravenously injected with ^{99m}Tc-RC-160, which specifically bound to pCIS-A549 cell-derived tumors. To study a synergistic inhibitory effect on tumor growth, ^{131}I-RC-160 and 5-FC were injected alone or together into mice bearing tumors via their tail veins. The results showed that the combination treatment of those two agents inhibited pCIS-A549 cell-derived tumor growth significantly more than ^{131}I-RC-160 or 5-FC treatment alone did [21]. These findings suggest that hSSTr2 reporter based therapy can combine with prodrug gene therapy to achieve enhanced antitumor effect and provides a novel treatment for lung cancer.

7. Conclusion

At present there are a number of tracers available for NET imaging. Their uptake is dependent upon different biological mechanisms, predominantly the expressions of SSTRs on tumor cell membranes. SRS with [^{111}In-DTPA^{0}]octreotide has played an important role in the diagnosis and staging of NETs. With the advent of PET technique, positron-emitting tracers were developed and seem to be more encouraging. ^{68}Ga-DOTA-peptides used for PET or PET/CT imaging are hopeful of being routinely utilized to visualize NETs. PRRT is a most promising therapy for patients with inoperable and/or metastasized NETs. Treatment with ^{90}Y-DOTATOC and ^{177}Lu-DOTATATE has been shown to be relatively safe, and most patients had high objective tumor response after the therapy, especially the combined treatment of the two radiopeptides. In addition, hSSTr2 reporter gene based imaging and therapy are feasible in SSTR negative or weakly positive tumors by means of gene transfer technique. Radiolabeled SST analogs can be delivered to transfected tumors, which provides a new specific approach to imaging gene expressions and killing tumor cells. Furthermore, a synergistic therapeutic effect can be achievable by dual gene transfer of hSSTr2 reporter gene and a second therapeutic gene such as TK or CD gene. Though excellent results have been achieved with regard to hSSTr2 reporter gene based imaging and radionuclide therapy in SSTR negative or weakly positive tumors, additional preclinical and especially translational and clinical researches are needed to obtain further proof of value.

Abbreviations

SST: Somatostatin
SSTR: Somatostatin receptor
SSTR2: Somatostatin receptor subtype 2
NETs: Neuroendocrine tumors
hSSTr2: Human somatostatin receptor subtype 2
GEP-NET: Gastroenteropancreatic neuroendocrine tumor
SRS: Somatostatin receptor scintigraphy
PET: Positron emission tomography
PRRT: Peptide receptor radionuclide therapy
SPECT: Single photon computed emission tomography
TK: Thymidine kinase
CD: Cytosine deaminase
CT: Computed tomography
MRI: Magnetic resonance imaging
WB DWI: Whole-body diffusion-weighted MR imaging
APUD: Amine precursor uptake and decarboxylation
CR: Complete remission
PR: Partial remission
SD: Stable disease
PD: Progressive disease
NSCLC: Non-small-cell lung cancer
HSV: Herpes simplex virus
Ad: Adenovirus
CAR: Coxsackie adenovirus receptor.

Conflict of Interests

The authors declare that they have no conflict of interests.

Acknowledgments

This work is partly sponsored by National Science Foundation of China (no. 30672396) and Zhejiang Provincial Program for the Cultivation of High-level Innovative Health Talents.

References

[1] D. Cuevas-Ramos and M. Fleseriu, "Somatostatin receptor ligands and resistance to treatment in pituitary adenomas," *Journal of Molecular Endocrinology*, vol. 52, no. 3, pp. R223–R240, 2014.

[2] A. Sundin, U. Garske, and H. Örlefors, "Nuclear imaging of neuroendocrine tumours," *Best Practice and Research: Clinical Endocrinology & Metabolism*, vol. 21, no. 1, pp. 69–85, 2007.

[3] S. W. J. Lamberts, E. P. Krenning, and J.-C. Reubi, "The role of somatostatin and its analogs in the diagnosis and treatment of tumors," *Endocrine Reviews*, vol. 12, no. 4, pp. 450–482, 1991.

[4] L. C. Sun and D. H. Coy, "Somatostatin receptor-targeted anticancer therapy," *Current Drug Delivery*, vol. 8, no. 1, pp. 2–10, 2011.

[5] M. C. Frühwald, M. S. O'Dorisio, T. Pietsch, and J. C. Reubi, "High expression of somatostatin receptor subtype 2 (sst_2) in medulloblastoma: implications for diagnosis and therapy," *Pediatric Research*, vol. 45, no. 5, part 1, pp. 697–708, 1999.

[6] M. Volante, R. Rosas, E. Allìa et al., "Somatostatin, cortistatin and their receptors in tumours," *Molecular and Cellular Endocrinology*, vol. 286, no. 1-2, pp. 219–229, 2008.

[7] M. Theodoropoulou and G. K. Stalla, "Somatostatin receptors: from signaling to clinical practice," *Frontiers in Neuroendocrinology*, vol. 34, no. 3, pp. 228–252, 2013.

[8] I. Virgolini, T. Traub, M. Leimer et al., "New radiopharmaceuticals for receptor scintigraphy and radionuclide therapy," *Quarterly Journal of Nuclear Medicine*, vol. 44, no. 1, pp. 50–58, 2000.

[9] M. Sorschag, P. Malle, and H.-J. Gallowitsch, "Nuclear medicine in NET," *Wiener Medizinische Wochenschrift*, vol. 162, no. 19-20, pp. 416–422, 2012.

[10] T. Shah, I. Kulakiene, A.-M. Quigley et al., "The role of 99mTc-depreotide in the management of neuroendocrine tumours," *Nuclear Medicine Communications*, vol. 29, no. 5, pp. 436–440, 2008.

[11] I. Virgolini, I. Szilvasi, A. Kurtaran et al., "Indium-111-DOTA-lanreotide: biodistribution, safety and radiation absorbed dose in tumor patients," *Journal of Nuclear Medicine*, vol. 39, no. 11, pp. 1928–1936, 1998.

[12] M. Gabriel, C. Decristoforo, D. Kendler et al., "68Ga-DOTA-Tyr3-octreotide PET in neuroendocrine tumors: comparison with somatostatin receptor scintigraphy and CT," *Journal of Nuclear Medicine*, vol. 48, no. 4, pp. 508–518, 2007.

[13] E. C. Etchebehere, A. de Oliveira Santos, B. Gumz et al., "68Ga-DOTATATE PET/CT, 99mTc-HYNIC-octreotide SPECT/CT, and whole-body MR imaging in detection of neuroendocrine tumors: a prospective trial," *Journal of Nuclear Medicine*, vol. 55, no. 10, pp. 1598–1604, 2014.

[14] P. Sharma, S. Arora, A. Mukherjee et al., "Predictive value of 68Ga-DOTANOC PET/CT in patients with suspicion of neuroendocrine tumors: is its routine use justified?" *Clinical Nuclear Medicine*, vol. 39, no. 1, pp. 37–43, 2014.

[15] D. J. Kwekkeboom, W. W. de Herder, C. H. J. van Eijck et al., "Peptide receptor radionuclide therapy in patients with gastroenteropancreatic neuroendocrine tumors," *Seminars in Nuclear Medicine*, vol. 40, no. 2, pp. 78–88, 2010.

[16] M. A. Muros, M. Varsavsky, P. Iglesias Rozas et al., "Outcome of treating advanced neuroendocrine tumours with radiolabelled somatostatin analogues," *Clinical and Translational Oncology*, vol. 11, no. 1, pp. 48–53, 2009.

[17] S. Khan, E. P. Krenning, M. Van Essen, B. L. Kam, J. J. Teunissen, and D. J. Kwekkeboom, "Quality of life in 265 patients with gastroenteropancreatic or bronchial neuroendocrine tumors treated with [177Lu-DOTA0,Tyr3]octreotate," *Journal of Nuclear Medicine*, vol. 52, no. 9, pp. 1361–1368, 2011.

[18] L. Buscail, N. Saint-Laurent, E. Chastre et al., "Loss of sst2 somatostatin receptor gene expression in human pancreatic and colorectal cancer," *Cancer Research*, vol. 56, no. 8, pp. 1823–1827, 1996.

[19] K. R. Zinn, D. J. Buchsbaum, T. R. Chaudhuri, J. M. Mountz, W. E. Grizzle, and B. E. Rogers, "Noninvasive monitoring of gene transfer using a reporter receptor imaged with a high-affinity peptide radiolabeled with 99mTc or 188Re," *Journal of Nuclear Medicine*, vol. 41, no. 5, pp. 887–895, 2000.

[20] S. P. Singh, L. Han, R. Murali et al., "SSTR2-based reporters for assessing gene transfer into non-small cell lung cancer: evaluation using an intrathoracic mouse model," *Human Gene Therapy*, vol. 22, no. 1, pp. 55–64, 2011.

[21] M. Yuan, J. Wang, J. Deng et al., "Combination therapy in A549 cells," *Nuclear Medicine and Biology*, vol. 37, no. 3, pp. 317–326, 2010.

[22] R. Zhao, W. Yang, Z. Wang, G. Li, W. Qin, and J. Wang, "Treatment of transplanted tumor of lung adenocarcinoma A549 transfected by human somatostatin receptor subtype 2 (hsstr2) gene with 188Re-RC-160," *Nuclear Medicine and Biology*, vol. 37, no. 8, pp. 977–987, 2010.

[23] H. Zhang, M. A. Moroz, I. Serganova et al., "Imaging expression of the human somatostatin receptor subtype-2 reporter gene with 68Ga-DOTATOC," *Journal of Nuclear Medicine*, vol. 52, no. 1, pp. 123–131, 2011.

[24] B. E. Rogers, S. F. McLean, R. L. Kirkman et al., "In vivo localization of [111In]-DTPA-D-Phe1-octreotide to human ovarian tumor xenografts induced to express the somatostatin receptor subtype 2 using an adenoviral vector," *Clinical Cancer Research*, vol. 5, no. 2, pp. 383–393, 1999.

[25] B. E. Rogers, J. J. Parry, R. Andrews, P. Cordopatis, B. A. Nock, and T. Maina, "MicroPET imaging of gene transfer with a somatostatin receptor-based reporter gene and 94mTc-demotate 1," *Journal of Nuclear Medicine*, vol. 46, no. 11, pp. 1889–1897, 2005.

[26] K. Meyer, J.-C. Irminger, L. G. Moss et al., "Sorting human β-cells consequent to targeted expression of green fluorescent protein," *Diabetes*, vol. 47, no. 12, pp. 1974–1977, 1998.

[27] S. Bhaumik, X. Z. Lewis, and S. S. Gambhir, "Optical imaging of *Renilla* luciferase, synthetic *Renilla* luciferase, and firefly luciferase reporter gene expression in living mice," *Journal of Biomedical Optics*, vol. 9, no. 3, pp. 578–586, 2004.

[28] K. Okuwaki, M. Kida, T. Mikami et al., "Clinicopathologic characteristics of pancreatic neuroendocrine tumors and relation of somatostatin receptor type 2A to outcomes," *Cancer*, vol. 119, no. 23, pp. 4094–4102, 2013.

[29] A. Sundin, "Radiological and nuclear medicine imaging of gastroenteropancreatic neuroendocrine tumours," *Best Practice and Research: Clinical Gastroenterology*, vol. 26, no. 6, pp. 803–818, 2012.

[30] G. Cotugno, M. Aurilio, P. Annunziata et al., "Noninvasive repetitive imaging of somatostatin receptor 2 gene transfer with positron emission tomography," *Human Gene Therapy*, vol. 22, no. 2, pp. 189–196, 2011.

[31] R. Cescato, S. Schulz, B. Waser et al., "Internalization of sst2, sst3, and sst5 receptors: effects of Somatostatin agonists and antagonists," *Journal of Nuclear Medicine*, vol. 47, no. 3, pp. 502–511, 2006.

[32] J. C. Reubi, B. Waser, R. Cescato, B. Gloor, C. Stettler, and E. Christ, "Internalized somatostatin receptor subtype 2 in neuroendocrine tumors of octreotide-treated patients," *Journal of Clinical Endocrinology and Metabolism*, vol. 95, no. 5, pp. 2343–2350, 2010.

[33] C. Fottner, E. Mettler, M. Goetz et al., "In vivo molecular imaging of somatostatin receptors in pancreatic islet cells and neuroendocrine tumors by miniaturized confocal laser-scanning fluorescence microscopy," *Endocrinology*, vol. 151, no. 5, pp. 2179–2188, 2010.

[34] D. J. Buchsbaum, T. R. Chaudhuri, and K. R. Zinn, "Radiotargeted gene therapy," *Journal of Nuclear Medicine*, vol. 46, supplement 1, pp. 179s–186s, 2005.

[35] I. Velikyan, A. Sundin, J. Sörensen et al., "Quantitative and qualitative intrapatient comparison of 68Ga-DOTATOC and 68Ga-DOTATATE: net uptake rate for accurate quantification," *Journal of Nuclear Medicine*, vol. 55, no. 2, pp. 204–210, 2014.

[36] C. Kratochwil, F. L. Giesel, F. Bruchertseifer et al., " ^{213}Bi-DOTATOC receptor-targeted alpha-radionuclide therapy induces remission in neuroendocrine tumours refractory to beta radiation: a first-in-human experience," *European Journal of Nuclear Medicine and Molecular Imaging*, vol. 41, no. 11, pp. 2106–2119, 2014.

[37] K. K. Wong, R. T. Waterfield, M. C. Marzola et al., "Contemporary nuclear medicine imaging of neuroendocrine tumours," *Clinical Radiology*, vol. 67, no. 11, pp. 1035–1050, 2012.

[38] D. J. Kwekkeboom, B. L. Kam, M. van Essen et al., "Somatostatin receptor-based imaging and therapy of gastroenteropancreatic neuroendocrine tumors," *Endocrine-Related Cancer*, vol. 17, no. 1, pp. R53–R73, 2010.

[39] L. Shan, "^{18}F-Fluoroethyl triazole-βAG-[(D)-Phe^1-c(Cys^2-Tyr^3-(D)-Trp^4-Lys^5-Thr^6-Cys^7)Thr^8]," in *Molecular Imaging and Contrast Agent Database (MICAD)*, National Center for Biotechnology Information, Bethesda, Md, USA, 2004.

[40] E. Bombardieri, M. Maccauro, E. De Deckere, G. Savelli, and A. Chiti, "Nuclear medicine imaging of neuroendocrine tumours," *Annals of Oncology*, vol. 12, supplement 2, pp. S51–S61, 2001.

[41] E. Ur, J. Bomanji, S. J. Mather et al., "Localization of neuroendocrine tumours and insulinomas using radiolabelled somatostatin analogues, 123I-Tyr3-octreotide and 111In-pentatreotide," *Clinical Endocrinology*, vol. 38, no. 5, pp. 501–506, 1993.

[42] R. Srirajaskanthan, I. Kayani, A. M. Quigley, J. Soh, M. E. Caplin, and J. Bomanji, "The role of 68Ga-DOTATATE PET in patients with neuroendocrine tumors and negative or equivocal findings on 111In-DTPA-octreotide scintigraphy," *Journal of Nuclear Medicine*, vol. 51, no. 6, pp. 875–882, 2010.

[43] G. Hildebrandt, K. Scheidhauer, C. Luyken et al., "High sensitivity of the in vivo detection of somatostatin receptors by111Indium (DTPA-octreotide)-scintigraphy in meningioma patients," *Acta Neurochirurgica*, vol. 126, no. 2-4, pp. 63–71, 1994.

[44] R. Lebtahi, J. le Cloirec, C. Houzard et al., "Detection of neuroendocrine tumors: 99mTc-P829 scintigraphy compared with 111In-pentetreotide scintigraphy," *Journal of Nuclear Medicine*, vol. 43, no. 7, pp. 889–895, 2002.

[45] G. G. Bural, F. Lieberman, and J. M. Mountz, "Use of 111in-pentetreotide scan in a subject with treatment refractory atypical meningioma," *Clinical Nuclear Medicine*, vol. 39, no. 4, pp. 342–345, 2014.

[46] E. Bombardieri, V. Ambrosini, C. Aktolun et al., "111In-pentetreotide scintigraphy: procedure guidelines for tumour imaging," *European Journal of Nuclear Medicine and Molecular Imaging*, vol. 37, no. 7, pp. 1441–1448, 2010.

[47] M. Pavel, E. Baudin, A. Couvelard et al., "ENETS consensus guidelines for the management of patients with liver and other distant metastases from neuroendocrine neoplasms of foregut, midgut, hindgut, and unknown primary," *Neuroendocrinology*, vol. 95, no. 2, pp. 157–176, 2012.

[48] U.-F. Pape, A. Perren, B. Niederle et al., "ENETS consensus guidelines for the management of patients with neuroendocrine neoplasms from the jejuno-ileum and the appendix including goblet cell carcinomas," *Neuroendocrinology*, vol. 95, no. 2, pp. 135–156, 2012.

[49] E. M. Blanchet, V. Martucci, and K. Pacak, "Pheochromocytoma and paraganglioma: current functional and future molecular imaging," *Frontiers in Oncology*, vol. 1, article 58, 2012.

[50] W. Xia, X. Zhang, F. Yu et al., "Experimental study of 99mTc-depreotide preparation and its affinity with A549 cell," *Frontiers in Bioscience*, vol. 16, no. 7, pp. 2527–2539, 2011.

[51] R. Axelsson, G. Herlin, M. Bth, P. Aspelin, and K. G. Kölbeck, "Role of scintigraphy with technetium-99m depreotide in the diagnosis and management of patients with suspected lung cancer," *Acta Radiologica*, vol. 49, no. 3, pp. 295–302, 2008.

[52] M. Rodrigues, S. Li, M. Gabriel, D. Heute, M. Greifeneder, and I. Virgolini, "^{99m}Tc-depreotide scintigraphy versus ^{18}F-FDG-PET in the diagnosis of radioiodine-negative thyroid cancer," *Journal of Clinical Endocrinology and Metabolism*, vol. 91, no. 10, pp. 3997–4000, 2006.

[53] B. van den Bossche, S. van Belle, F. de Winter, A. Signore, and C. Van De Wiele, "Early prediction of endocrine therapy effect in advanced breast cancer patients using 99mTc-depreotide scintigraphy," *Journal of Nuclear Medicine*, vol. 47, no. 1, pp. 6–13, 2006.

[54] A. Asnacios, F. Courbon, P. Rochaix et al., "Indium-111-pentetreotide scintigraphy and somatostatin receptor subtype 2 expression: new prognostic factors for malignant well-differentiated endocrine tumors," *Journal of Clinical Oncology*, vol. 26, no. 6, pp. 963–970, 2008.

[55] T. Belhocine, J. Foidart, P. Rigo et al., "Fluorodeoxyglucose positron emission tomography and somatostatin receptor scintigraphy for diagnosing and staging carcinoid tumours: correlations with the pathological indexes p53 and Ki-67," *Nuclear Medicine Communications*, vol. 23, no. 8, pp. 727–734, 2002.

[56] I. Kayani, J. B. Bomanji, A. Groves et al., "Functional imaging of neuroendocrine tumors with combined PET/CT using 68Ga-DOTATATE (Dota-DPhe1, Tyr3-octreotate) and 18F-FDG," *Cancer*, vol. 112, no. 11, pp. 2447–2455, 2008.

[57] D. Wild, H. R. Mäcke, B. Waser et al., "68Ga-DOTANOC: a first compound for PET imaging with high affinity for somatostatin receptor subtypes 2 and 5," *European Journal of Nuclear Medicine and Molecular Imaging*, vol. 32, no. 6, p. 724, 2005.

[58] P. Sharma, S. Arora, V. S. Dhull et al., "Evaluation of (68)Ga-DOTANOC PET/CT imaging in a large exclusive population of pancreatic neuroendocrine tumors," *Abdominal Imaging*, vol. 40, no. 2, pp. 299–309, 2015.

[59] C. B. Johnbeck, U. Knigge, and A. Kjær, "PET tracers for somatostatin receptor imaging of neuroendocrine tumors: current status and review of the literature," *Future Oncology*, vol. 10, no. 14, pp. 2259–2277, 2014.

[60] T. D. Poeppel, I. Binse, S. Petersenn et al., "^{68}Ga-DOTATOC versus ^{68}Ga-DOTATATE PET/CT in functional imaging of neuroendocrine tumors," *The Journal of Nuclear Medicine*, vol. 52, no. 12, pp. 1864–1870, 2011.

[61] D. Wild, J. B. Bomanji, P. Benkert et al., "Comparison of 68Ga-DOTANOC and 68Ga-DOTATATE PET/CT within patients with gastroenteropancreatic neuroendocrine tumors," *Journal of Nuclear Medicine*, vol. 54, no. 3, pp. 364–372, 2013.

[62] E. Bombardieri, M. Maccauro, M. R. Castellani et al., "Radioisotopic imaging of neuroendocrine tumours. Which radiopharmaceutical and which diagnostic procedure?" *Minerva Endocrinologica*, vol. 26, no. 4, pp. 197–213, 2001.

[63] A. Nikolaou, D. Thomas, C. Kampanellou et al., "The value of 11C-5-hydroxy-tryptophan positron emission tomography in neuroendocrine tumor diagnosis and management: experience from one center," *Journal of Endocrinological Investigation*, vol. 33, no. 11, pp. 794–799, 2010.

[64] R. Junik, P. Drobik, B. Małkowski, and K. Kobus-Błachnio, "The role of positron emission tomography (PET) in diagnostics of gastroenteropancreatic neuroendocrine tumours (GEP NET)," *Advances in Medical Sciences*, vol. 51, pp. 66–68, 2006.

[65] G. A. Kaltsas, D. Papadogias, P. Makras, and A. B. Grossman, "Treatment of advanced neuroendocrine tumours with radiolabelled somatostatin analogues," *Endocrine-Related Cancer*, vol. 12, no. 4, pp. 683–699, 2005.

[66] G. Kaltsas, J. J. Mukherjee, P. N. Plowman, and A. B. Grossman, "The role of chemotherapy in the nonsurgical management of malignant neuroendocrine tumours," *Clinical Endocrinology*, vol. 55, no. 5, pp. 575–587, 2001.

[67] J. Vogel, A. S. Atanacio, T. Prodanov et al., "External beam radiation therapy in treatment of malignant pheochromocytoma and paraganglioma," *Frontiers in Oncology*, vol. 4, article 166, 2014.

[68] A. Mohamed, M. P. Blanchard, M. Albertelli et al., "Pasireotide and octreotide antiproliferative effects and sst2 trafficking in

human pancreatic neuroendocrine tumor cultures," *Endocrine-Related Cancer*, vol. 21, no. 5, pp. 691–704, 2014.

[69] M. Fani, H. R. Maecke, and S. M. Okarvi, "Radiolabeled peptides: valuable tools for the detection and treatment of cancer," *Theranostics*, vol. 2, no. 5, pp. 481–501, 2012.

[70] E. P. Krenning, M. de Jong, P. P. M. Kooij et al., "Radiolabelled somatostatin analogue(s) for peptide receptor scintigraphy and radionuclide therapy," *Annals of Oncology*, vol. 10, supplement 2, pp. S23–S29, 1999.

[71] L. B. Anthony, E. A. Woltering, G. D. Espenan, M. D. Cronin, T. J. Maloney, and K. E. McCarthy, "Indium-111-pentetreotide prolongs survival in gastroenteropancreatic malignancies," *Seminars in Nuclear Medicine*, vol. 32, no. 2, pp. 123–132, 2002.

[72] E. S. Delpassand, J. Sims-Mourtada, H. Saso et al., "Safety and efficacy of radionuclide therapy with high-activity in-111 pentetreotide in patients with progressive neuroendocrine tumors," *Cancer Biotherapy and Radiopharmaceuticals*, vol. 23, no. 3, pp. 292–300, 2008.

[73] A. Capello, E. P. Krenning, W. A. P. Breeman, B. F. Bernard, and M. de Jong, "Peptide receptor radionuclide therapy *in vitro* using [111In-DTPA0]octreotide," *Journal of Nuclear Medicine*, vol. 44, no. 1, pp. 98–104, 2003.

[74] M. V. Davì, L. Bodei, M. Ferdeghini et al., "Multidisciplinary approach including receptor radionuclide therapy with 90Y-DOTATOC ([90Y-DOTA0,Tyr3]-octreotide) and 177Lu-DOTATATE ([177Lu-DOTA0,Tyr3]-octreotate) in ectopic Cushing syndrome from a metastatic gastrinoma: a promising proposal," *Endocrine Practice*, vol. 14, no. 2, pp. 213–218, 2008.

[75] D. J. Kwekkeboom, W. H. Bakker, P. P. Kooij et al., "[^{177}Lu-DOTA^{0},Tyr^{3}]octreotate: comparison with [^{111}In-DTPA^{0}]octreotide in patients," *European Journal of Nuclear Medicine*, vol. 28, no. 9, pp. 1319–1325, 2001.

[76] M. Ginj, K. Hinni, S. Tschumi, S. Schulz, and H. R. Maecke, "Trifunctional somatostatin-based derivatives designed for targeted radiotherapy using auger electron emitters," *Journal of Nuclear Medicine*, vol. 46, no. 12, pp. 2097–2103, 2005.

[77] S. Vinjamuri, T. M. Gilbert, M. Banks et al., "Peptide receptor radionuclide therapy with 90 Y-DOTATATE/90 Y-DOTATOC in patients with progressive metastatic neuroendocrine tumours: assessment of response, survival and toxicity," *British Journal of Cancer*, vol. 108, no. 7, pp. 1440–1448, 2013.

[78] L. Bodei, M. Cremonesi, C. M. Grana et al., "Yttrium-labelled peptides for therapy of NET," *European Journal of Nuclear Medicine and Molecular Imaging*, vol. 39, supplement 1, pp. S93–S102, 2012.

[79] F. Forrer, C. Waldherr, H. R. Maecke, and J. Mueller-Brand, "Targeted radionuclide therapy with ^{90}Y-DOTATOC in patients with neuroendocrine tumors," *Anticancer Research*, vol. 26, no. 1, pp. 703–707, 2006.

[80] C. Waldherr, M. Pless, H. R. Maecke, A. Haldemann, and J. Mueller-Brand, "The clinical value of [90Y-DOTA]-D-Phe1-Tyr3-octreotide (90Y-DOTATOC) in the treatment of neuroendocrine tumours: a clinical phase II study," *Annals of Oncology*, vol. 12, no. 7, pp. 941–945, 2001.

[81] D. J. Kwekkeboom, W. W. de Herder, B. L. Kam et al., "Treatment with the radiolabeled somatostatin analog [177Lu-DOTA0,Tyr3]octreotate: toxicity, efficacy, and survival," *Journal of Clinical Oncology*, vol. 26, no. 13, pp. 2124–2130, 2008.

[82] M. Sansovini, S. Severi, A. Ambrosetti et al., "Treatment with the radiolabelled somatostatin analog ^{177}Lu-DOTATATE for advanced pancreatic neuroendocrine tumors," *Neuroendocrinology*, vol. 97, no. 4, pp. 347–354, 2013.

[83] E. Seregni, M. Maccauro, C. Chiesa et al., "Treatment with tandem [90Y]DOTA-TATE and [177Lu] DOTA-TATE of neuroendocrine tumours refractory to conventional therapy," *European Journal of Nuclear Medicine and Molecular Imaging*, vol. 41, no. 2, pp. 223–230, 2014.

[84] A. Imhof, P. Brunner, N. Marincek et al., "Response, survival, and long-term toxicity after therapy with the radiolabeled somatostatin analogue [90Y-DOTA]-TOC in metastasized neuroendocrine cancers," *Journal of Clinical Oncology*, vol. 29, no. 17, pp. 2416–2423, 2011.

[85] L. Nisa, G. Savelli, and R. Giubbini, "Yttrium-90 DOTATOC therapy in GEP-NET and other SST2 expressing tumors: a selected review," *Annals of Nuclear Medicine*, vol. 25, no. 2, pp. 75–85, 2011.

[86] M. de Jong, W. A. P. Breeman, R. Valkema, B. F. Bernard, and E. P. Krenning, "Combination radionuclide therapy using ^{177}Lu and ^{90}Y-labeled somatostatin analogs," *Journal of Nuclear Medicine*, vol. 46, no. 1, supplement, pp. 13S–17S, 2005.

[87] A. Romer, D. Seiler, N. Marincek et al., "Somatostatin-based radiopeptide therapy with [^{177}Lu-DOTA]-TOC versus [^{90}Y-DOTA]-TOC in neuroendocrine tumours," *European Journal of Nuclear Medicine and Molecular Imaging*, vol. 41, no. 2, pp. 214–222, 2014.

[88] J. C. Reubi, J.-C. Schär, B. Waser et al., "Affinity profiles for human somatostatin receptor subtypes SST1-SST5 of somatostatin radiotracers selected for scintigraphic and radiotherapeutic use," *European Journal of Nuclear Medicine*, vol. 27, no. 3, pp. 273–282, 2000.

[89] F. Forrer, H. Uusijärvi, D. Storch, H. R. Maecke, and J. Mueller-Brand, "Treatment with 177Lu-DOTATOC of patients with relapse of neuroendocrine tumors after treatment with 90Y-DOTATOC," *Journal of Nuclear Medicine*, vol. 46, no. 8, pp. 1310–1316, 2005.

[90] S. M. Bison, M. W. Konijnenberg, M. Melis et al., "Peptide receptor radionuclide therapy using radiolabeled somatostatin analogs: focus on future developments," *Clinical and Translational Imaging*, vol. 2, no. 1, pp. 55–66, 2014.

[91] F. Graf, J. Fahrer, S. Maus et al., "DNA double strand breaks as predictor of efficacy of the alpha-particle emitter Ac-225 and the electron emitter Lu-177 for somatostatin receptor targeted radiotherapy," *PLoS ONE*, vol. 9, no. 2, Article ID e88239, 2014.

[92] S. T. Palayoor, J. L. Humm, R. W. Atcher, J. J. Hines, and R. M. Macklis, "G2M arrest and apoptosis in murine T lymphoma cells following exposure to 212Bi alpha particle irradiation," *Nuclear Medicine and Biology*, vol. 20, no. 6, pp. 795–805, 1993.

[93] T. K. Nayak, J. P. Norenberg, T. L. Anderson, E. R. Prossnitz, M. G. Stabin, and R. W. Atcher, "Somatostatin-receptor-targeted α-emitting ^{213}Bi is therapeutically more effective than β—emitting 177Lu in human pancreatic adenocarcinoma cells," *Nuclear Medicine and Biology*, vol. 34, no. 2, pp. 185–193, 2007.

[94] M. Miederer, G. Henriksen, A. Alke et al., "Preclinical evaluation of the α-particle generator nuclide 225Ac for somatostatin receptor radiotherapy of neuroendocrine tumors," *Clinical Cancer Research*, vol. 14, no. 11, pp. 3555–3561, 2008.

[95] J. P. Norenberg, B. J. Krenning, I. R. H. M. Konings et al., "^{213}Bi-[DOTA^{0},Tyr^{3}]octreotide peptide receptor radionuclide therapy of pancreatic tumors in a preclinical animal model," *Clinical Cancer Research*, vol. 12, no. 3, part 1, pp. 897–903, 2006.

[96] D. T. Goodhead, "Mechanisms for the biological effectiveness of high-LET radiations," *Journal of Radiation Research*, vol. 40, supplement, pp. 1–13, 1999.

[97] K. Matthews, P. E. Noker, B. Tian et al., "Identifying the safety profile of Ad5.SSTR/TK.RGD, a novel infectivity-enhanced bicistronic adenovirus, in anticipation of a phase I clinical trial in patients with recurrent ovarian cancer," *Clinical Cancer Research*, vol. 15, no. 12, pp. 4131–4137, 2009.

[98] S. M. Verwijnen, P. A. E. S. Smith, R. C. Hoeben et al., "Molecular imaging and treatment of malignant gliomas following adenoviral transfer of the herpes simplex virus-thymidine kinase gene and the somatostatin receptor subtype 2 gene," *Cancer Biotherapy and Radiopharmaceuticals*, vol. 19, no. 1, pp. 111–120, 2004.

[99] K. H. Kim, I. Dmitriev, J. P. O'Malley et al., "A phase I clinical trial of Ad5.SSTR/TK.RGD, a novel infectivity-enhanced bicistronic adenovirus, in patients with recurrent gynecologic cancer," *Clinical Cancer Research*, vol. 18, no. 12, pp. 3440–3451, 2012.

[100] K. Higashi, S. Hazama, A. Araki et al., "A novel cancer vaccine strategy with combined IL-18 and HSV-TK gene therapy driven by the hTERT promoter in a murine colorectal cancer model," *International Journal of Oncology*, vol. 45, no. 4, pp. 1412–1420, 2014.

[101] K. R. Zinn, T. R. Chaudhuri, V. N. Krasnykh et al., "Gamma camera dual imaging with a somatostatin receptor and thymidine kinase after gene transfer with a bicistronic adenovirus in mice," *Radiology*, vol. 223, no. 2, pp. 417–425, 2002.

[102] M. ter Horst, S. M. Verwijnen, E. Brouwer et al., "Locoregional delivery of adenoviral vectors," *Journal of Nuclear Medicine*, vol. 47, no. 9, pp. 1483–1489, 2006.

[103] V. Akerstrom, C. Chen, M. S. Lan, and M. B. Breslin, "Adenoviral insulinoma-associated protein 1 promoter-driven suicide gene therapy with enhanced selectivity for treatment of neuroendocrine cancers," *Ochsner Journal*, vol. 13, no. 1, pp. 91–99, 2013.

[104] C. Capasso, M. Garofalo, M. Hirvinen, and V. Cerullo, "The evolution of adenoviral vectors through genetic and chemical surface modifications," *Viruses*, vol. 6, no. 2, pp. 832–855, 2014.

[105] M. G. Castro, M. Colfi, T. J. Wilson et al., "Adenoviral vector-mediated gene therapy for gliomas: coming of age," *Expert Opinion on Biological Therapy*, vol. 14, no. 9, pp. 1241–1257, 2014.

[106] E. Zinn and L. H. Venberghe, "Adeno-associated virus: fit to serve," *Current Opinion in Virology*, vol. 8, pp. 90–97, 2014.

[107] D. Ibraheem, A. Elaissari, and H. Fessi, "Gene therapy and DNA delivery systems," *International Journal of Pharmaceutics*, vol. 459, no. 1-2, pp. 70–83, 2014.

[108] L. S. Young, P. F. Searle, D. Onion, and V. Mautner, "Viral gene therapy strategies: from basic science to clinical application," *Journal of Pathology*, vol. 208, no. 2, pp. 299–318, 2006.

[109] J. A. McCart, N. Mehta, D. Scollard et al., "Oncolytic vaccinia virus expressing the human somatostatin receptor SSTR2: molecular imaging after systemic delivery using ^{111}In-pentetreotide," *Molecular Therapy*, vol. 10, no. 3, pp. 553–561, 2004.

[110] D. E. Hruby, "Vaccinia virus vectors: new strategies for producing recombinant vaccines," *Clinical Microbiology Reviews*, vol. 3, no. 2, pp. 153–170, 1990.

[111] N. Wang, H. Zhang, B.-Q. Zhang et al., "Adenovirus-mediated efficient gene transfer into cultured three-dimensional organoids," *PLoS ONE*, vol. 9, no. 4, Article ID e93608, 2014.

[112] S. Nair, D. T. Curiel, V. Rajaratnam, C. Thota, and A. Al-Hendy, "Targeting adenoviral vectors for enhanced gene therapy of uterine leiomyomas," *Human Reproduction*, vol. 28, no. 9, pp. 2398–2406, 2013.

[113] F. McCormick, "Cancer gene therapy: fringe or cutting edge?" *Nature Reviews Cancer*, vol. 1, no. 2, pp. 130–141, 2001.

[114] V. Kundra, F. Mannting, A. G. Jones, and A. I. Kassis, "Noninvasive monitoring of somatostatin receptor type 2 chimeric gene transfer," *Journal of Nuclear Medicine*, vol. 43, no. 3, pp. 406–412, 2002.

[115] A. Hemminki, N. Belousova, K. R. Zinn et al., "An adenovirus with enhanced infectivity mediates molecular chemotherapy of ovarian cancer cells and allows imaging of gene expression," *Molecular Therapy*, vol. 4, no. 3, pp. 223–231, 2001.

[116] M. van Essen, E. P. Krenning, B. L. R. Kam, M. de Jong, R. Valkema, and D. J. Kwekkeboom, "Peptide-receptor radionuclide therapy for endocrine tumors," *Nature Reviews Endocrinology*, vol. 5, no. 7, pp. 382–393, 2009.

[117] O. Akinlolu, K. Ottolino-Perry, J. A. McCart, and R. M. Reilly, "Antiproliferative effects of 111In- or 177Lu-DOTATOC on cells exposed to low multiplicity-of-infection double-deleted vaccinia virus encoding somatostatin subtype-2 receptor," *Cancer Biotherapy and Radiopharmaceuticals*, vol. 25, no. 3, pp. 325–333, 2010.

[118] M. Takahashi, T. Sato, T. Sagawa et al., "E1B-55K-deleted adenovirus expressing E1A-13S by AFP-enhancer/promoter is capable of highly specific replication in AFP-producing hepatocellular carcinoma and eradication of established tumor," *Molecular Therapy*, vol. 5, no. 5, pp. 627–634, 2002.

[119] B. E. Rogers, K. R. Zinn, C.-Y. Lin, T. R. Chaudhuri, and D. J. Buchsbaum, "Targeted radiotherapy with [90Y]-SMT 487 in mice bearing human nonsmall cell lung tumor xenografts induced to express human somatostatin receptor subtype 2 with an adenoviral vector," *Cancer*, vol. 94, supplement 4, pp. 1298–1305, 2002.

[120] L.-P. Chai, Z.-F. Wang, W.-Y. Liang et al., "In vitro and in vivo effect of 5-FC combined gene therapy with TNF-alpha and CD suicide gene on human laryngeal carcinoma cell line Hep-2," *PLoS ONE*, vol. 8, no. 4, Article ID e61136, 2013.